NORTHWESTERN UNIVERSITY

Self-Dispersed Crumpled Graphene Nanoparticles for Lubrication

A DISSERTATION

SUBMITTED TO THE GRADUATE SCHOOL
IN PARTIAL FULFILLMENT OF THE REQUIREMENTS

for the degree

DOCTOR OF PHILOSOPHY

Field of Materials Science and Engineering

By

Xuan Dou

EVANSTON, ILLINOIS

December 2018

ABSTRACT

Ultrafine particles are often used as lubricant additives because they can enter tribological contacts to reduce friction and protect surfaces from wear. They tend to be more stable than molecular additives under high thermal and mechanical stresses during rubbing. However, in lubricant oil, ultrafine particles tend to aggregate together to reduce the effective dispersed concentration. Although the surfactants could bind to nanoparticle surface and facilitate their dispersion in lubricant oil, they could be rubbed off or decomposed under the harsh tribological conditions. Therefore, the lubrication performance will be compromised. And it is highly desirable for these particles to remain well dispersed in oil without relying on molecular ligands.

Previously, our lab discovered that the nano-meter sized crumpled graphene balls which have unique aggregation resistance property and here we report the use of crumpled graphene balls as a high-performance additive that can significantly improve the lubrication properties of polyalphaolefin base oil. Due to the aggregation resistant property, the tribological performance of crumpled graphene balls is only weakly dependent on their concentration in oil and readily exceeds that of other carbon additives such as graphite, reduced graphene oxide, and carbon black. Notably, polyalphaolefin base oil with only 0.01–0.1 wt % of crumpled graphene balls outperforms a fully formulated commercial lubricant in terms of friction and wear reduction.

Further, crumpled graphene balls were also evaluated as additives for commercially lubricant oils. They were found to improve the wear reduction of the commercially available oils at oil temperature ranging from room temp to 90C. However, the crumpled graphene balls did not significantly change the oils' friction reduction, suggesting that the current formulation will not be negatively affected by crumpled graphene balls, probably due to its aggregation resistance and no interferences with other molecular additives. On the other hand, it could further improve the wear reduction by being added into the commercial lubricant oil.

In conclusion, crumpled graphene has great potential as a lubricant additive material. Because of their unique particle shape and aggregation resistance property, crumpled graphene balls can reduce the friction and wear between metal mechanical parts, showing improvements over other carbon-based additives and a fully formulated commercial lubricant. Finally, crumpled graphene balls can be easily introduced into commercially available lubricants to further enhance their lubrication performance, especially in wear reduction.

ACKNOWLEDGEMENTS

The author wants to thank the Office of Naval Research, Northwestern MRSEC and Air Products & Chemicals for funding support.

I want to thank my advisor Prof. Jiaxing Huang for his continuous support, advice and help throughout my PhD career. I also want to thank all my committee members – Prof. Jiaxing Huang, Prof. Jane Wang, Prof. Yip-Wah Chung and Prof. Kenneth Shull – for their time and commitment.

I also want to thank all of my collaborators and friends, including Dr. Xingliang He and Dr. Andrew Koltonow, for their contributions to my work and their generous help throughout my PhD thesis; Dr. Chening Yeh and Ms. Alane Lim, for their suggestion on my thesis paper writing. Additionally, I want to thank Dr. Blake Johnson and Dr. Jie Ren in Prof. Wang's lab for their help in experiment modification and paper writing. They gave me lots of insightful suggestions on my tribological experiments.

Last but not least, I want to thank my family and friends for their encouragement and help. PhD study is not an easy journey, and I wouldn't have been able to finish it without their support.

Table of Contents

List of Tables, Figures and Illustrations

Tables

Figures

Chapter 1

A Review of Graphene's Application to Lubrication

1.1 Introduction

Friction and wear are inevitable at contacted interfaces of engineering components with relative motion. Both not only consume extra energy but also cause the material loss of surface contacts. Take automobile for example, the friction within the engines significantly reduces their energy efficiency - frictional losses in the engine and transmission account for up to 17% of fuel consumption[1]. In 2014, if friction and wear in engines and drivetrain were reduced by advanced tribological technologies, it could save the global economy as much as 450 billion euro plus 1.46 billion ton of carbon dioxide emission in the short term[2]. The application of lubricants reduces friction and wear within mechanical systems, helping to improve fuel efficiency and material durability. In response, scientists and engineers are searching for mitigating solutions in the new type of materials for tribological application. And graphene is such a material with great tribological potentials for friction and wear reduction owing to its inherent low friction and superior strength.

Graphene is a two-dimensional carbon material with a honeycomb structure, consisting of single layers of sp2-hybridized carbon atoms in two-dimensional six-carbon rings[3]. As the

building block of the widely used solid lubricant – graphite, graphene inherits graphite's ultralow-friction characteristics[4-5]. That is because a few graphene nanosheets usually are stacked in a lamellar structure bonded by weak Van der Waals' force, which leads to a state of low shear strength and the ease of shearing or delaminating. Also, graphene has low surface energy[6]. Therefore, graphene nanosheets with only atomic-scale thickness are easy to enter into the contact surfaces, and thus be able to avoid the direct solid contact to reduce adhesion and friction. Beside friction reduction, graphene is also a potential material with good wear resistance due to its hybridized sp2 orbitals of a carbon atoms covalently bonding to each other in a planar configuration with a short C-C bond length of 0.142 nm, which results in a high fracture stress measured around 130 Gpa with elastic modulus exceeding 1.0 TPa[7-8].

Since graphene was discovered[9], multiple researches have investigated its tribological behavior at the nanoscale by using the Atomic Force microscopy[10-14]. The molecular dynamic simulation was also fully utilized to help understand the principle of graphene's lubrication performance in the experiments[15-17]. However, the graphene's macroscale tribological applications remain relatively unexplored. Different with the tribological test at the nanoscale, the macroscale friction test applies higher force, faster sliding velocity and larger contact surfaces. The performance of wear reduction is also necessary to be taken into the consideration. Moreover, macroscale lubrication application has different experimental conditions due to the different requirements, for example, there are solid lubrication and liquid lubrication.

An up-to-date summary of graphene's tribological application at nanoscale enables us to understand the fundamental principles of this material for lubrication and its macroscopic tribological test will further help us better understand how graphene could reduce the mechanical friction and protect surfaces from wears as the surface treatment, solid lubricant additive, liquid lubricant additive and grease lubricant additive (as shown in Figure 1.1.1).

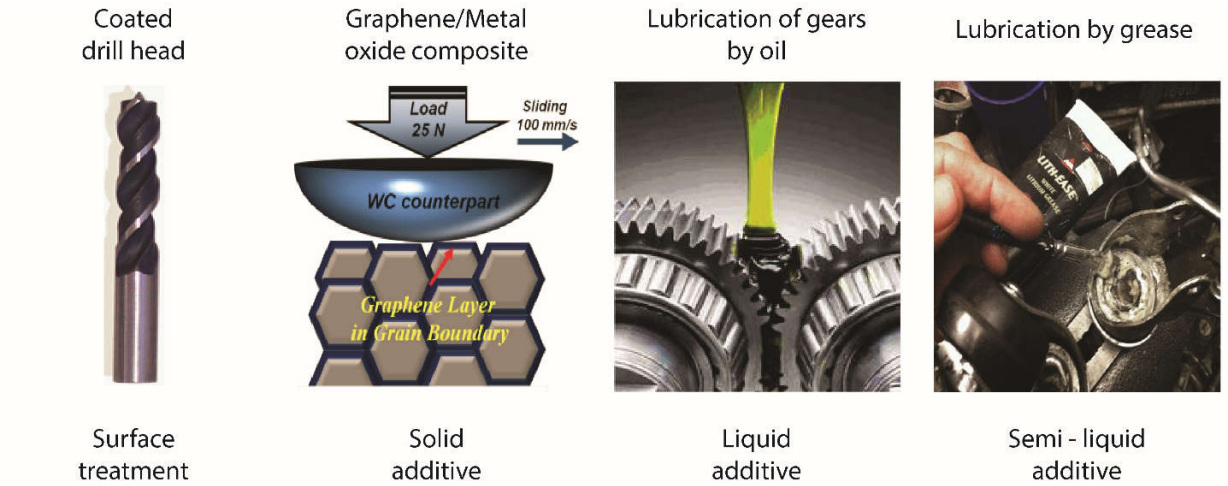

Figure 1.1.1 Tribological applications of graphene as the surface treatment, solid lubricant additive, liquid lubricant additive and grease lubricant additive

And in this thesis paper, we mainly focus on the liquid lubrication. Graphene materials are added into the lubricant oil as an additive material to further improve the lubrication performance. Lots of researches have been conducted in this field already.

1.2 Graphene's nanoscale lubrication

Researchers have proved that graphene shows friction reduction at the nanoscale. Atomic Force Microscope or Lateral Force Microscope was utilized to implement the friction test on single or multiple layers of graphene to identify what is the factors influencing graphene's friction performance at the nanoscale. One noticeable factor is the puckering effect: When an AFM tip makes a contact with loosely bounded thin layers of graphene sheets, the sheets can pucker locally due to the tip-sheet adhesion, leading to a larger contact area and thus a higher frictional resistance. In the case of thick layers of graphene, the thicker layer sheets minimize the puckering effect due to increased stiffness, so that the induced-contact area decreases as well and thereby reduce friction[14] (as shown in Figure 1.2.1). Other factors have also been identified that could influence graphene's friction performance due to the interaction fluctuation between the scanning tip and graphene surface which are all summarized in Table 1.2.1 below.

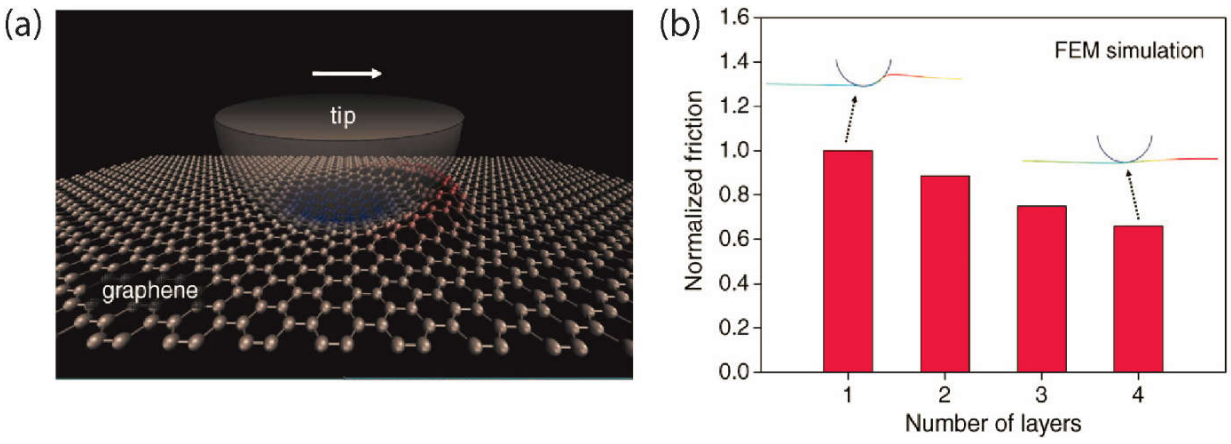

Figure 1.2.1 (a) the illustrated graph to show the formation of puckering effect due to the tip sliding. (b) The thicker layer is less likely to have puckering effect due to the increased stiffness, which results into lower friction force.

Table 1.2.1 Factors influencing the tribological performance of graphene in single-asperity contact

Influencing factor	Trend	Mechanism
Number of layers and Substrate	Increasing the number of layers will reduce the friction between the tip and graphene	~Instead of surface normal force, Van der Waals force is the source of friction and it decreases with increasing layers[11] ~During contacting, the tip will more easily cause localized wrinkles (puckering effect) for thinner layers, which resists sliding[14, 16, 18-19] ~Electron-phonon coupling of bilayer graphene lead into frictional energy loss comparing to single layer graphene[12] ~The thicker layers will increase the local contact stiffness and reduce the surface deformation which will cost less energy in the friction test comparing to thinner layers[20] ~The thinner layers are likely to have smaller interatomic space between layers due to the tip sliding, and therefore, increase the possibility to form the crosslinks which increase the interlayer friction[21] ~Number of layers is less relevant due to the subsurface contamination of the ink (NMP)[22]

	Friction is minimum for the single layer	~Suppression of pucker effect by tightly anchoring the graphene onto substrate[23-24]
Load dependence / Force hysteresis	The friction force has a hysteresis effect during loading/unloading process	~The adhesion between tip and graphene is stronger than the bounding force between graphene and substrate – which will keep out-of-plain deformation during unloading process[18, 25-26] ~In the humid environment, the water between the tip and graphene introduce the hysteresis effect[27]
Sliding orientation	There is a periodic or repeated friction variation of graphene based on periodically varied sliding orientation	~The friction variation is due the different bonds density based on lattice orientation[28-29] And the 60°periodicity is in consistent with periodicity of atomic structure of graphene[30-31]
Sliding velocity	Friction increase logarithmically with the sliding speed	~Viscoelasticity similarity – the increased velocity makes deflected graphene sheet less time to relax and therefore cause the increased friction force[11] ~Stick-slip effect – slip is the friction between the tip and top layer; stick is the friction between graphene layers[20]
Temperature	Friction rise when the temperature increase for the mechanically exfoliated graphene weakly adhered on a silica substrate	~The increasing temperature will result into the surface corrugation and further weaken the friction reduction[32]
Synthesis/ fabrication methods	Mechanically exfoliated graphene has better lubrication performance than the graphene made by chemical vapor deposition	~The lubrication property of graphene is related with its graphitic structure - defects will compromise the friction reduction performance[32-34]

Types (pristine, hydrogenated, fluorinated, oxidized graphene)	Compared with pristine graphene, the friction force of chemically modified graphene significantly increases	~The hydrogenation induced atomic roughness results into the interlocking of tip atoms and hydrogen atoms by bring them very close[35] ~Friction increase due to the strong local variation of interfacial potential energy, result from the highly localized negative charge over F atom[34, 36-37] ~ Due to the fluorination, the increased out of plane stiffness caused the friction increment[38]
AFM tip	Although there is no evidence showing the influence of different types of AFM tips, functionalized AFM tips do have varied friction behavior.	~ The friction force would increase with stronger tip – sample adhesion due to the functionlization[39]
Environment	Friction has a stochastic performance in water	~The stochastic friction behavior is because the water loses force memory much faster than the sliding of the tip[40]

Besides, a few researches have investigated the intrinsic friction behavior between graphene interlayers. The tribological behavior of the interface between graphene sheets is also affected by various factors (Table 1.2.2). Commensurate state, an indicator of symmetry, plays a key role in the interlayer friction between graphene nanosheets.

Table 1.2.2 Factors influencing the interlayer tribological performance of the graphenes

Influencing factor	Trend	Mechanism

Commensurate state	Higher friction in the commensurate (higher symmetry) than that in the incommensurate case (lower symmetry)	Stick-slip behavior in the commensurate state[15, 17, 36, 41-43]
Contact area	Higher friction when sliding on edge atoms than that on the atoms in interior areas in the incommensurate case	Edge atoms locally reconstruct to follow the structural registry of the substrate or vertically distort causing local pinning[42]
Interlayer distance	Lower friction for larger interlayer distance in the commensurate case	The registry strength between stacking graphene nanosheets decreases[41]
Defect and vacancy	Friction decrease when introduction of 5-7 defects and vacancies	Interlayer registry decrease[41]
Number of layers	Lower friction for thinner graphene that strongly anchored on the substrate	The stiffness of the sliding body weakens the stick-slip behavior, and stiffness increases with the thickness decreases[17]
Applied load	Higher load inducing higher friction for incommensurate graphene flakes on graphite	Vertical distortions of edge atoms transit sliding state from smooth sliding to stick-slip[44]
Substrate stiffness	Softer substrate giving rise to higher friction	Increase in deformation[42]
Type	Lower friction for a single hydrogenated graphene sheet sliding against another one	Electrons accumulation between the carbon and hydrogen atoms[45]
	Higher friction for graphene oxide than the pristine graphene	The hydrogen bond formation in the graphene oxide causes instability due to the local chemical change, which lead to a stronger energy dissipation and then result in a higher friction[46]
Full graphene or hexagonal flakes	Lower friction for hexagonal graphene flakes when sliding between two graphene layers	Graphene flakes have lower coverage of underlying graphene layers and they can move independent to each other within one

	period, which reduces sliding resistance[47]

Beyond fundamental research of graphene's lubrication mechanism, researchers also further explored graphene's potential application as the lubricant additive of the liquid lubricant. And it indicates that graphene has the ability to reduce friction and wear in liquid lubricant as well.

1.3 Stribeck Curve

For the liquid lubrication, graphene specifically fulfills its lubrication functionality in the so called the boundary lubrication regime, which is one of the three liquid lubrication regimes according to the Stribeck curve (as shown in Figure 1.3.1). Stribeck curve is used to characterize and define the three specific lubrication regimes according to the different lubrication mechanisms influenced by the relative speed, liquid viscosity and applied force[48-49]. Take automotive's gear box for example: in the hydrodynamic lubrication, the gears would spin at thousands rpm and sustain a certain amount of loading. The liquid film could be built up due to the high relative speed. Once the film thickness (h) is larger than the surface roughness (R), the surfaces could be completely separated by the thick liquid lubricant film. The prevention of surface contacts greatly reduces the friction and wear. The only factor to affect the friction coefficient in this region is the liquid's viscosity which will drag the surfaces' relative motion at high speed.

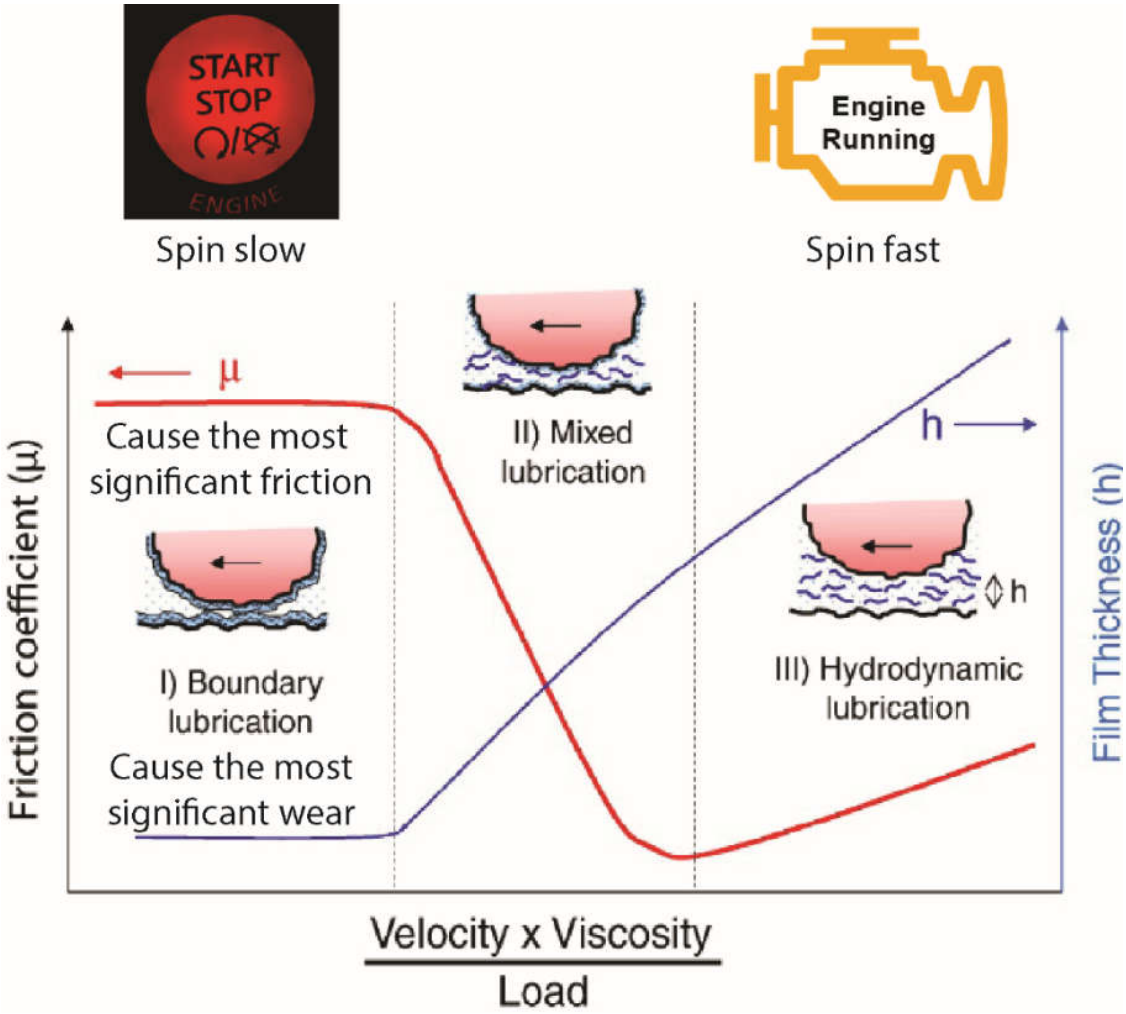

Figure 1.3.1 Stribeck curve categorized the liquid lubrication into three lubrication regimes including boundary lubrication, mixed lubrication and hydrodynamic lubrication. Engine start/stop correspond to boundary lubrication and Engine's running correspond to hydrodynamic lubrication region

However, for the engine's start/stop stage, its gears would spin at a lower speed compared to the normal spinning speed at thousands rpm. At this stage, the relatively low speed and comparable force level shift the lubrication region from the right to left side of Stribeck curve:

engine or gear parts would operate in the boundary lubrication. The liquid film would barely exist and its film thickness (h) is less than the roughness of the surface (R), results in two surfaces' direct contact. The surface asperities would rub with each other and leads to the most significant friction and surface wear. The lubricants added within graphene materials are designed to work in this region because graphene materials could be delivered to the friction spots and reduce the friction and wear by effectively separating the surface contacts. All the liquid lubrication research containing graphene operated in this boundary lubrication region.

To apply graphene as the lubricant additive, a well-dispersed graphene solution in lubricant oil is a necessary pre-request condition. The graphene should keep dispersed in lubricant for long enough time to maintain an effective concentration. But, graphene is inherently hydro/oil-phobic and hard to be dispersed in the most solvent, especially the hydrocarbon solvent which is the major component of lubricant oil. To fully disperse the graphene into lubricant oil, various efforts have been made and shown as below.

1.4 Adding Graphene as the Lubricant Additive

Graphene nanosheets could also fulfill its function of lubrication by being added into the lubricant oil as an additive material. As an additive, graphene nanosheets need to be dispersed in the lubricant oil and transported to the friction contact sites by the flow of liquid lubricant. Then graphene could further reduce the friction and wear by separating the

surface contacts. Better than the solid graphene coatings, liquid lubrication with additive materials avoids the need of frequently replenishing the coating materials.

Surfactant / Chemical modification assisted dispersion of graphene

Using surfactant is the most intuitive method to help graphene disperse in lubricant base oil. Lin, et al. use the stearic and oleic acid to functionalize the graphene sheets[4]. The FT-IR spectra of modified graphene (in Figure 1.4.1 b) shows the new peaks at 2862 and 2921 cm-1 featuring the CH2 and CH3 groups, which indicates that the graphene sheets were modified with long alkyl chains of oleic acid (as shown in Figure 1.4.1 a). The grafted organophilic group will help graphene better disperse into the lubricant base oil.

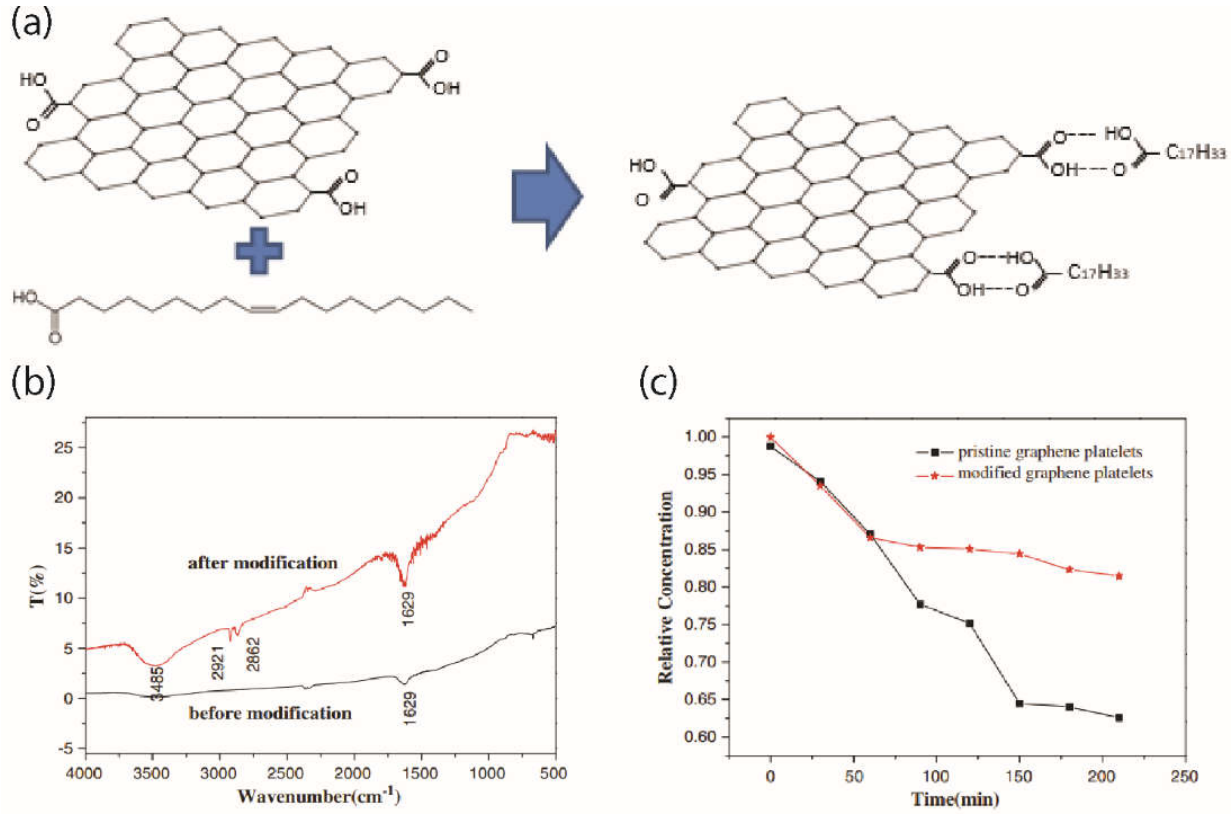

Figure 1.4.1 Liquid lubricant additive – (a) Graphene nanosheet is modified by oleic acid. (b) The FTIR spectra of pristine and modified graphene. (c) The concentration changes of pristine and modified graphene dispersion in base oil.

To further compare the dispersibility of pristine graphene with the modified graphene, the dispersion test was fulfilled by the centrifugation of lubricant oil dispersion of both materials at the same concentration. The UV-vis spectroscopy was used to identify their relative concentration change after the centrifugation (as shown in Figure 1.4.1 c). Eventually, the modified graphene was proved to have a much better dispersibility in the lubricant base oil, because it still maintained the relatively higher concentration. However, the aggregation and sedimentation of the pristine graphene led to almost 40% loss of the original concentration after the centrifugation.

For the tribological tests in schematic Figure 1.4.2 a, the base oil with merely 0.075%wt modified graphene was used for the pin-on-disk friction test in comparison with the base oil of the same concentrated modified graphite flakes and pure base oil. Among these three groups, the oil within modified graphene has the best performance of friction and wear reduction (in Figure 1.4.2 b-c). The SEM images of worn surfaces further indicated that the metal surface protected by the lubricant with the modified graphene almost had no significant sign of wear compared to the other two samples (Figure 1.4.2 d-f). For the test with pure base oil, the SEM images of the worn surface further indicated that the surface experience more severe damages because the base oil failed to effectively separate the

surface contact. The surface protected by the lubricant containing the modified graphite showed less severe but still noticeable wear tracks. The EDS analysis further verified that the wear track protected by modified graphene has the highest concentration of carbon elements. The research group concluded that the reason of modified graphene's better friction and wear reduction is because the thin sheets of the graphene could easily infiltrate into the friction contact area and transfer into the deposit layers of lubrication protective film to prevent the direct surface contact. And modified graphite is less effective due to its bigger size.

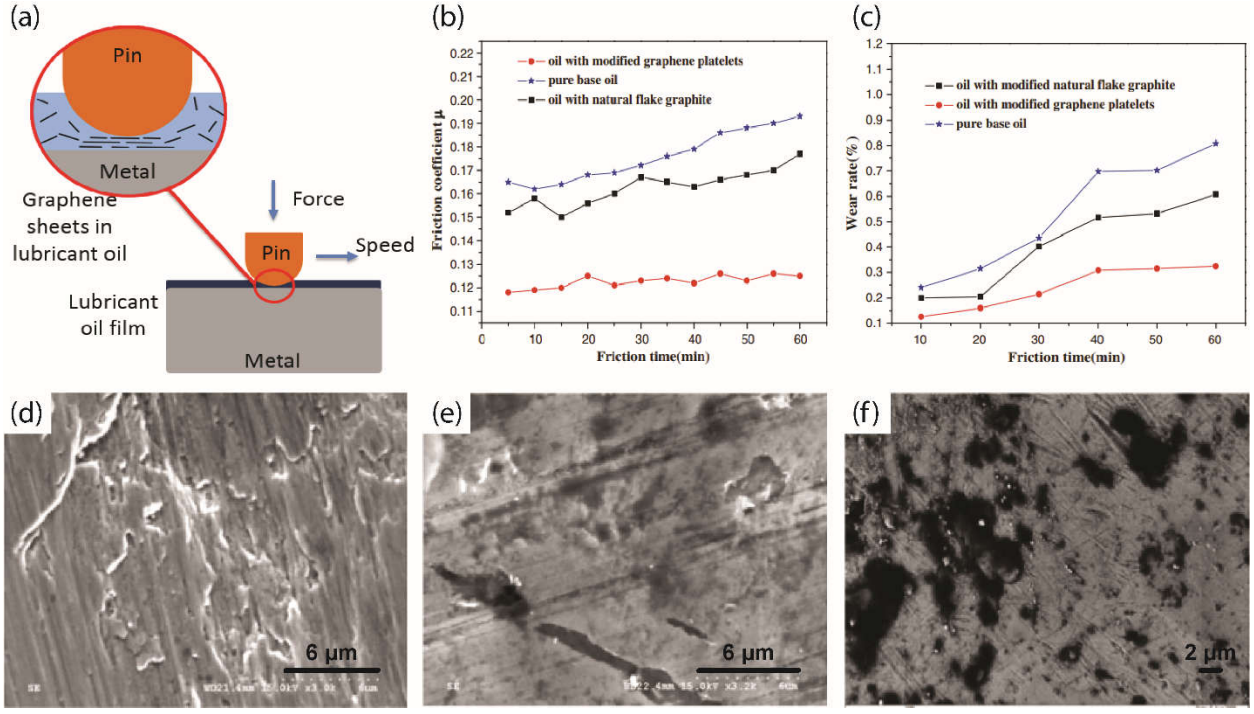

Figure 1.4.2 Liquid lubricant additive - (a) The schematic graph of the pin-on-disk lubrication process by the lubricant modified with graphene nanosheets. (b-c) The comparison of lubrication performance between the pure base oil, and the oil mixed with modified

graphene and modified graphite. (d-f) The SEM images of worn surfaces correspond to the wear test.

Besides oleic acid, Mungse, H et, al. used octadecylamine (ODA) to functionalize the rGO with long alkyl chains at rGO's edges and defect sites[50]. The modification greatly improves rGO sheets dispersibility in the 10-40W engine oil, which results in a better friction and wear reduction performance compared to the engine oil itself. Adding dispersant is another option to help graphene disperse in lube oil. Ota, Jyotiranjan et, al. mixed the poly isobutylene succinic imide-based dispersant into gear oil[51]. The modified gear oil could well disperse the graphene nanosheets. The dispersion of 0.5 wt% graphene not only had improved friction reduction but also had a better heat dissipation rate than the original gear oil as well. Eswaraiah et, al. also directly dispersed the r-GO reduced by the focused solar radiation into the engine oil[52]. The graphene maintains a very stable dispersion probably due to the dispersant contained in the engine oil. The addition of only 0.025 mg/ml graphene outperform the original engine oil by 80 and 33% for the friction and wear reduction.

The impact of graphene's concentration variation on lubrication performance

Further, Zhang, et al. found out that there exists an optimal additive concentration of graphene in the lubricant base oil leading to the best lubrication performance with the maximum friction and wear reduction[53]. And the influence of concentration variation indeed reflects on the friction (Figure 1.4.3 b) and wear test (as shown in Figure 1.4.3 c-e). Zhang, et al. did the tribological test on a wide range of graphene's concentration from 0 – 5 wt.%. They

found out that there is a range of optimal additive concentration around 0.06 wt.%. With the same experiment condition, the modified lubricant at the optimum concentration has the lowest friction coefficient and lowest wear rate. The friction curve and wear curve share the same trends. The lower and higher concentrations perform worse than the optimum concentration. As shown in the Figure 1.4.3 a, it further explains that if the concentration of graphene as lubricant additive is too low, there would not be sufficient materials to cover the contact surface. Therefore, it could result in the dry friction in the boundary lubrication region without protective material. Or if the concentration is too high, it might intentionally cause jamming or aggregation which deteriorate the lubrication performance. High concentration would also speed up graphene nanosheets' aggregation which further compromise its lubrication performance. Therefore, the extreme concentration will hurt the lubrication performance.

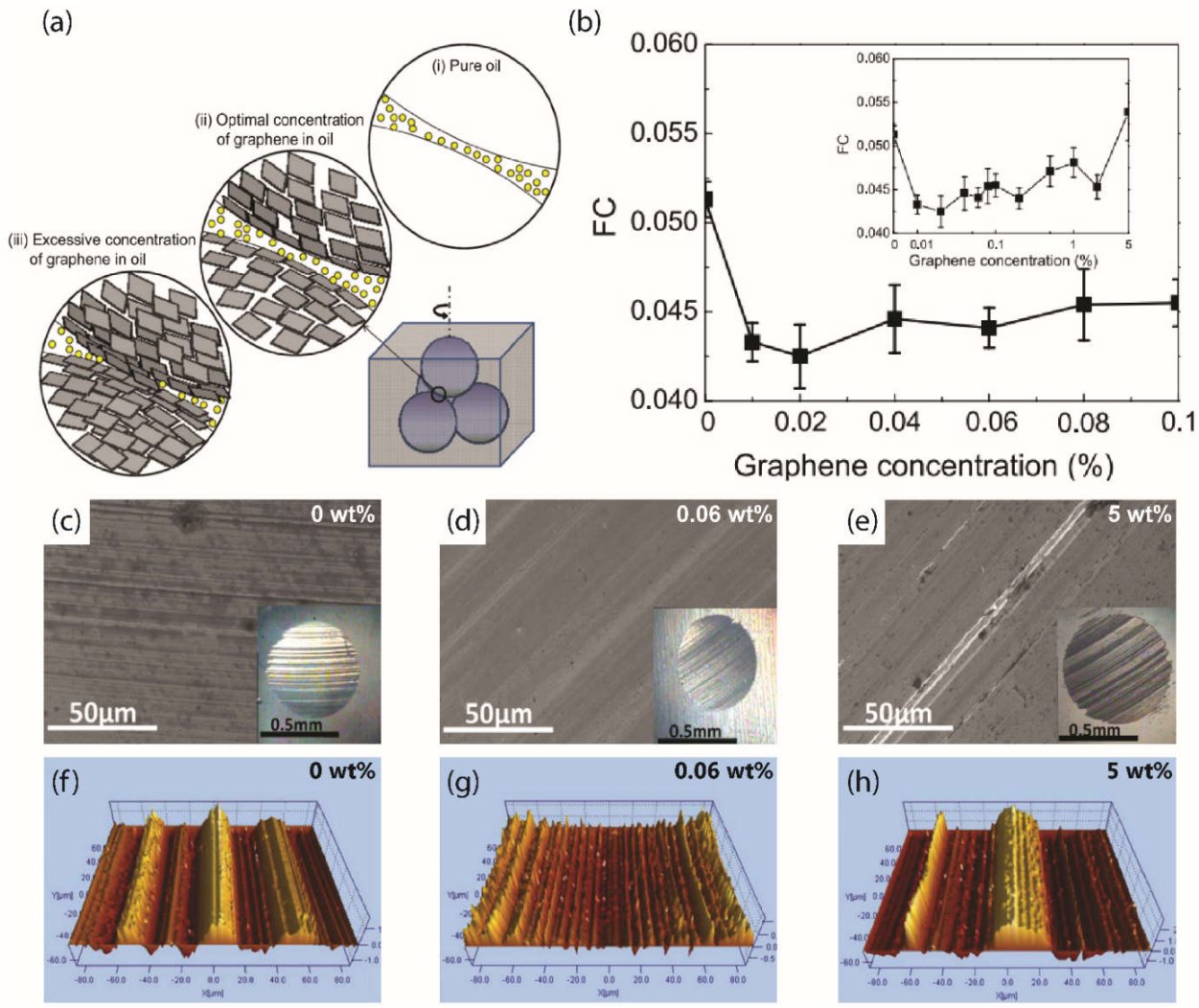

Figure 1.4.3 Optimal concentration of functionalized graphene in oil for friction and wear reduction. (a) The schematic graph of four-ball friction test with the lubricant oil modified with various concentrated graphene. (b) The performance of the friction tests varied at a wide range of concentrations of graphene. (c-h) The wear scars of the balls correspond to the graphene's concentration of 0 wt%, 0.06 wt% and 5 wt%.

In addition, Zin, V et, al. applied carbon nano-horn as the lubricant additive in the Poly-Alkylene Glycol (PAG)[54]. And this specific nano-horn shaped material could transform into

the nano-star structure, which could maintain a very stable dispersion in PAG oil without any surfactant or chemical modification. The reason of the good dispersibility in oil might be similar to the crumpled graphene balls: nano-horn particles' dahlia structure could prevent them from aggregation. At the optimum concentration of 0.2 wt%, the carbon nanohorn dispersion outperforms the pure PAG oil by 18% and 75% for friction and wear reduction.

All in all, various types of dispersion methods we introduced here have been developed to improve graphene's stability in the lubricant medium. And below is a more comprehensive list summarizing the up-to-date methods to make lubricant stably contain graphene as an additive.

Table 1.4.1 Various dispersion methods of graphene additive

Approaches	Methods	Base lubricant
Surfactant/ chemical modification	Oleic acid	Ploy-Alpha-olefin(PAO) oil[55]; 350SN oil[4];
	Alkyne-functionalization (Octadecylamine ; alkyl imidazolium ionic liquids)	10W-40 commercial oil[50]; hexadecane [56]; Group II 500N petroleum oil [57]; Ionic liquids[58-59]
	Reduction of graphite oxide by KOH	PAO oil [60]
	Amino-terminated block copolymer	Deionized(DI) water [61]; Polyethylene glycol [61]
	Sorbitol monooleate (span-80)	Paraffin oil; PAO Oil[62-63]
	Poly isobutylene succinic imide	Linear alkyl benzene[51]; API Gr I and II lube oils[51]
	Triton X-100	DI water[64]
	Sodium dodecyl sulfate	DI water[65]

Non-surfactant	Transform	Folding graphene naonosheets into crumpled balls	PAO4 oil[66]
		Single graphene wrapped individually to form nanohorns and then connected in the stars-like shape	Poly-alkylene glycol oil[54, 67]
	Mechanical stirring force		Esterified bio-oil[68-69]; polyalkylene glycol[70]; Perfluoropolyether[68]; engine oil[52]; mineral oil[62]

The synergy effect of graphene and other materials as lubricant additives

Not only limited in functioning as the only component for friction and wear reduction, graphene could also be mixed with other functional materials which will cause the synergy effect to further improve the lubrication performance. Those mixture materials could also be applied as a surface coating, solid lubricant additive and liquid lubricant additive. Representative research works will be briefly introduced below to illustrate the idea of the synergy effects and a more comprehensive summary of up-to-date researches of graphene-based mixture materials is listed in the table. 4.

For the surface coating, Pu, J et, al. [71] could use the multistep self-assembly method to make a hybrid graphene – C60 film onto the silicon surface: graphene was deposited on the silicon substrate and C60 was further chemisorbed on to the graphene surface. And AFM was used to test and compare the friction reduction performance of this hybrid film at the nanoscale with other samples including the graphene film on silicon and C60 film on the silicon. It turns

out that the hybrid film of graphene and C60 has the best lubrication performance, which is largely due to the synergy effect between the graphene and C60: the C60 could reduce the friction due to its ball bearing effect because of its tiny ball shape. And graphene could further deploy its load carrying and wear resistance functions. The combination of graphene and C60 perform better than the individual material. Similarly, at the macroscale, Berman, D et, al. [72] discovered the superlubricity by applying graphene and nanodiamond particle together. That is because the graphene layer will be scrolled during the sliding and it will wrap the nanodiamond particle. The coated particle will not only deploy its ball bearings effect, but enhance its mechanical strength due to the graphene coverage. And the friction reduction of both materials outperforms the individual material under the same experiment condition.

Self-lubricated composite could also apply the graphene based mixture to further improve the lubrication performance. One example is the work done by Yan, Z et al.[73]: They mixed both the multilayer graphene and Ti3SiC2 into the Ni3Al metal matrix. The new composite containing both materials has better wear and friction reduction than the composite with the only graphene or Ti3SiC2 individually. The synergy of graphene and Ti3SiC2 not only increase the materials hardness which results in an improved wear reduction, but also further expand the appropriate working temperature range by combining graphene's lower temperature range and Ti3SiC2's higher temperature range.

Besides the solid lubricant, graphene could also have cooperative effect with other particle materials as lubricant additives. Bai, G et, al. came up with the idea of making the hybrid

mixture of CeO2 nanoparticle and graphene nanosheets to synergize the functionality of both nanoparticle and nanosheets[74-75] in lubricant oil. The graphene nanosheets provide a template for the growth and attachment of uniform distributed nanoparticles, and those nanoparticles on the nanosheets prevent the aggregation of graphene nanosheets as spacers. This composite material has much better dispersion in lubricant oil than the pristine graphene. The combination of CeO2 nanoparticle and graphene nanosheets effectively prevent the graphene stacking and CeO2 particle aggregation. As the polishing particles, CeO2 also could increase the hardness of the mixtures and have the ball bearing effect, which enable the mixtures to sustain the higher shear force. Therefore, its tribological properties get significant improvement. The friction and wear reduction of the lubricant oil dispersion of these similar composite materials outperform all the other related groups in comparison.

Table 1.4.2 The synergy effects of materials containing graphene

Applications		Materials	Synergy
Surface coating	Nano	Graphene–C60 hybrid films[71]	Graphene deploy load-carrying and wear resistant function, C60 reduce the friction due to its ball bearing[71]
	Macro	Graphene nanosheets (GNS) combined with nanodiamond[76], ionic liquids (IL)[77], diamond-like carbon (DLC) / ionic liquid[72], Cu/WC[78] respectively	Nanodiamond has ball bearing effect and it scrolls up the GNS as a wrap-up coating, further improve its mechanical strength[76]; lubrication is fulfilled by GNS's load carrying phase and IL's lubrication function[77]; DLC film has load bearing effect and friction

			reduction is fulfilled by IL and GNS[72], WC particles increase the hardness of the lubricating coating containing GNS and make the coating not easily split[78]
Composites	Metal matrix	Cu-carbon fibers-reduced graphene oxide (rGO)[79]; Ag-WC-Graphene (G) [80]; Ni_3Al-Ti_3SiC_2-G[73]; TiAl-Ag-G[81-82]; TiAl-MoS_2 nanospheres-G[83];	The filler material reinforces the composite and improve the hardness and strength for wear reduction[79]; Improve the load bearing effect for friction reduction[80, 83]; Form a lubrication film to reduce the friction and wear[80-81, 83-84]; Provide a skeleton for other filler materials[82]; Expand lubrication temperature ranges[73];
	Ceramic matrix	Al_2O_3-carbon nanotubes-G[85]	Graphene forms into tribofilm and CNT improve the fracture toughness[85]
	Polymer matrix	Polytetrafluoretyhylene (PTFE) -nomex -Mo_2C-G[86]; bismaleimide –MoS_2-rGO[87]; bismaleimide-Fe_3O_4-G[88]; poly(phenol-formaldehyde resin)-carbon fibers-Fe_3O_4-G[89]; nylon 66-polytetrafluoroethylene-G[90]; polycaprolactam-solid paraffin-G[91]; polymide-carbon nanotubes-G[92]; epoxy-ZnS-rGO[93]	Filler materials provide high load-carrying capacity[86, 92]; Form a lubrication film to suppress the friction and wear[86, 88, 90, 92-93]; the toughness of composite is enhanced by filler[87, 91]; Nanoparticle act as spacers to prevent graphene from restacking[88-89, 93]; PTFE is only good at friction reduction, graphene addition supply the wear reduction function[90]; melted paraffin have lubrication effect after frictional heat absorption[91];
Lubricant oils addition	Graphene nanosheets with CeO_2 [74], ZrO_2[75], Ag[94], Cu[95], carbon quantum		Nanoparticles act as spacers to prevent graphene from restacking[74-75, 94-96]; Nanoparticles have load-bearing property and could increase the

	dots[96], WS_2[97], polyaniline nanotubes[95] respectively	composite hardness with graphene[74-75, 95]; Enhanced deposition of nanoparticles as a film for surface protection and easy sliding interface[94-95, 97];

1.5 Conclusion and outlook

The recent developments of graphene's tribological application as lubricant or lubricant additive at nanoscale and macroscale level are highlighted. The nanoscale research of graphene indicates its huge tribological potential for macroscopic lubrication application and it could be applied to all the four major lubrication types including surface treatment, solid lubricant additive, liquid lubricant additive and grease additive depends on different lubrication requirements.

Chapter 2

Crumpled graphene balls' aggregation resistance

（Material in this chapter is reproduced in part with permission from reference 121, "Compression and Aggregation-Resistant Particles of Crumpled Soft Sheets" by Luo, J. Y.; Jang, H. D.; Sun, T.; Xiao, L.; He, Z.; Katsoulidis, A. P.; Kanatzidis, M. G.; Gibson, J. M.; Huang, J. X. Compression and Aggregation-Resistant Particles of Crumpled Soft Sheets. Acs Nano 2011, 5, 8943-8949）

2.1 Introduction

The 2D nanosheet materials like graphene can easily form aggregations due to the strong Van der Waals force. Especially for those material processing involving potential compression and stacking, it would be hard to efficiently separate the aggregated sheets for following material processing. Numerous methods have been developed to solve this problem, including tailoring the solvent-graphene interactions or employing dispersing agents. However, once the dispersion of nanosheets dry out, the sheets would aggregate and still could not re-disperse themselves into new solvent anymore. And it is crucial to develop a type of nanoparticle which could be well self-dispersed in solvent without any surfactant

or chemical functionalization. Here, our group developed an aerosol-assisted capillary compression process to transfer graphene oxide nanosheets into crumpled graphene nanoparticles. This nanoparticle material has excellent compression and aggregation-resistant properties, which was further validated in the comparison test with graphene nanosheets sample. Its aggregation resistant property was enabled by the plastically deformed ridges due to the pi-pi stacking of those ridges. Those ridges further result into lower contact surface of this nanoparticle and strengthen its stiffness upon the compression due to the strength hardening effect.

2.2 Experiments

Synthesis

GO was prepared by a modified Hummers' method[98] as reported elsewhere[99]. GO dispersions in water with various concentrations were nebulized by an ultrasonic atomizer (1.7 MHz, UN-511, Alfesa Pharm Co., Japan) to form aerosol droplets, which were carried by N2 gas at 1 L/min to fly through a horizontal tube furnace (tube diameter = 1 in.) preheated at a desired temperature. The power of the nebulizer was set at the same level for all experiments. A Teflon filter was placed at the exhaust[100] to collect the crumpled particles.

Material processing

Solution processing was typically done by first dispersing the powder samples in water or methanol by gentle shaking or sonication, and then filtration to collect the powders. The particles can also disperse in many other solvents known to be poor for dispersing GO or r-GO such as acetone, toluene, and cyclohexane. Slow heating was done in a N2 atmosphere by first heating the GO samples from room temperature to 400 °C at a rate of 3 °C/min, and holding them at 400 °C for another 2 h. Thermal shock[101] was done by rapidly inserting the samples into a hot tube furnace at 400 °C to trigger the explosive exfoliation, and heating them for another 5 min. Microwave reduction[102] of GO was done by irradiating the samples in a commercial microwave oven at 1250 W for 1 min. Hydrazine reduction was done by fluxing GO in hydrazine at 80 °C for 12 h. Mechanical compression was done by pelletizing the dried samples in a die with a diameter of either 3 or 20 mm.

Characterization

SEM images were taken on a FEI NOVA 600 SEM microscope. The size distributions of crumpled particles were obtained by counting 100 particles of each sample in SEM images. To study the morphological evolution of GO, Si wafers were placed along the aerosol flying pathway as indicated by positions 1–4 in Figure 1, collecting samples before and during different stages of heating.

2.3 Results and Discussion

Crumpled Particles from Rapidly Evaporating Aerosol Droplets

The aerosol process is made by three parts: the ultrasonic nebulizer, pre- heated tuber furnace and collecting filter as shown in Figure 2.3.1 A. For the manufacturing process: the graphene oxide nanosheets dispersion was added into the nebulizer and was further generated into microdroplets containing graphene oxide nanosheets; the flowing carrier gas further carried the microdroplets through the pre-heated tube furnace; Inside the tube furnace, the microdroplet started to evaporate and shrink. The capillary force of microdroplet started to compress the nanosheets and gradually turned them into a crumpled nanoparticle. And filter will collect all the crumpled nanoparticles. To further validate the transformation path of crumpled graphene, the silicon wafers were placed inside the quartz tube to collect the nanoparticles made from spot 1-4 and was further inspected under SEM, as shown in Figure 2.3.1 B. From spot 1-3, it was just a pile of graphene oxide sheets and it eventually formed into crumpled graphene nanoparticle at spot 4.

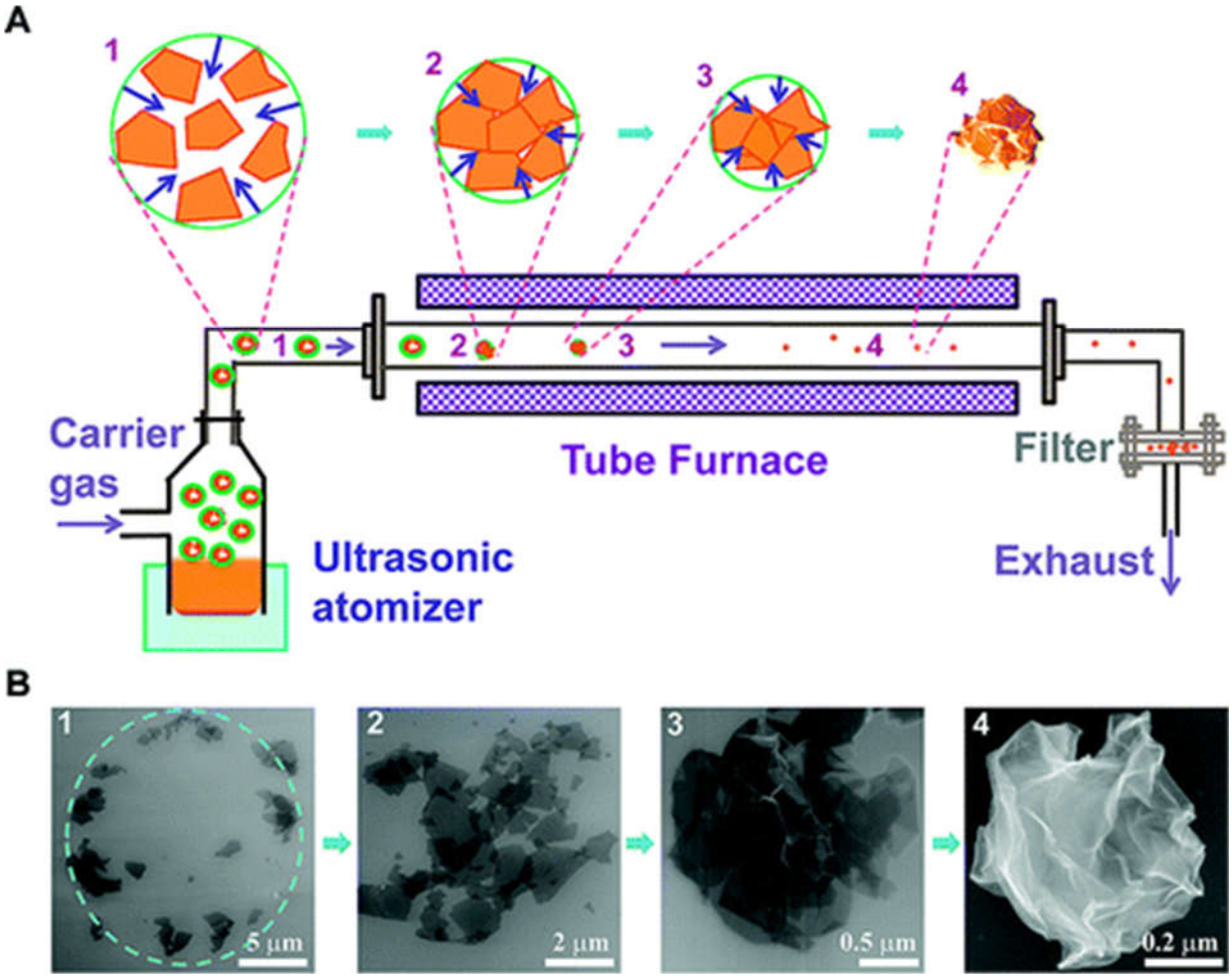

Figure 2.3.1 Particles of crumpled GO sheets by rapid isotropic compression in evaporating aerosol droplets. (a) Schematic drawings illustrating the experimental setup and the evaporation-induced crumpling process. Aerosol droplets containing GO sheets were nebulized and rapidly evaporated by passing through a preheated tube furnace. (b) SEM images of four samples collected along the flying pathway from spots 1 to 4 showing the typical morphologies of deposited GO evolving from (b1) sparse sheets in a "coffee-ring" pattern, (b2) clustered and tiled sheets, (b3) aggregated sheets with extensive wrinkles, to (b4) the final 3D crumpled, ball-like particle.

To further control the size of crumpled graphene balls, there are two methods: either control the size of micro-droplets or tune the concentration of graphene oxide nanosheets in solvent. The size of crumpled graphene balls is directly related to the layer numbers of graphene oxide nanosheets in a single microdroplet. The bigger crumpled particle contains more layers of graphene oxide sheets, the smaller particle has less layers. In order to get a better understanding of the crumpled particle size, different sizes of crumpled graphene nanoparticles were made based on varied concentration of graphene oxide sheets in solvent as shown in Figure 2.3.2. Three different concentrations were used (0.2 mg/ml, 1 mg/ml, 5 mg/ml). And with the same operation procedure, three different sizes of corresponding crumpled graphene nanoparticles were made at 200nm, 400nm and 800nm in diameter.

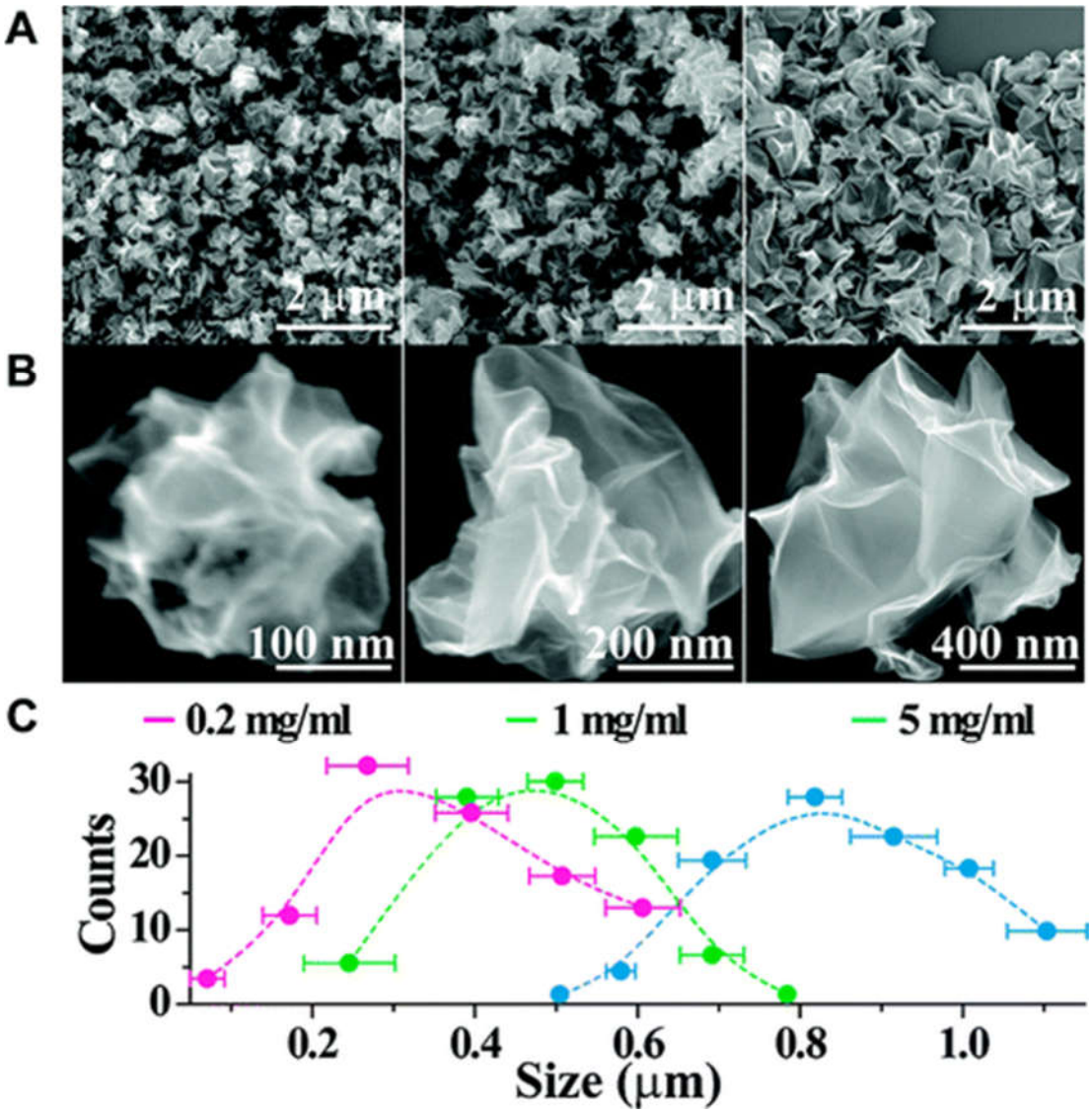

Figure 2.3.3 The size of the crumpled particles and the degree of crumpling can be tuned by the concentration of GO in the aerosol droplets as shown in the (a) low magnification overview and (b) representative high magnification single particle SEM images. (c) The average size of the particles decreased from around 800 or 500 nm to 250 nm when the GO concentration was reduced from 5 or 1 mg/mL to 0.2 mg/mL, respectively. The dotted lines are drawn as a guide to the eye.

Because crumpled graphene nanoparticles have plastically deformed ridges, it could further prevent aggregation. In Figure 2.3.3, to further test the aggregation resistance performance, the reduced graphene oxide sheets were compressed into a pellet to compare with crumpled graphene nanoparticles pellets under the compression pressure at 55 MPa. To test the aggregation resistance, those pellets were re-dispersed into the solvent. However, the pellet of reduced graphene oxide nanosheets could not re-disperse into the solvent. They would form into aggregates, and the pellet of crumpled graphene nanoparticles could easily be re-dispersed into the solvent with gentle shakes by hands. After re-shaking the solution, a few solution drops were taken and observed under SEM microscope when it was dried up. From the SEM pics in Figure 2.3.3 E and G, the crumpled graphene balls were distributed slatternly on the substrate without any signs of aggregation. And the reduced graphene oxide has formed into aggregates already.

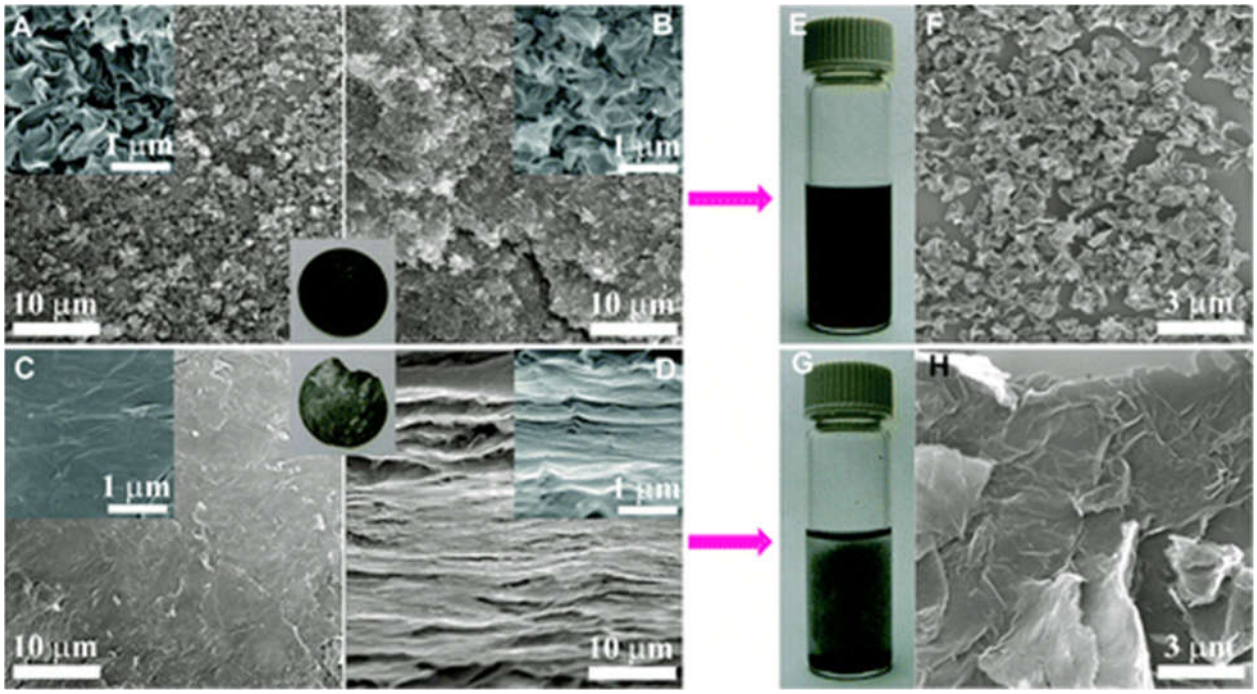

Figure 2.3.3 Compressed pellet of crumpled r-GO particles (inset of panels a and b) has rough and isotropic microstructures as shown in the SEM images taken at both (a) the surface and (b) cross section due to their near-spherical, pointy shape. In contrast, flat r-GO sheets restack along the compressing direction, resulting in a highly anisotropic pellet (inset of c, d) with (c) very smooth surface and (d) lamellar cross section. (e,f) The pellet of the crumpled particles can be readily dispersed by gentle hand-shaking after being compressed at 55 MPa. (g,h) However, the pellet of regular r-GO sheets cannot be redispersed due to extensive aggregation.

2.4 Conclusion

Particles of crumpled GO and r-GO (i.e., chemically modified graphene) sheets have been obtained by capillary compression in rapidly evaporating aerosol droplets of GO. The average size of the crumpled, near-spherical particles is in the sub micrometer range and can be tuned by the concentration of the starting GO concentration. As is with a crumpled paper ball, the crumpled graphene is also stabilized by plastically deformed ridges, and thus does not unfold or collapse during various types of solution processing or chemical or heating treatments. The crumpled particles exhibit strain-hardening behaviors, thus making them remarkably resistant to aggregation in both solution and dried states. They remain largely intact and dispersible after chemical treatments, wet processing, annealing, and even pelletizing at high pressure. Compared to the regular, flat sheets processed under the same conditions, the crumpled particles consistently have higher surface areas. In addition, the surface area of crumpled particles is more robust, and much less sensitive to the material processing history. The dimensional transition associated with the mechanical deformation effectively solves the aggregation problem of graphene without the need for any modification to material composition or surface properties. Therefore, such a crumpled form of graphene should benefit applications relying on the high surface area of graphene.

Chapter 3

A Continuous Method of Making Crumpled Graphene Balls

3.1 Introduction

Crumpled graphene nanoparticles have broad potential applications in energy storage such as capsulation materials of silicon nanoparticles to further improve their performance significantly. In the general manufacturing route, an intermediate material called graphene oxide nanosheet is necessary to make crumpled graphene nanoparticle. However, this intermediate material is made through a complex chemical and physical synthesis process, which involves a significant amount of energy, corrosive chemicals and time. It would be desirable if the crumpled graphene balls could be made directly from the raw graphite powder without those intermediate steps mentioned above.

Previously, researchers have already investigated the possibility of using sonication to exfoliate graphite flakes into thin layers of graphene sheets without using chemical exfoliation method[103]. They demonstrated exfoliation of bulk Transition Metal Dichalcogenide (TMD) crystals into mono- and few- layer nanosheets in the common solvents by exposing the layered material to ultrasonic waves in the solvent[104-106]. The cavitation bubbles that collapsed into jets with high energy were generated from the

ultrasonic waves, and therefore exfoliated the layered nanosheets. They were able to exfoliate various 2D materials including graphene, h-BN, TMDs and TMOs by using this ultrasonic technique in common solvents such as N-Methyl-2-Pyrrolidone (NMP).

Inspired by previous exfoliation work, here we developed a continuous manufacturing process of making crumpled graphene balls directly from raw graphite particles, which is the modification and improvement of the previous manufacturing process of making crumpled graphene balls. This improved method makes the manufacturing process of crumpled graphene nanoparticles more efficient and green by directly nebulizing graphite powders instead of graphene oxide nanosheets without any materials pre-processing steps. Replacing graphene oxide sheets with raw graphite powders as starting materials eliminates the intermediate process of exfoliating graphite into graphene, which generally involves a huge amount of time (usually one-two weeks), corrosive chemicals and energy.

In this process, graphite powders are exfoliated into graphene nanosheets during nebulization. The microdroplets generated from nebulization only carry the lighter particles such as exfoliated graphene nanosheets materials through the pre-heated tube furnace by the nitrogen gas flow. The gas flow is unable to carry the heavier graphite particle due to the natural gravity subsidence. Only those thinner sheets carried in the liquid microdroplets go through the entire process, and the crumpled graphene nanoparticles are collected at the end of the tube based on this gravitational–assistant selection process.

3.2 Experiment

Material processing

Different from the previous method of making crumpled graphene, this continuous method directly used raw graphite powders instead of graphene oxide. Graphite powders (purchased from Asbury Carbon, mesh size 100) were directly dispersed in water at a concentration of 4 mg/ml, and the exact same aerosol process was utilized for the continuous manufacturing of crumpled graphene balls.

Aerosol process

Graphite dispersion in water was added into the nebulizer., which is the same one used in the previous work. The nebulizer intensity was tuned at its maximum level, which was five times the intensity for nebulization of r-GO. A pre-heated tube furnace was attached to the nebulizer to further dry up the liquid micro-droplets, and a filter was used to collect the final products.

Characterization

Similar to the process mentioned in Chapter 2, the crumpled particles were formed due to the different heating stages of the oven. To study the morphological evolution of crumpled particles formed from graphite powders, Si wafers were placed along the aerosol flying pathway as indicated by positions 1–3 in Figure 3.1, which collected samples before and

during different stages of heating. The microstructures of collected samples were further observed under SEM (JOEL SU 8030).

3.3 Results and discussion

As shown in Figure 3.3.1, graphite dispersion was added into the nebulizer, and the tube furnace was heated at 400 °C. After nebulizer was turned on, it started to exfoliate the graphite powders into thinner graphene sheets. At the same time, nebulization generated micro-droplets containing the lighter graphene sheets. The nitrogen gas flow carried the nebulized water droplets through the pre-heated tube furnace, and the droplets quickly evaporated under high temperature. The capillary force on the surface of droplets further compressed the inside nanosheets isotropically into a crumpled-ball structure. Eventually, all the nanoparticles were collected at the end of the tube by a filter. Even though our group previously used a similar experimental setup, this continuous method has different principles of making crumpled graphene balls comparing to the previous aerosol method.

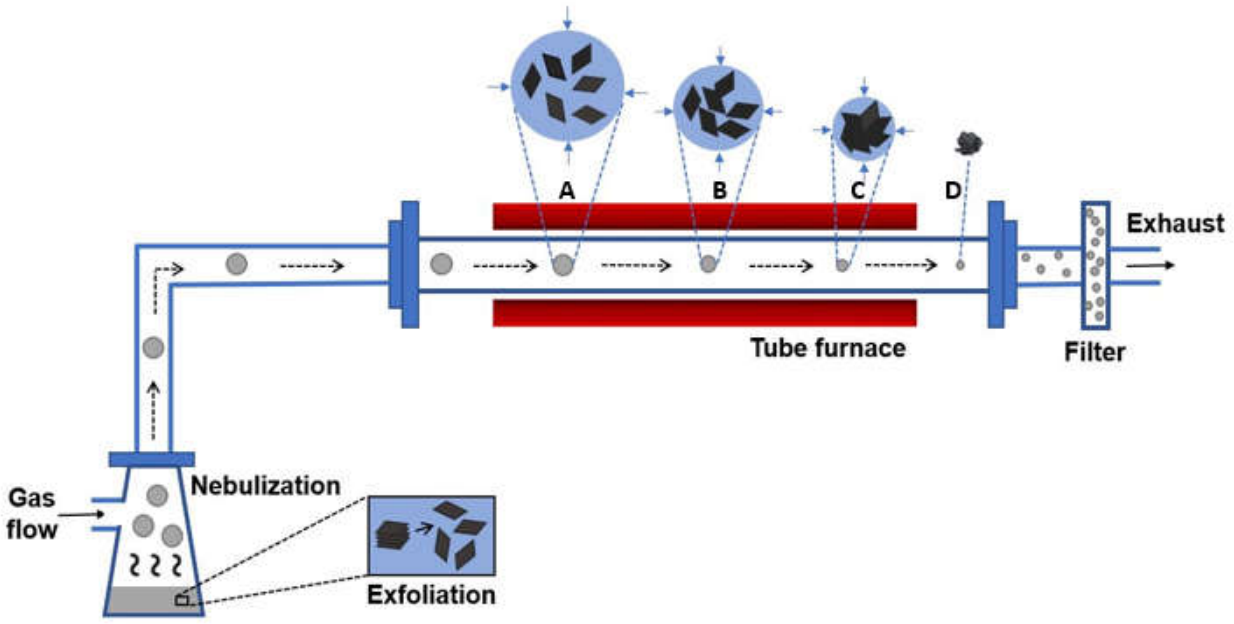

Figure 3.3.1 Schematic drawings illustrating the experimental setup and the evaporation-induced crumpling process. Aerosol droplets containing exfoliated graphite sheets were nebulized and rapidly evaporated by passing through a preheated tube furnace. During this process, the nebulization had the exfoliation functionality to further exfoliate big graphite flakes into thinner graphene sheets. And samples are collected at different spots inside the tube (from A to B)

Within the nebulization, graphite powders in the dispersion were further exfoliated, which resulted in a dispersion containing different sizes of nanoparticles including thicker graphite flakes and thinner exfoliated graphene sheets. At the same time, it generated micro-droplets containing the dispersed materials during the nebulization. Only those droplets containing flakes with relatively smaller sizes and lower weights or those containing exfoliated sheets could be delivered into the pre-heated tube with the nitrogen carrier gas.

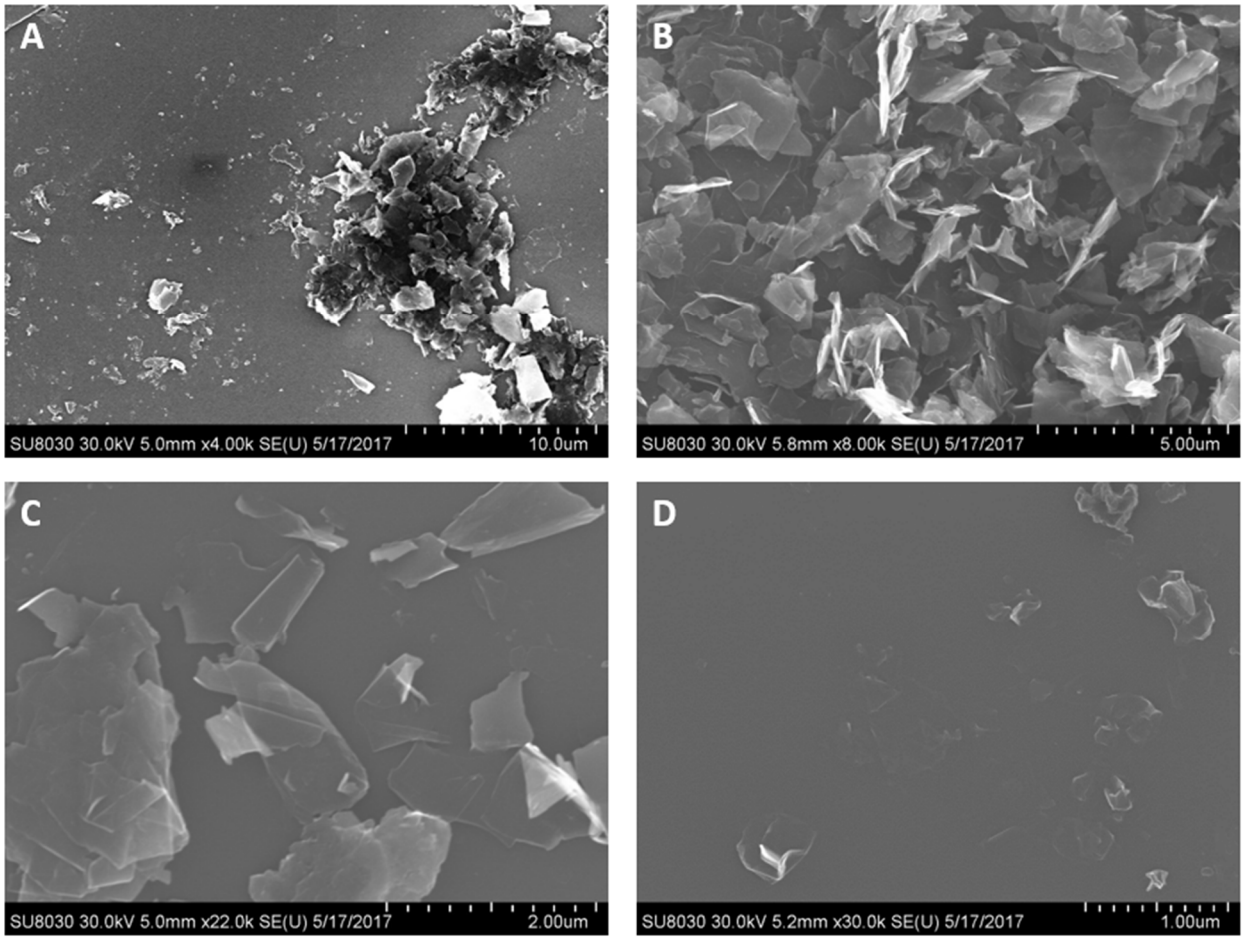

Figure 3.3.2 The SEM images of the products collected at different locations inside of the pre-heated tube furnace along the flying pathway from the spot A (the beginning) to the spot D (the end). (a) Aggregated chucks of graphite flakes are found at the spot A, and (b, c) there are relatively small and thin sheets deposited on the substrates at spots B and C. (d) Eventually the crumpled particles are collected at the very end of the flying pathway - spot D.

To further validate the idea of the gravitational-assisted selection process, the products made at different positions inside the pre-heated tube were collected on the silicon wafers.

SEM images in Figure 3.3.2. correspond to different spots in the pre-heated quartz tube along the carrier gas flying path. (A) is at the beginning of the glass tube and (D) is closed to the end of the tube. Figure 3.3.2 (a) show lots of bigger chunks and aggregates deposited on the substrate, which might be the smaller sized graphite particles. A trend can be observed from Figures 3.3.2a to d, indicating the deposited particles become smaller and less packed as they travel through the tube. Comparing Figure 3.3.2 (c) with (d), the particles in (c) still have the sheet morphology probably because the droplet in spot C was still wet and did not form into a crumpled particle by plastic deformation. Also, the size and weight of the particle at spot C should still be larger than those of the sheets at spot D. Figure 3.3.2 (d) shows that the microdroplets contain smaller nanosheets and they can be carried by gas and go through the entire pre-heated tube. Water in the droplets is fully evaporated, and the capillary force of the droplet crumples the sheets into a crumpled structure. However, for those larger sized sheets, they were not able to travel through long flying paths and sedimented inside the tube or even didn't enter the tube at all.

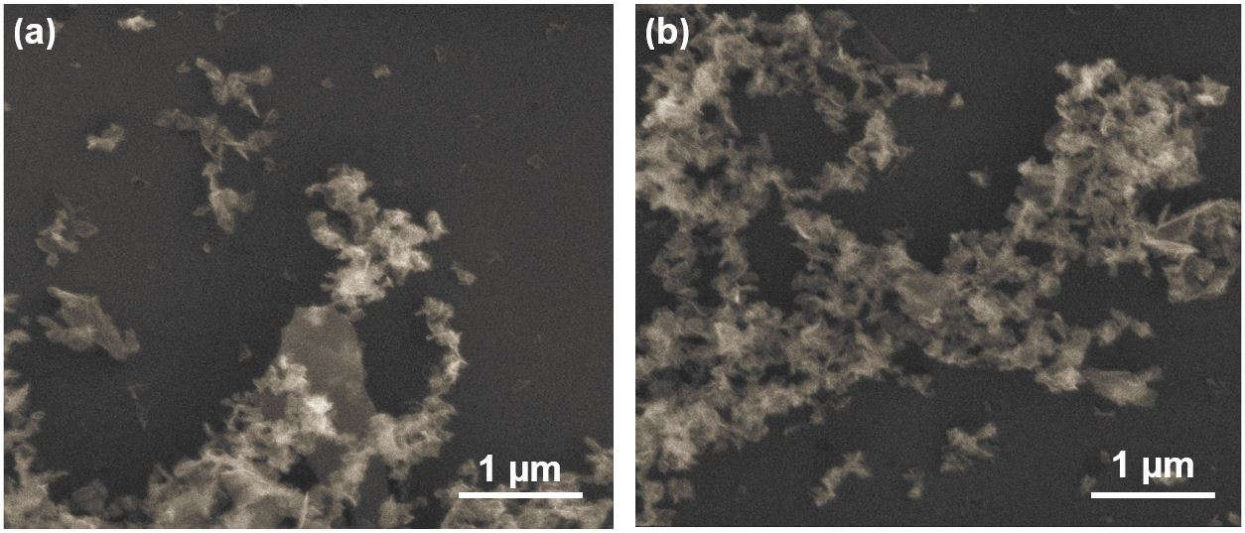

Figure 3.3.3 The SEM images of the final products collected from the filter papers. (a) and (b) both indicate that the final products were crumpled graphene nanoparticles, and the sizes of the particles were approximately around 100-200 nm in diameter.

The products collected on the filter papers were observed under SEM as shown in Figure 3.3.3. The resembled particles have already been crumpled. They have a smaller particle size compared with the crumpled particles made from the chemical exfoliated graphene oxide. This might result from two reasons: 1. Difference between the exfoliation quality: only the smaller sheets were able to be exfoliated, and a sonicator of high power is necessary in order to get more larger sheets. 2. The microdroplet containing both smaller sheets and bigger sheets or flakes could not make it to the end of the flying path. In order to improve the quality, powerful pre-sonication should be applied, and an additional step is needed to sediment large sheets or flakes, followed by taking the supernatant containing only thinner and lighter exfoliated sheets.

3.4 Conclusion

A continuous fabrication method is utilized to improve the efficiency/economy of the manufacturing process for crumpled graphene nanoparticles by modifying an operational condition – replacing the graphene oxide nanosheets with their raw material: graphite. Chemically exfoliated graphene oxide sheets were used in the original process. However, the preparation process of graphene oxide nanosheets consumes a huge amount of corrosive chemicals, water and energy. In this modified manufacturing process, nebulization mechanically exfoliates graphite flakes into thinner graphene sheets. The microdroplets can carry lighter particles such as graphene sheets but not the bigger and heavier graphite particles which are likely to subside. Eventually, only the crumpled graphene nanoparticles will be collected at the end of the tube.

However, compared to the chemical exfoliated nanosheets, the production rate of monolayer nanosheets was at most a few tens of percent of the original raw material. And there are still improvements to be made on this method. For example, try to use a more powerful sonicator for efficient mechanical exfoliation, and use a longer quartz tube to fulfill the gravitational selection process with higher purity.

Chapter 4

Crumpled graphene's application for lubrication

（Material in this chapter is reproduced in part with permission from reference 66, "Self-dispersed crumpled graphene balls in oil for friction and wear reduction" by Dou, X.; Koltonow, A. R.; He, X. L.; Jang, H. D.; Wang, Q.; Chung, Y. W.; Huang, J. X. Proceedings of the National Academy of Sciences of the United States of America 2016, 113, 1528-1533）

4.1 Introduction

Lubricants reduce friction between contacting surfaces and thus increase the energy efficiency of engines and other machines. They can also reduce wear, thereby extending the life of tribological components. Many types of ultrafine particles have been studied as lubricant additives[107-108] because they can enter contact regions between sliding surfaces and protect them from direct mechanical contact [48, 108]. This makes ultrafine particles effective for reducing friction and wear in the boundary regime, such as during startup or low-speed operation of an engine, when the lubricant film at these contacts is too thin to prevent direct metal-metal contact. Further, because of the high shear stresses and sometimes high local temperatures at these contacts, molecular additives can be rubbed off, decomposed, or simply fail to provide a sufficiently thick coverage for friction reduction and

wear protection. Therefore, ultrafine particles are appealing by virtue of their size and their chemical and thermal stability under tribological conditions. However, it is challenging to disperse ultrafine particles in lubricating oils. Typically, this requires surface functionalization with surfactant-like substances, which themselves are prone to degradation under tribological conditions, leading to unstable lubrication properties. Therefore, it would be highly desirable if ultrafine particle additives can remain self-disperse in lubricant oil without the use of ligands.

This work was inspired by the analogy with crumpled paper mentioned previously. A crumpled piece of paper in the shape of a ball has a rough surface texture, which reduces the area of contact when placed on top of a flat sheet of paper or in an assembly of crumpled paper balls, resulting in minimal adhesion. Because of the multiple folding, crumpled paper balls become strain-hardened (and thus stiffer) under mechanical stress, so they can largely maintain their shape and shape-induced nonstick properties[109-111]. One might expect, then, that ultrafine particles in the shape of crumpled paper balls could be well dispersed in oil and have superior lubrication properties. Such miniaturized crumpled structures were first realized with graphene-based materials using an aerosol capillary compression approach[110]. Just as how a crumpled paper ball is made by isotropically compressing a sheet of paper with one's hands, flat graphene-based sheets suspended in nebulized aerosol droplets are isotropically compressed during solvent evaporation, leading to the final crumpled ball morphology. The resultant sub-micron-sized crumpled graphene balls indeed have properties analogous to those of crumpled paper, including strain hardening and

aggregation resistance. The morphology of crumpled graphene balls is highly stable in the solid state and when dispersed in liquids. They do not unfold or collapse even after heating or pelletizing. Since they consistently do not form intimate contact with each other, their inter-particle van der Waals attraction is so weak that they can be individually dispersed in nearly any solvent, including lubricant oils, without the need for any chemical functionalization. In spite of their compact appearance, crumpled graphene balls have a great deal of free volume and solvent-accessible surface area inside, making them an effective absorber of oil, which could be released upon compression, ensuring uninterrupted wetting of the contact area. These properties should make them highly desirable for tribological applications. In this work, we demonstrate that crumpled graphene ball is indeed a superior friction modifier when compared with other carbon additives such as graphite powders, chemically exfoliated graphene sheets, and carbon black[50, 112-118]. Remarkably, base oil with just 0.01 wt. % to 0.1 wt. % of crumpled graphene balls is more effective in friction and wear reduction than a fully formulated commercial lubricant.

4.2 Experiments

Preparation of tested materials

Graphite was purchased from Sigma-Aldrich. Carbon black was purchased from VWR. Lubricant PAO4 base oil was purchased from Exxon-Mobil. The steel disks for friction tests were machined from an E52100 steel bar, and the disk surfaces were machine-polished to a mirror finish with surface roughness Ra of around 5 nm measured by an interferometer. The

steel balls, 3/8" in diameter and made of M50 steel, were purchased from McMaster-Carr and used as received. GO was made by a modified Hummers method [98] described previously [119]. Crumpled graphene balls have been obtained by capillary compression in rapidly heated evaporating aerosol droplets of graphene oxide sheets. An ultrasonic atomizer (1.7 Mhz, UN-511 Alfesa Pharm Co., Japan) was used to generate aerosol droplets of aqueous graphene oxide solution at a concentration of 1.5 mg/mL. Nitrogen flow was used to carry those droplets through a 400ºC tube furnace. Particles were collected at the end of the tube furnace using a Millipore Teflon filter with 200 nm pore size. Those partially reduced crumpled GO particles were further reduced at 700ºC in argon for an hour. Reduced graphene oxide (r-GO) was synthesized by hydrazine reduction of GO in water and collected by filtration based on a previous report[120].

Tribology tests

Lubricant additives (graphite, carbon black and crumpled graphene balls) were added to the PAO4 base oil (density = 0.82 g/ml) and sonicated for 30 minutes in a water-bath ultrasonic cleaner UC-32D, 125W. Due to its poor dispersibility, the filtered r-GO was tip-sonicated (150W) for 10 min before sonicating in a water bath for 20 min. Before testing, the polished 52100 steel disks and steel ball were sonicated in acetone for 5 minutes to remove any possible residual contaminants. The metal disk was then fixed tightly in the holder of the tribotester, and plastic pipettes were used to transfer 3 mL of freshly mixed lubricant solution onto the disk. The tests were conducted at a linear speed of 10 mm/s, a constant vertical force of 10 N (maximum Hertzian contact pressure ~ 1 GPa), and ambient

temperature and humidity. The experimental duration was 2000s and 4000s respectively for the 0.01 wt. % and 0.1 wt. % concentration of each carbon-based additive. Each sample was tested at least twice under identical conditions.

Characterization of wear tracks

Before each SEM observation, the metal disk was cleaned in hexane for 3 minutes to remove the residual lubricant oil and was then air-dried. SEM images were recorded using a LEO 1525 microscope. Before optical profilometry, the steel disk was further sonicated in acetone to completely remove all the debris and lubricant materials. A Zygo® NewView™ 7300 optical surface profiler was used to identify and analyze the 3D topography of the wear track. The wear volume was defined as the amount of metal removed from a single track in the course of an experiment and was estimated by numerically integrating the surface height (from optical profilometry) over the area at eight different points along the track. Wear coefficient is given by the following equation:

$$\text{Wear coefficient (K)} = \frac{\text{Wear volume } (m^3) \times \text{Surface hardness } (Pa)}{\text{Normal load } (N) \times \text{Sliding distance } (m)}$$

Vickers hardness measurements of steel disks were determined to be 575±10.4 kgf/mm^2 (~5.64 GPa) by a Struters Duramin microhardness tester. The measurements were repeated three times for each disk.

4.3 Results and Discussion

Dispersion and aggregation-resistant properties of crumpled graphene balls

The tribological performance of crumpled graphene balls was investigated in comparison to three other widely studied carbon additives: graphite platelets, reduced graphene oxide sheets (r-GO, *a.k.a.* reduced graphene oxide), and carbon black. Powders of these carbon materials (0.01-0.1 wt. %) were sonicated in the lubricant base oil (polyalphaolefins type-4, PAO4) until they were fully dispersed with no residual solids remaining. All four additives can initially disperse in the base oil right after sonication (Figure 4.3.1 a). However, agglomeration was apparent in the dispersions of graphite platelets, r-GO sheets, and carbon black powders after a few hours. After 20 hours, crumpled graphene balls were still dispersed in the oil, but the other three carbon materials were fully sedimented (Figure 4.3.1 b). The microstructures of the four carbon additives were observed with the scanning electron microscope (SEM). The sonicated graphite platelets are typically around 1-3 microns in lateral dimension and 40-60 nm in thickness (Figure 4.3.1 c). Although they disperse initially, they are prone to aggregation due to their flat, disk-like shape, which can form intimate inter-particle contact and generate strong attraction. Similarly, the r-GO sheets also tend to restack to form large chunks a few hours after sonication (Figure 4.3.1 d). The primary particles in carbon black powders are about 50 nm in diameter. They aggregate into micron-sized clusters, which can be broken down to sub-micron pieces by sonication (Figure 4.3.1 e). Carbon black powders can stay dispersed for about 5-10 hours. The dispersion of crumpled graphene balls, which are around 500 nm in diameter, is the most

stable, because their shape prevents them from forming tight stacking, hence preventing aggregation (Figure 4.3.1 f). After a few days, all the dispersed carbon additives shown in Figure 4.3.1 a and 4.3.2 b will sediment in the oil. Upon shaking, sedimented graphite platelets, r-GO sheets, and carbon black powders can re-disperse in oil; however, having already aggregated, they will precipitate again quickly. Optical microscopic observation of the shaken oil samples reveals that of the four samples, only crumpled graphene balls can be finely re-suspended, while the other three oil samples contain large, persistent micron-sized aggregates.

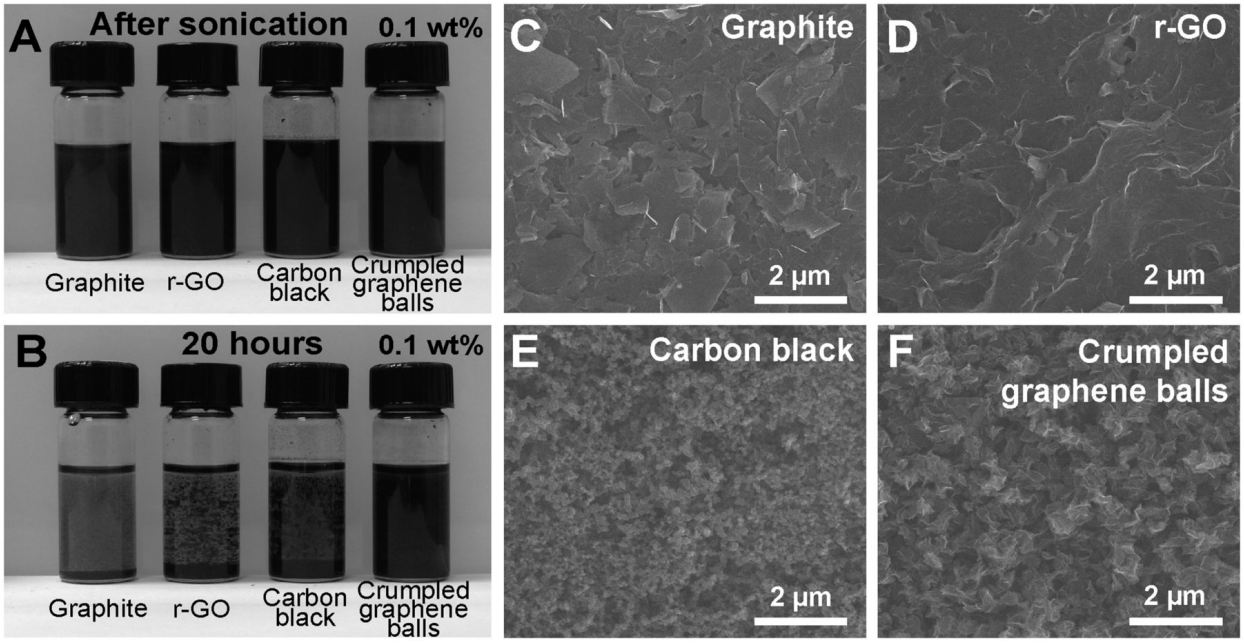

Figure 4.3.1 Dispersion properties of four carbon additives in the lubricating oil. Dispersion of four carbon additives, all at 0.1 wt %, in PAO4 (A) immediately after sonication and (B) 20 h after sonication; (C–F) SEM images of drop-casted powders of graphite, r-GO, carbon black,

and crumpled graphene balls, respectively. The crumpled graphene balls stay dispersed due to their aggregation-resistant properties. The solid content for all the dispersions is 0.1 wt %.

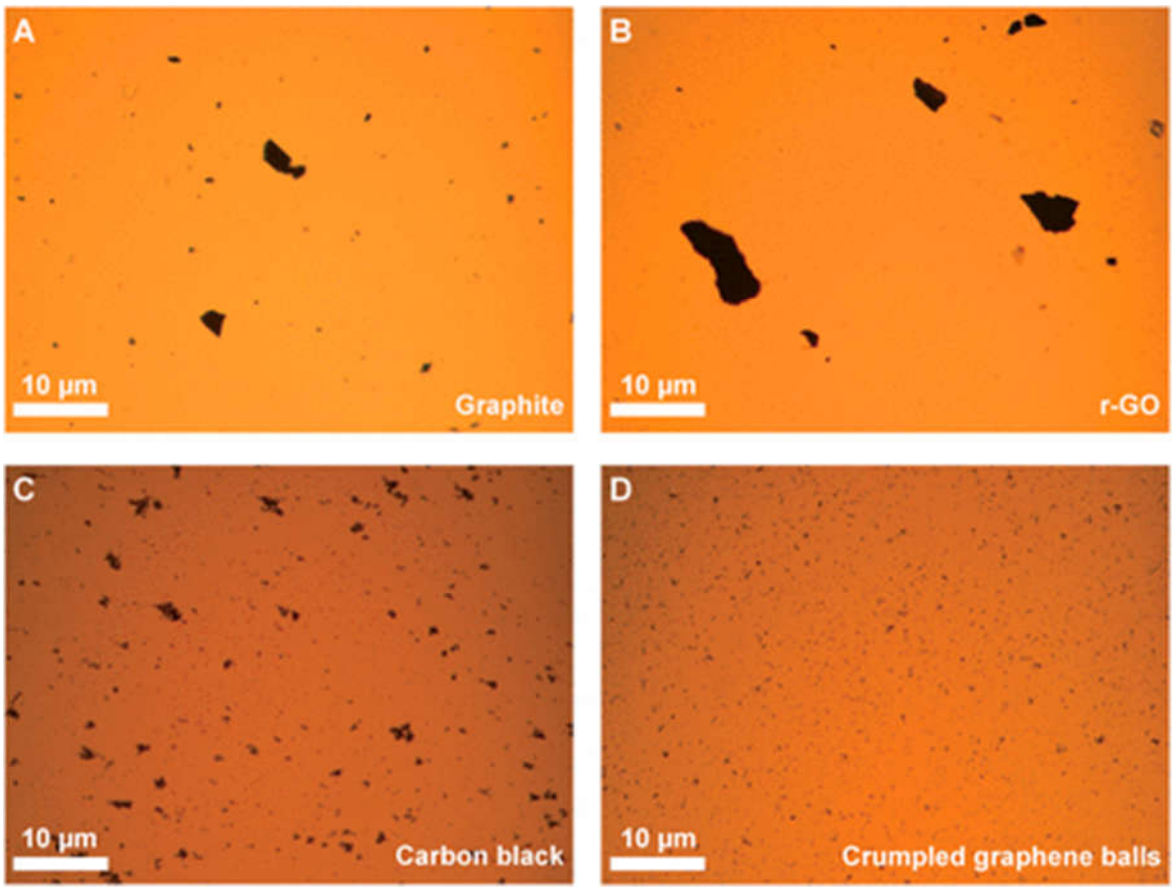

Figure 4.3.2 Optical microscopy images corresponding to the vials shown in Fig. 1A showing that (A) graphite, (B) r-GO, and (C) carbon black powders form large aggregates with uneven sizes in the PAO4 base oil, whereas (D) crumpled graphene balls are much more finely dispersed.

A pin-on-disk tribometer (Figure 4.3.3 a and Figure 4.3.3 b) was used to study the tribological properties of the carbon-based additives in PAO4 base oils [117]. The pin and the disk were

made of M50 steel ball (Ø 9.53 mm, surface roughness Ra ~ 17 nm) and E52100 steel (Ø 30 cm, Ra ~ 5 nm), respectively. In order to keep the tribological test in the boundary lubrication regime, testing parameters were chosen to ensure that the thickness of the lubricant film was smaller than the surface roughness [118]. According to the Hamrock-Dowson equation [121], this condition can be met by applying a 10 N load to the pin while the linear sliding speed of the disk relative to the pin is 10 mm/s. The maximum Hertzian contact pressure was about 1 GPa [122]. In order to test if the crumpled graphene balls can sustain this high pressure, static compression experiments were performed first by using the same pin-on-disk configuration with a 10 N load. Crumpled graphene balls drop-casted onto a polished steel disk formed a uniform film. The steel ball left a nearly circular contact area of around 300 μm in diameter. The SEM overview image of this area shows that some patches of crumpled graphene balls were removed with the ball, exposing the surface of the steel disk. However, crumpled graphene balls remaining in the contact area did not appear flattened or severely deformed. The resistance of crumpled graphene ball to compression is attributed to its strain-hardening property due to the multiple folds created within the ball during its formation. Upon further compression, more folds can be generated, leading to increased stiffness. Results shown in suggest that crumpled graphene balls can survive the high pressure while remaining its crumpled ball shape.

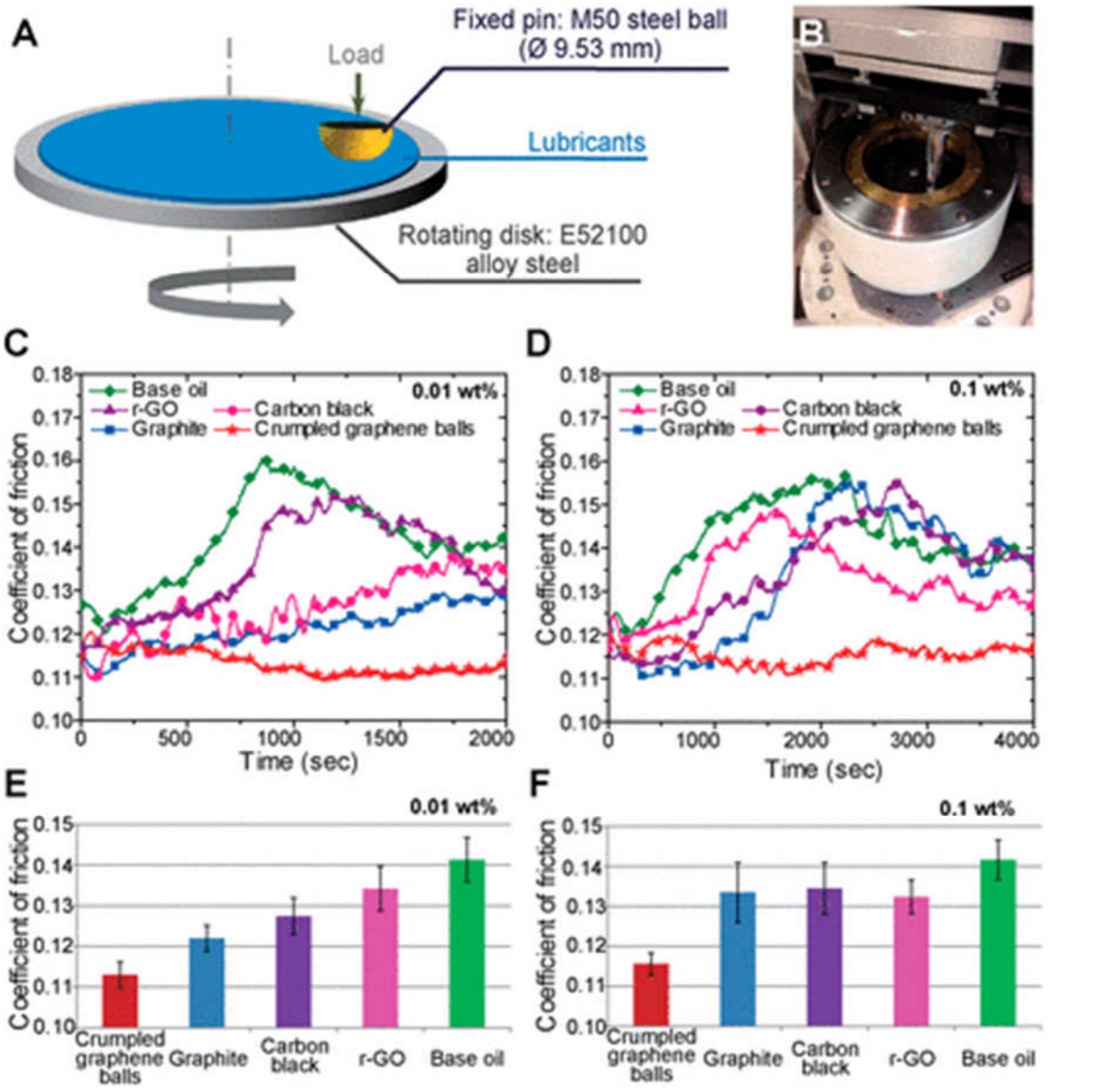

Figure 4.3.3 Coefficient of friction using PAO4 base oil with and without carbon additives. (A) Schematic illustration and (B) photo showing the pin-on-disk geometry of the tribometer; C and D show the variation of coefficient of friction as a function of time using PAO4 base oil and with 0.01 wt % and 0.1 wt % carbon-based additives, respectively. The corresponding bar charts in E and F show the friction values averaged over the entire duration of the test.

For both concentrations, crumpled graphene balls are found to be the most effective carbon additive for friction reduction.

Self -dispersed crumpled graphene balls as friction modifiers

Friction testing results are shown in Figures 4.3.3 c through f. Steel surfaces lubricated with the base oil display an initial increase in the friction coefficient followed by a decrease to a lower steady state value. This type of run-in behavior is fairly typical and is due to the wear of asperities at the contact surfaces resulting in increased real area of contact and hence reduced contact pressure. The friction curve for r-GO is similar to that of the base oil. Among all the carbon-based additives, crumpled graphene ball gives the lowest friction coefficient: only 0.01 wt. % of crumpled graphene is needed to reduce the friction coefficient by 20% compared with the base oil. In practice, a good additive should maintain consistent performance over a range of concentrations so that local concentration fluctuations and/or material loss do not disrupt the functionality of the additive. Therefore, tests were also conducted at higher loading, 0.1 wt. %. This high concentration (Figure 4.3.3 d) results in no significant improvement in friction performance for r-GO, while graphite and carbon black display poorer performance, probably due to easier aggregation at higher concentration. Such larger aggregates are likely to be poorly dispersed and cannot protect contacting surfaces. In fact, interaction among these larger aggregates could induce jamming during the friction test, leading to increased friction coefficient [123]. By contrast, crumpled graphene displays consistent friction behavior at this higher concentration. Its self-dispersion and

aggregation-resistant properties are primarily responsible for this consistently low friction over this range of concentration.

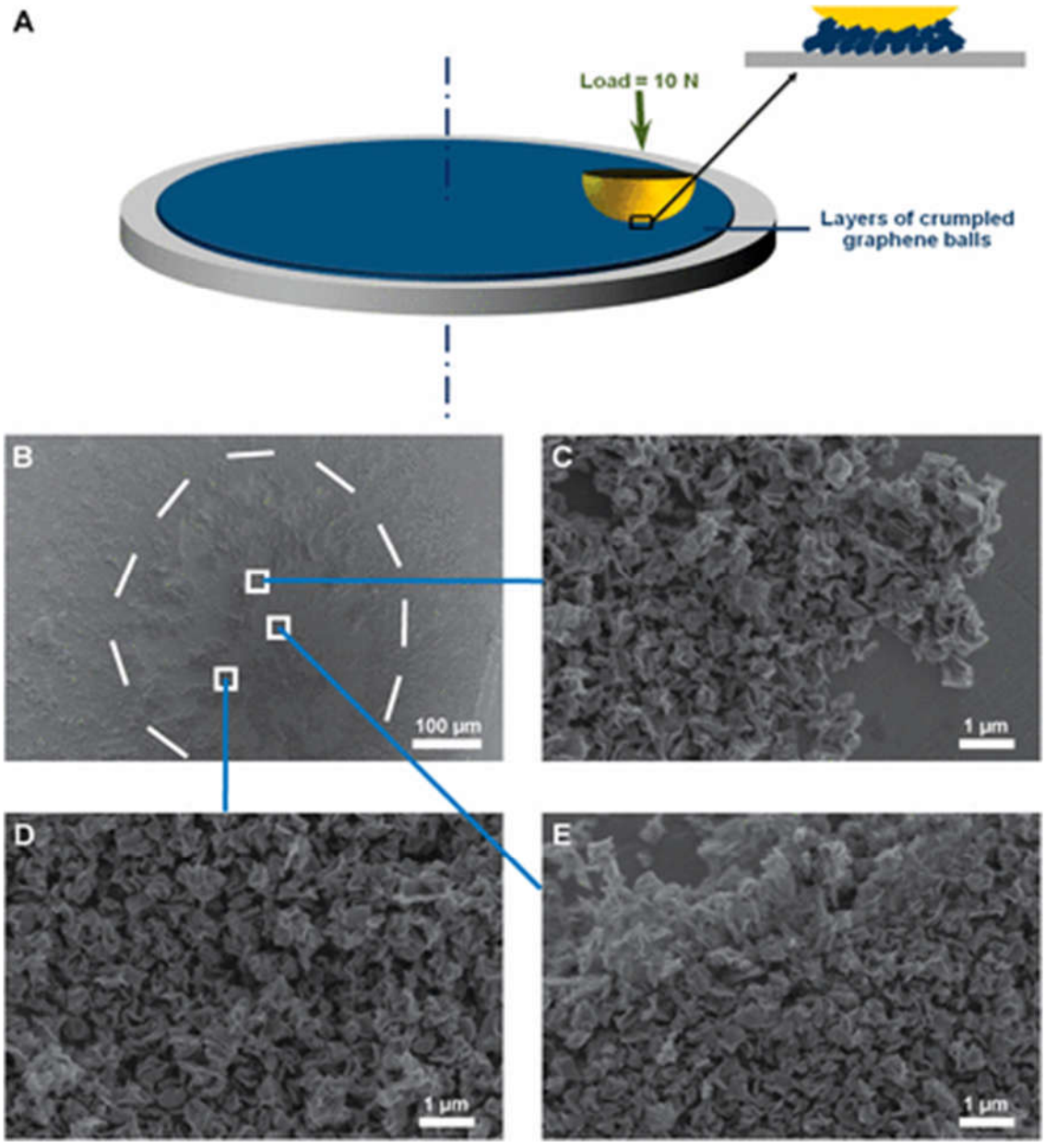

Figure 4.3.4 (A) Schematic illustration showing crumpled graphene balls being compressed between the pin and the disk on a pin-on-disk tribometer. The load on the pin was set at 10

N. (B) SEM image of the area of crumpled graphene coated disk right beneath the pin. The white dashed line outlines the contact area of the pin. Some particles were removed by the pin after the test. High-magnification images (C–E) taken on the residues within the contact area show no apparent shape change or deformation after compression.

After the friction tests, the wear surfaces were imaged by SEM. Some carbon-based particles were left on the wear track. Severe aggregation was observed for all carbon-based additives (Figures 4.3.5 a to c) except crumpled graphene balls (Figures 4.3.5 d). Intact crumpled graphene balls can be seen filling the grooves of the wear tracks and are separated from each other clearly. Evidently, the strain-hardening property of crumpled nanostructure prevents excessive deformation and damage during friction.

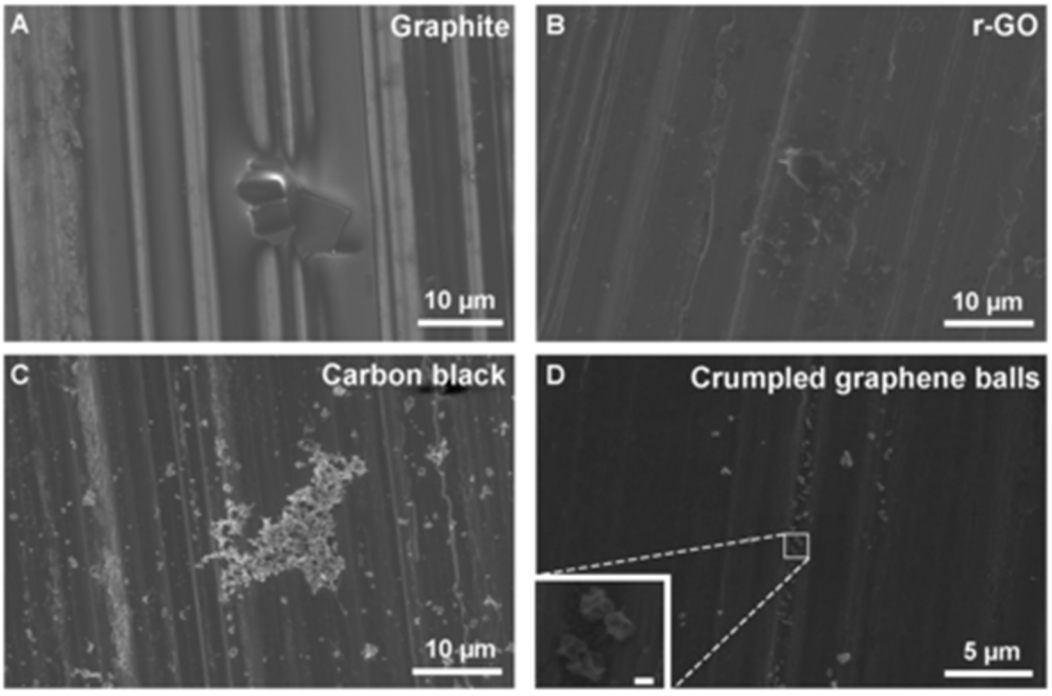

Figure 4.3.5 SEM images of remaining carbon additives in the wear tracks after tribological tests. (A) Graphite, (B) r-GO, (C) carbon black, and (D) crumpled graphene balls. Only crumpled graphene balls remain aggregation-free. (Scale bar in the Inset, 200 nm.)

Wear reduction by self -dispersed crumpled graphene balls

In addition to the substantial friction reduction, noteworthy improvements in wear reduction were also observed in our experiments. In Figure 4.3.5, SEM images of the wear tracks already suggest that oil modified with crumpled graphene balls is qualitatively more effective in reducing wear than the other three carbon additives. Quantitative examination of the wear tracks was conducted with white light interferometer, which generated a 3D map of the surface. Wear coefficients for oils modified with additives at two different concentrations are shown in Figure 4.3.7 a and b. For both 0.01 and 0.1 wt. %, crumpled graphene ball is significantly more effective than other carbon additives for wear reduction. The apparent wear coefficient difference in pure base oil between the two tests arises from the different testing times – because the most significant wear tends to occur at the beginning of the test, the wear coefficient calculated from the longer test should be lower. r-GO sheets, which did not reduce the coefficient of friction greatly, also failed to provide effective wear reduction; it showed the same apparent decrease in wear coefficient as the base oil when tested at a higher concentration for a longer time. Similar to what was observed for friction coefficient, the wear reduction performance of graphite platelets and carbon black additives also degrades at higher concentrations.

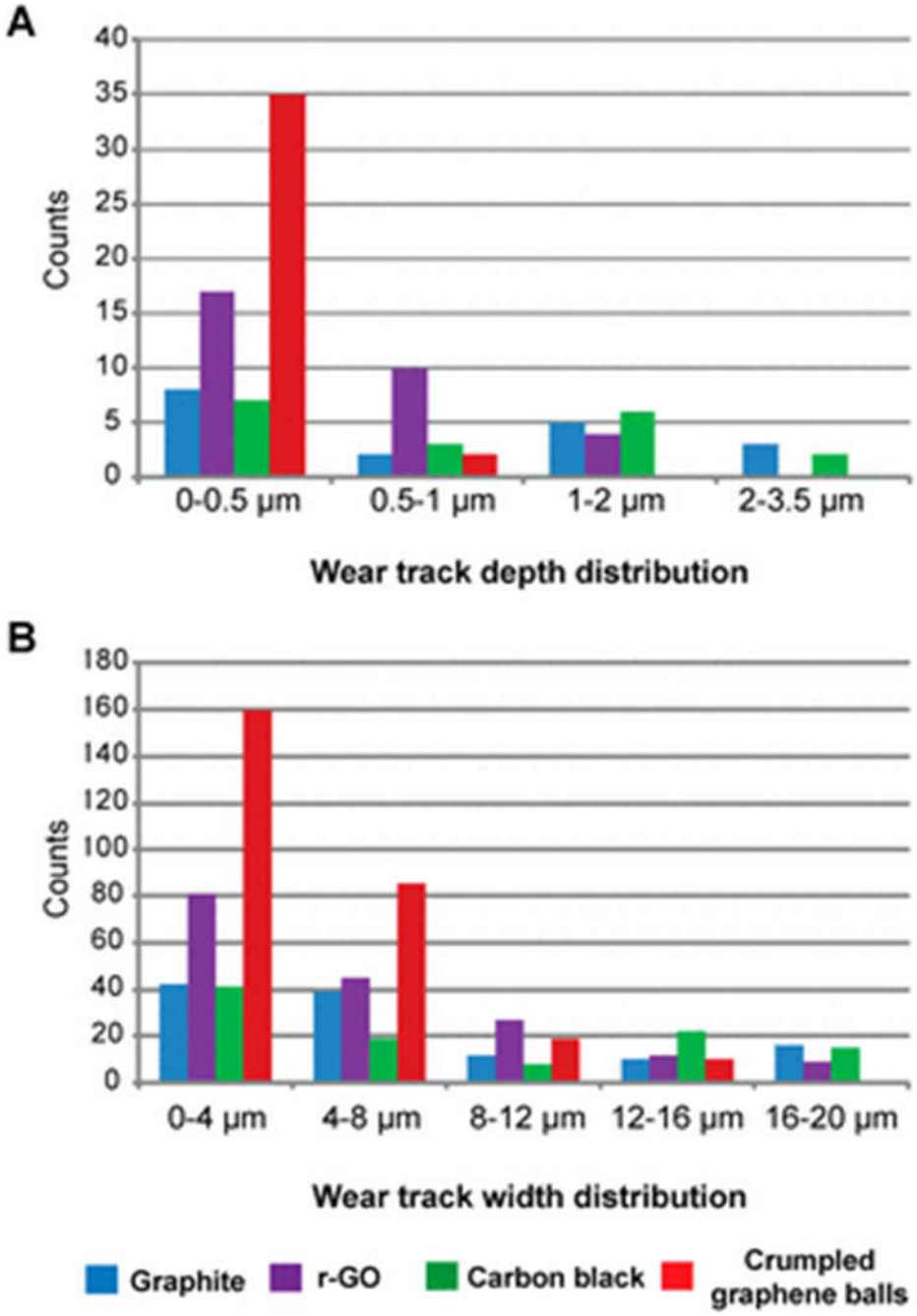

Figure 4.3.6 (A) Width and (B) depth distribution of wear tracks corresponding to those shown in Figure 4.3.7.

Meanwhile, varying the concentration has comparatively little effect on the wear coefficient for the lubricant with crumpled graphene balls. A detailed analysis of the wear tracks is presented in Figure 4.3.6 Compared to the other three additives, crumpled graphene balls generated shallower (0-0.5 μm), narrower (0-4 μm), and more uniform wear tracks. In contrast, wear tracks generated by other carbon additives are deeper (1-3.5 μm) and wider (12-20 μm), with a broader size distribution. It is significant that the use of crumpled graphene ball prevents the formation of wear tracks larger or deeper than 10 μm, because such wear tracks tend to generate large debris that can inflict severe abrasive wear [124-126]. Compared to the use of the base oil, the self-dispersed crumpled graphene additives are able to eliminate wear by ~85 % (red bars in Figure 4.3.6).

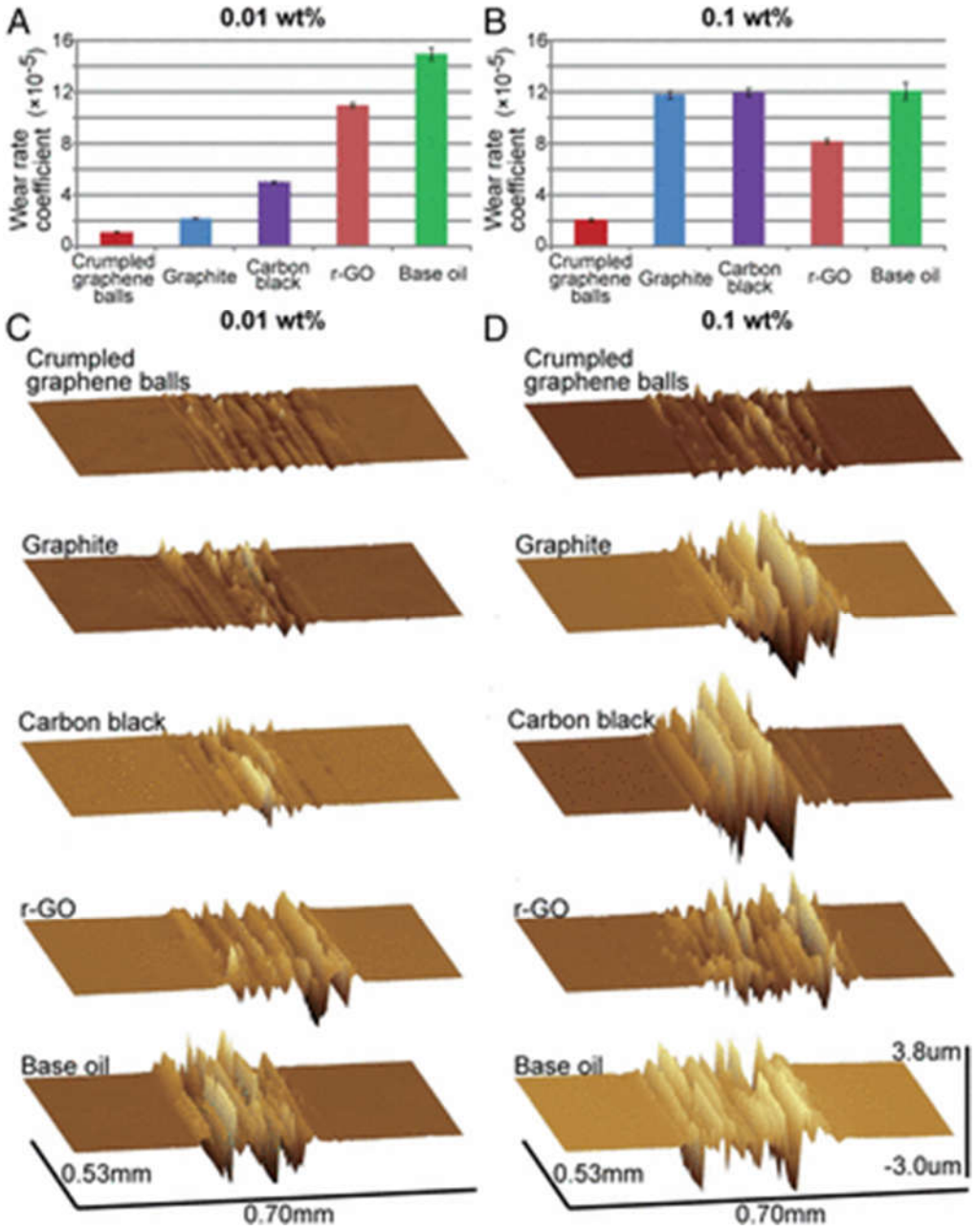

Figure 4.3.7 Wear coefficients of PAO4 base oil with and without carbon additives. The bar charts in A and B compare the wear coefficients of the base oil itself and samples with 0.01 wt % and 0.1 wt % carbon additives, respectively. The corresponding 3D profile images of the wear tracks are shown in C and D. It is evident that crumpled graphene balls can better protect the steel surface from wear.

Benchmarking against fully formulated commercial lubricant

The base oil modified with 0.1 wt. % crumpled graphene balls was also tested for comparison with a polyalphaolefin-based commercial lubricant 5W30 (Figure 4.3.8 a). Both 5W30 and crumpled-graphene-ball-modified PAO4 outperform the base oil, with comparable coefficients of friction. 5W30 has organic molecular friction modifiers which bind to the metal surface and decrease adhesion, making it effective for friction reduction. However, crumpled graphene balls are more effective in wear reduction. The difference is evidently revealed by the wear track profiles shown in Figure 4.3.8 c and d. The surface lubricated by 5W30 still yielded deep and wide wear tracks at tens of micron scale. However, crumpled graphene balls can provide better protection of the surfaces, leaving a much smoother wear track, as shown by the profile (Fig. 4.3.8 d).

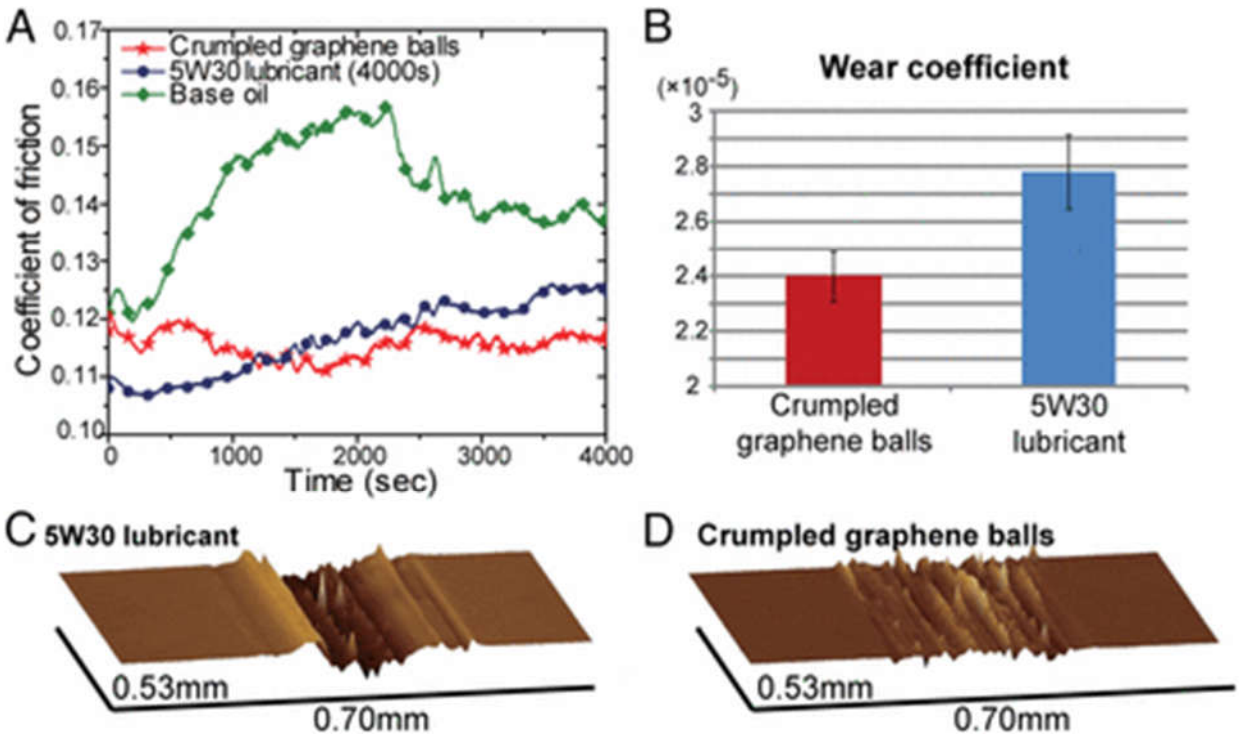

Figure 4.3.8 Comparison of lubrication between crumpled graphene balls in PAO4 base oil and commercial lubricant 5W30. At 0.1 wt % of loading level, the PAO4 base oil modified by crumpled graphene balls outperforms the fully formulated lubricant 5W30 (additives up to 10 wt %) as shown in the comparison of (A) coefficient of friction, (B) wear coefficient, and (C and D) 3D profile images of the wear tracks.

4.4 Conclusion

In summary, addition of crumpled graphene balls to PAO4 base oil results in superior friction and wear performance, due largely to their aggregation-resistant property. This unique property makes them more stable in the base oil than other carbon-based materials, such as graphite, r-GO, and carbon black. Aggregation makes other carbon-based materials lose their ability to prevent the contact of two surfaces, negatively impacting friction and wear performance. In contrast to other carbon additives, whose tribological properties are sensitive to their concentration, crumpled graphene balls deliver consistently good performance between 0.01 and 0.1 wt. % concentration. It was found that crumpled graphene balls reduce friction coefficient and wear coefficient by about 20% and 85% respectively with respect to the base oil. Furthermore, base oil modified with crumpled graphene balls alone outperforms a fully formulated 5W30 lubricant in terms of friction and wear reduction. The combination of aggregation resistance, self-dispersion, and mechanical

properties of crumpled graphene particles makes them an attractive material for tribological applications.

Chapter 5

Crumpled graphene as an additive for commercial Lubricant

5.1 Introduction

Crumpled graphene balls could improve the base lubricant oil performance and it would be worthy of knowing if it could also improve the lubrication performance of commercial lubricant oil. Commercial lubricant oil is more complicated because it contains various types of lubricant additives to fulfill different functions such as anti-foaming, anti-oxidation, anti-wear, demulsification, rust inhibition and friction / wear reduction. Base oil, the main component of commercial lubricant oil, consisting of 60 to 70 percent of the product. Although commercial lubricant oil is versatile in friction and wear reduction, crumpled graphene balls might still have its own advantages. As mentioned before, we mainly focus on wear and friction modifiers. Most friction and wear additives are molecular chemicals. However, they have two main drawbacks: 1. Under harsh tribological environment, molecular additives may desorb or deplete from the binding surfaces. 2. These molecular additives may also intervene with other types of lubricant additives and results into a bad dispersion of either or neither other additives. Therefore, it could compromise the lubrication performance in general. That is why more and more nanoparticles were applied into lubricant oil as lubricant additives. Because they could infiltrate into the surface contact

and further reduce the friction and wear. On the other hand, nanoparticle materials are more chemically and thermally stable than the molecular additives.

Experiments in Chapter 4 demonstrated that crumpled graphene balls reduce friction and wear in base oil, showing enhanced performance over other carbon additives. Furthermore, base oil modified with crumpled graphene ball and commercial lubricant oil 5W-30 exhibit comparable performance in friction reduction, with crumpled-graphene-modified oil having the added benefit of a more stable performance over time. 3D topography of a wear track also indicated that the crumpled graphene balls can better protect a metal surface from wear compared to the commercial lubricant oil.

However, all those experiments related with crumpled graphene balls were conducted in the lubricant base oil previously. To further explore the lubrication potentials of this material, we further disperse our crumpled graphene balls into the commercial lubricant oil and further test its performance to see if there are any improvements on the friction and wear reduction for commercial lubricant oil.

Although commercial lubricant oil contains various types of the additive molecular and materials, the aggregation resistance property could enable crumpled graphene fully dispersed in the commercial lubricant oil even under the higher oil temperature at 90-100 degree. Because the commercial lubricant contains the viscosity modifier and other additive materials, the viscosity is higher than the PAO base lubricant oil, and the higher viscous

lubricant oil enables crumpled graphene ball to maintain a more stable dispersion for at least a week. The crumpled graphene balls were added into commercial lubricant oil at 0.01wt%. And there were no significant improvements on friction reduction, however, it indeed could further improve the wear reduction by 25% compared to commercial lubricant oil themselves. And it further reveals the potential of crumpled graphene balls a potential lubricant additive in the liquid lubricant for automobile and other industrial applications.

5.2 Experiment

Materials processing

Similar as the previous experiments, the crumpled graphene balls were made by the same aerosol process with the same set-ups. The same batch of graphene oxide samples was used to make the crumpled graphene particles for this dispersion and friction test.

Dispersion test

The commercial lubricant oil was bought from the market as the dispersion solvent in this dispersion test. 3ml lubricant oil was used and 0.01wt% of crumpled graphene balls were dispersed in the solvent through vigorous sonication. And dispersed sample will be kept in oil staticly to observe its dispersion stability. To further investigate the dispersion condition under the high temperature (90-100 C), a preheated oil bath was used to provide the comparable and simulated high-temperature environment.

Tribological test

A high-temperature tribo-tester was used for the all the friction test in this session. The operating temperature was set up to 90 C. For the tribological test, the lubricant oil was well spread onto the disk surface first and the equipment will raise the temperature to the target temp and then, the friction test would start. The only difference between this tribometer and previous one is the heating unit. For the testing disk, the hardness is lower for this session. From the friction test, the coefficient of friction will be collected, and the wear track will be further inspected with the white-light interferometer.

5.3 Results and discussion

In the real practical applications, lubrication usually operates in the environment within various temperature ranges including low temp (-20C – 5C), room temp (10-35C), and high temp (70C+). Lubricant and its additives should be able to work properly in the relatively wide range of temperatures depending on lubrication requirements and objectives. In this session, we will further explore the performance comparison between commercial lubricant oil with the modified commercial lubricant oil sample containing the crumpled graphene nanoparticles under the room temperature and high temperature.

Room temperature experiment

The dispersion of crumpled graphene nanoparticles in commercial lubricant oil is excellent because the viscosity modifier enables a higher viscosity for commercial lubricant oil over

the PAO base oil which makes crumpled nanoparticles more stably disperse in oil for at least a week.

Figure 5.3.1 A week-long dispersion test between the modified commercial lubricant oil (left side) and the modified PAO base oil with crumpled graphene nanoparticles (right side) at same concentration at room temperature

The similar friction test was conducted with the same type stainless steel disk, a high-temperature tribo-tester and commercial lubricant oil samples w/o crumpled graphene balls. The experimental condition was the same compared to the friction test in Chap 4. In this friction test, 0.01 wt% of crumpled graphene balls were sonicated into the commercial lubricant oil until the additives were fully dispersed. The pure commercial lubricant oil and the modified commercial lubricant oil with crumpled graphene balls were well spread onto the steel disk and the fixed steel ball applies the 10N pressure on the rotating disk with 10mm/s linear velocity. As shown in the Figure 5.3.2, the results of friction coefficient for this friction test at room temperature are comparable between pure commercial lubricant oil and the oil modified with crumpled graphene balls. However, for the commercial

lubricant oil, there was still a more typical running-in behavior at the very beginning of friction test. And eventually, they all reached to relatively more stable lubrication performance.

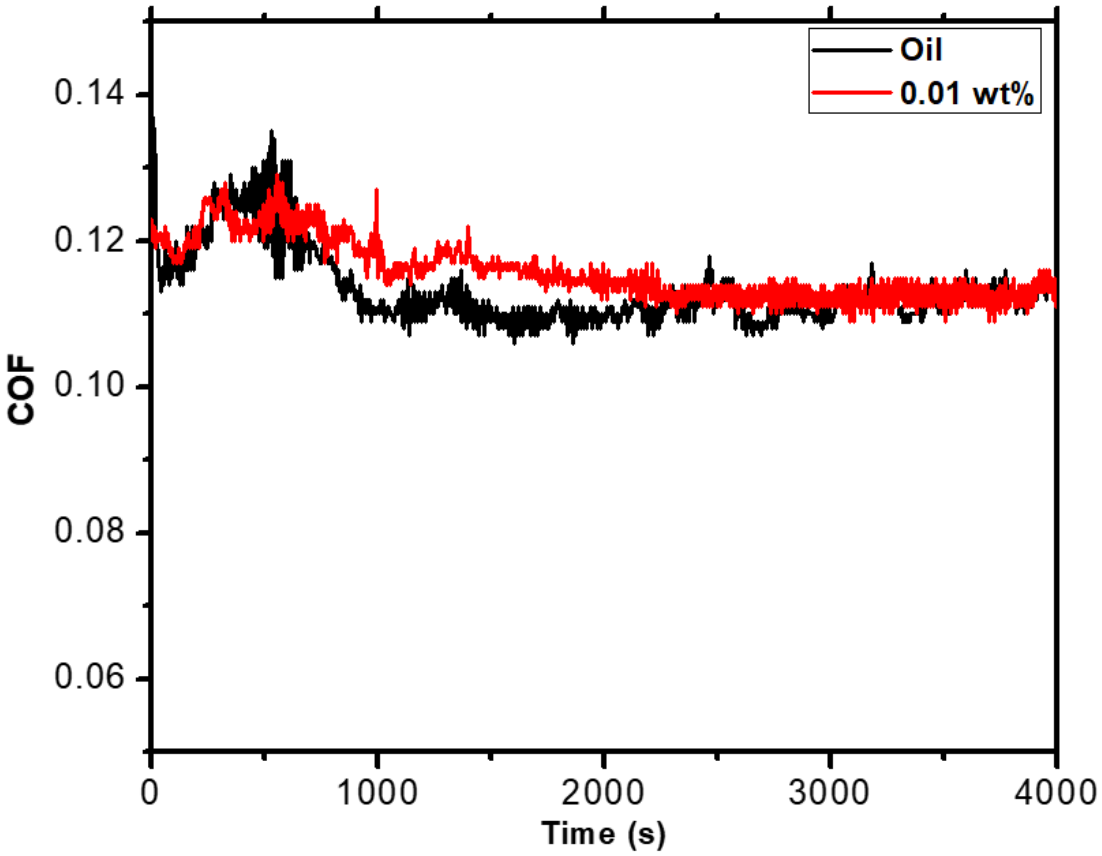

Figure 5.3.2 The coefficient friction curve of friction test between commercial lubricant oil and modified commercial lubricant oil with 0.01 wt% crumpled graphene balls.

For the wear reduction performance as shown in the figure 5.3.3, the wear tracks were further investigated through the white-light interferometer which could give us a detailed understanding of the surface profile data. The figure 5.3.3 (a) and (b) compare the surface profile of the two wear tracks corresponding to two different lubrication samples. It is hard

to observe the difference between the two wear tracks. And figure 5.3.3 (b) further extract the cross-section profile of two wear tracks and could give a more intuitive sense of the differences. The red curve corresponds to the wear track protected by the modified commercial lubricant oil containing 0.01 wt% crumpled graphene nanoparticles. And its wear track is shallower than the wear track protected by the pure commercial lubricant oil: the deepest wear trenches for pure oil is about 140nm; on the contrast, the deepest wear valley for the modified oil is about 80 nm. That is because crumpled graphene balls could effectively protect the surface wear as a wear modifier. Its aggregation resistance property enables it to infiltrate into surface contact and separate them from contacting each other and therefore reduce the wear. Although it didn't significantly improve or compromise the friction reduction, it did improve the wear reduction performance. The chemical stability of crumpled graphene balls prevents it from interfering with other lubricant additives containing different surfactants. In general, crumpled graphene balls are more effective in wear reduction when added into the commercial oil in the room temperature range.

(a)

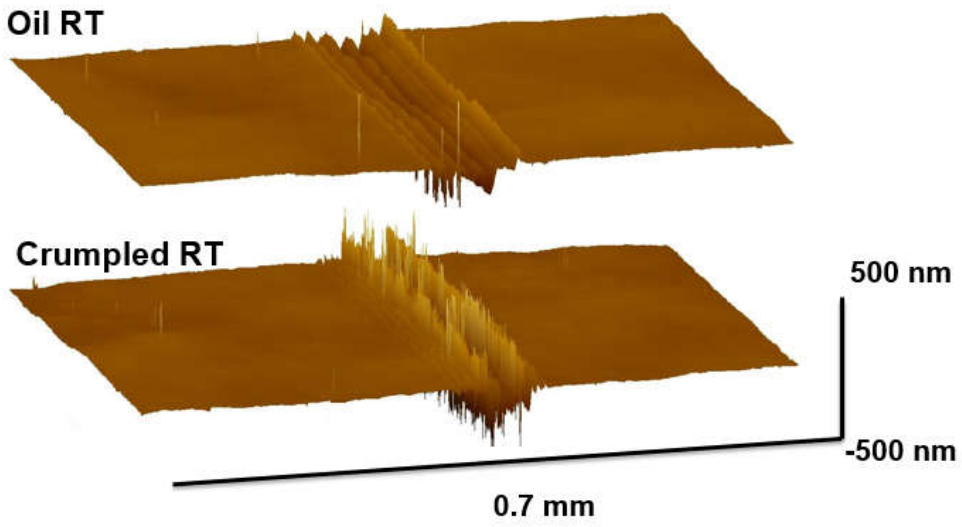
Oil RT
Crumpled RT
500 nm
-500 nm
0.7 mm

(b)

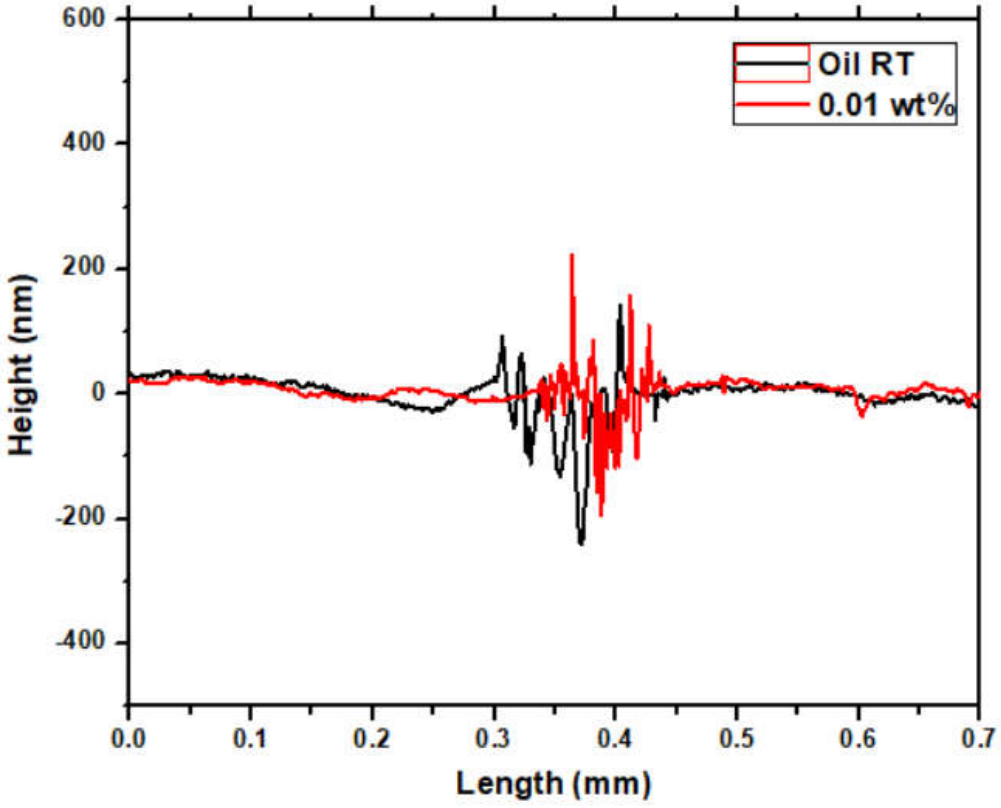
Oil RT
0.01 wt%
Height (nm)
Length (mm)
600
400
200
0
-200
-400
0.0
0.1
0.2
0.3
0.4
0.5
0.6
0.7

Figure 5.3.3 The comparison of the cross-section profile of wear track lubricated with commercial lubricant oil and the modified commercial lubricant oil with 0.01 wt%. (a) The 3D profile image of wear track generated from white light interferometer (b) 2D Cross section profile of the wear tracks

High temperature experiment

Sometimes, mechanical parts need to operate under the high temperature. For example, auto mobile's engine will rise to hundreds of degrees C after its cold start. Therefore, it is important for lubricant oil to maintain a relatively stable lubrication performance in such a wide temperature range. Especially, under the high temperature, the physical and chemical property of lubricant oil might also change and potentially influence the performance of its lubricant additives, for example, the viscosity. That is why it is also necessary to further test crumpled graphene balls' lubrication performance under the high temperature.

But first, it is important to test its dispersibility in the PAO base lubricant oil and commercial lubricant oil. With the previous dispersion test at the room temperature, we know that the 0.1 wt% crumpled graphene could stably disperse in PAO base oil for more than a day. Here we did the dispersion test in PAO base oil and commercial lubricant oil at the temperature of 90C within a pre-heated oil bath. This temperature is comparable to the temperature of cooling water for the engine. Because lubricant oil is also circulated inside of the engine.

As shown in Figure 5.3.4, it is the dispersion test in PAO base oil. And the crumpled graphene balls could only maintain the stable dispersion in 5 min. Why the particle sediment so fast compared to the room temperature? Because of the high temperature, the viscosity of PAO base oil significantly dropped, and the lowered viscosity could not hold the stable nanoparticle dispersion anymore. On the other hand, for the commercial lubricant oil, as shown in Figure 5.3.4, the dispersion test in hot oil bath indicated that crumpled graphene balls could maintain a stable dispersion for at least 24 hours. The reason why crumpled graphene nanoparticles have a much better dispersibility in hot lubricant oil is due to the functional surfactant in the commercial lubricant oil. The commercial lubricant oils have multiple lubricant additives deploying different functionality to maintain the stable lubrication performance in varies environment including the viscosity modifier which could maintain relatively stable viscosity even under high temperature and high speed. Further, it also contains the dispersant chemicals to facilitate the stable dispersion of crumpled graphene balls in commercial lubricant oil even under the high temperature.

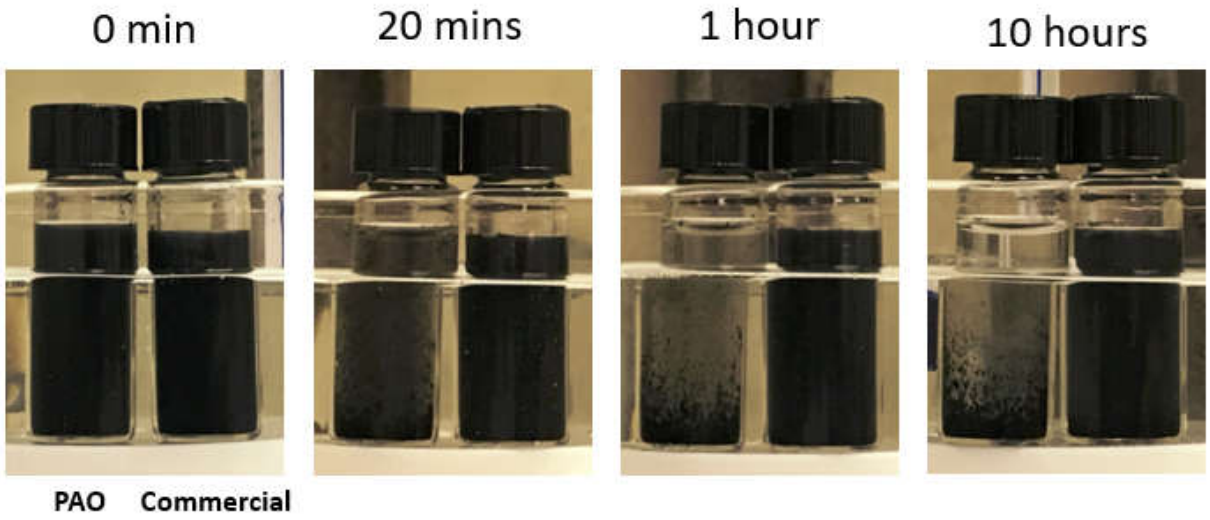

Figure 5.3.4 The dispersion test between the modified commercial lubricant oil (right side) and the modified PAO base oil with crumpled graphene nanoparticles (left side) at same concentration at room temperature

For the friction and wear test, the high temperature tribo-tester was used. The operating temperature was set up to 90 C to compare with dispersion test temperature. And whole friction test was also implemented for 4000 secs. From the friction coefficient curve, as shown in Figure 5.3.5, the lubrication of the two groups including pure commercial lubricant oil and the modified oil with crumpled graphene balls are comparable. Similar to the friction test at room temperature, both testing groups have a stable lubrication performance. Crumpled graphene didn't significantly improve nor compromise the friction reduction performance of commercial lubricant oil.

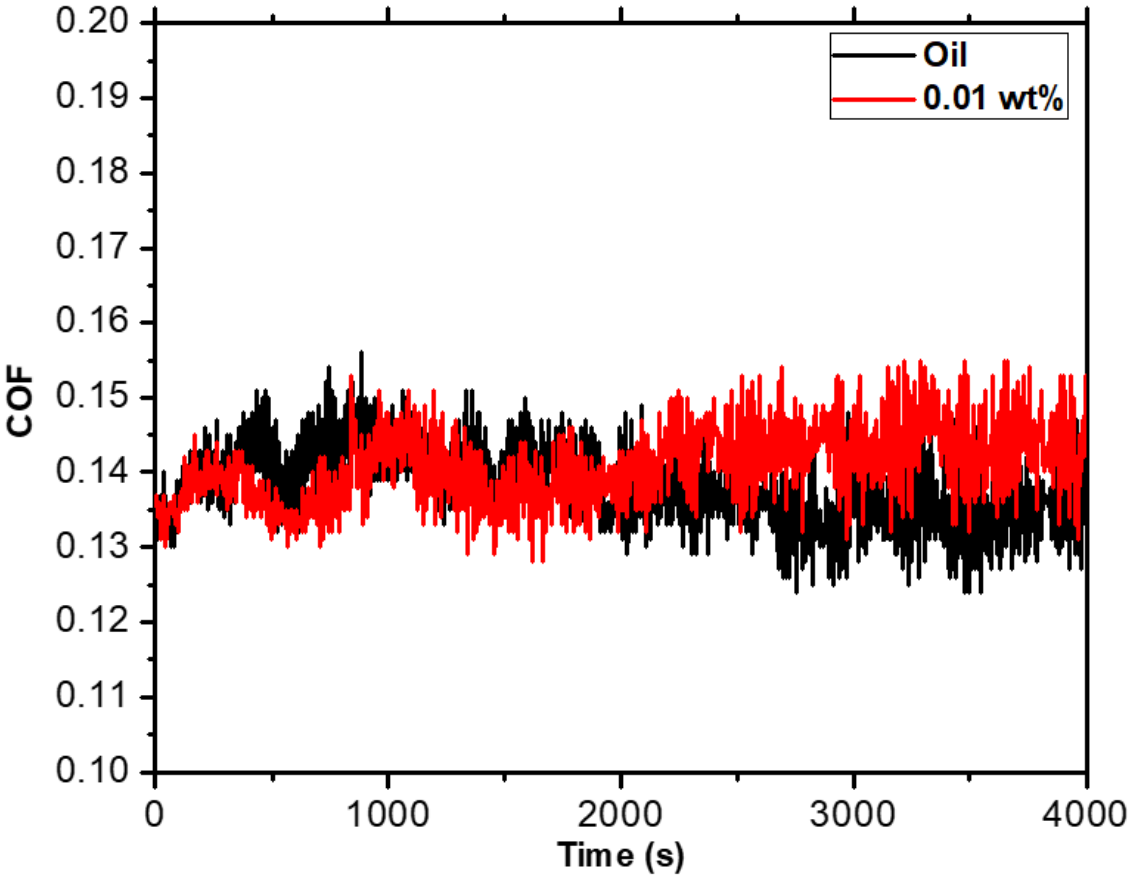

Figure 5.3.5 The friction coefficient curve for the high temperature friction test between commercial lubricant oil and the modified commercial lubricant oil with crumple graphene balls

(a)

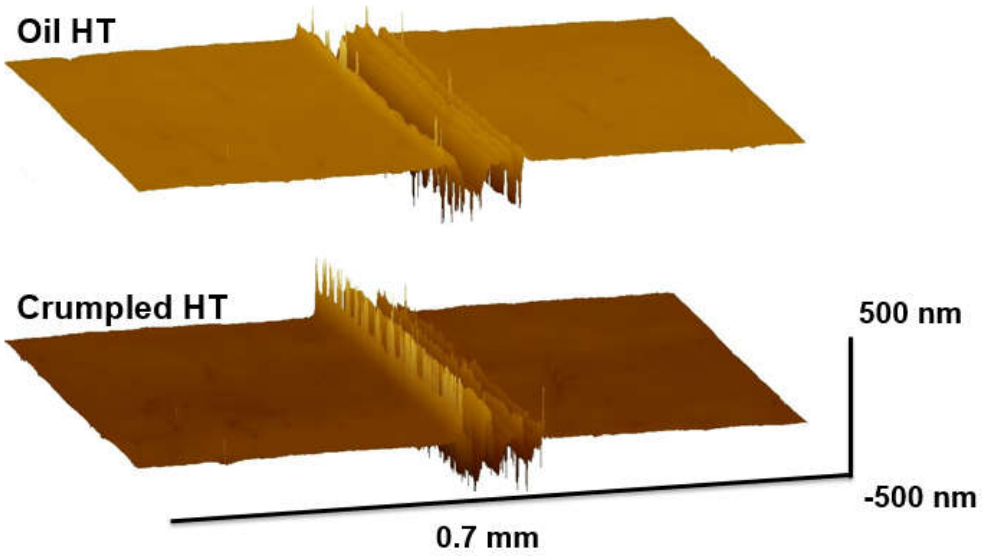
Oil HT
Crumpled HT
500 nm
-500 nm
0.7 mm

(b)

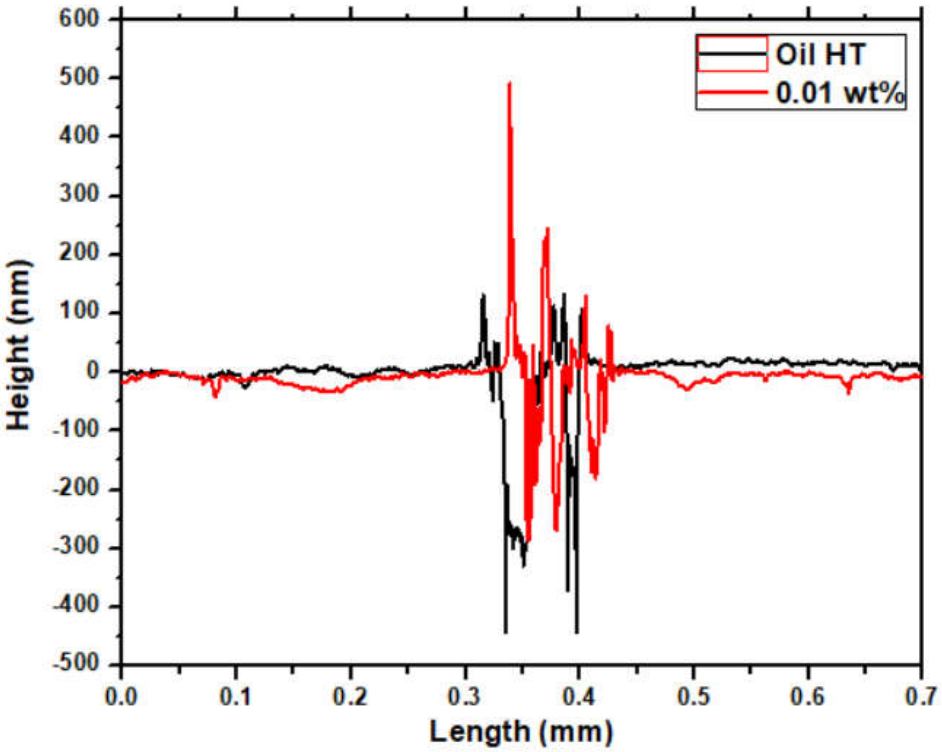
Oil HT
0.01 wt%
Height (nm)
Length (mm)
600
500
400
300
200
100
0
-100
-200
-300
-400
-500
0.0
0.1
0.2
0.3
0.4
0.5
0.6
0.7

Figure 5.3.6 The comparison of the cross-section profile of wear track lubricated with commercial lubricant oil and the modified commercial lubricant oil with 0.01 wt% under the high temperature at 90 C (a) The 3D profile image of wear track generated from white light interferometer (b) 2D Cross section profile of the wear tracks

Moreover, for the wear test shown in the Figure 5.3.6, the modified oil with crumpled graphene balls had better wear reduction performance than the pure commercial lubricant oil. Although the wear tracks of two experimental groups have the comparable width, but the wear track of the sample containing crumpled graphene balls has shallow profile than the other pure commercial lubricant oil sample, which indicates that crumpled graphene balls have a great potential in wear reduction for the commercial lubricant oil even under the higher oil temperature.

5.4 Conclusion and Future work

In this session, the high-temperature tribology test was fulfilled within the commercial lubricant oil system. The comparison between the pure commercial lubricant oil and the commercial lubricant oil modified with crumpled graphene balls further help us explore the lubrication performance of crumpled graphene balls. Considering the well-established formula and performance of commercial lubricant oil we used, crumpled graphene balls could further improve the wear reduction performance by being added into the commercial oil without any functionalization or any other steps. Although crumpled graphene balls could

not further boost the performance of friction reduction of commercial oil, it didn't hurt its original lubrication performance, which indicates its compatibility with the formula system of commercial oil.

The reason why crumpled graphene balls could not further improve the friction reduction performance is due to the contained friction modifier molecular in the commercial lubricant oil. The fully formulated commercial oil is versatile already.

Further, to understand why crumpled graphene balls are more stable in commercial oil. It would be better to make a dispersion test comparing PAO 10 base oil with commercial lubricant oil, which have a comparable viscosity so that it could check if it is the high viscosity or the other dispersants in the commercial oil. For the surface wear, it would be better to do the EDX or Raman spectra to check if there is any tribo-film formed from the anti-wear molecular in the commercial oil, like ZDDP. Besides, lubrication application is not limited to the liquid form. Other applications including lubricant grease and extreme high-pressure lubricant also could take the advantage of crumpled graphene balls' lubrication potentials. And it would be interesting to further explore the possibility in those areas as well.

Chapter 6

Making 1D Structure

Besides the project related with crumpled graphene for lubrication application, I also had the chances to work on the other two projects. The first project was related to the templated-assistant gold nanowire growth based on imprinting technique without using any surfactants. The gold nanowire project explored the possibility of synthesizing the high aspect ratio Au nanowires within a confined physical geometry. And the second project was about strain induced curling polymer strip. The curling polymer strip further explored how the strain induced helical structure was formed due to the stretching and different strain property distributed in the polymer cross-section.

Part I: Template-assisted, surfactant-free synthesis of gold nanowires on substrate

6.1.1 Introduction

Long Gold (Au) nanowires have promise as multifunctional conduits that couple plasmonic, electronic, mechanical and surface chemical functions for probing small area samples. Such

nanowires, usually with multiple twinned inner structure and single crystalline surface have been very difficult to make without the traditional surfactant mediated syntheses. Because those surfactants could cap the surface of gold seed nanoparticles and further guided them to grow into the various structures like nanowire or star shape. They are essential elements for size/shape control synthesis and stabilization of as-synthesized nanoparticles. For these purposes, excessive surfactants or capping agents should be used. However, the excessive amount of surfactants[120, 127-132] like CTAB and PVP are hard to remove after the synthesis[133-134]. As a result, these residues can bring much difficulty to subsequent material processing steps and degrade the material performance in some applications such as catalysis, surface enhanced Raman spectroscopy (SERS), and electronic devices, in which the surface of metal nanoparticles is directly related to their applications. Even during the removal or post-removal process, the nanowires will form into agglomeration and other potential problems. Therefore, there is a need to use non-surfactant method to synthesize the gold nanowire. And luckily, it is possible to achieve this objective by using a new gold precursor developed by my previous colleague Dr. Kwonnam Sohn, the principle of this gold precursor is because it contains the NMP and H_2O_2, the hydrogen peroxide could reduce the reduce the Au (3+) into Au (1+). And NMP will further stabilize the hydrogen peroxide by forming the NMP-H_2O_2 adduct. Under certain external experiment condition including heating, UV lighting, etc. The reduction of Au (1+) to Au will initiate and gold seed particles would be formed. In this section, the gold nanowire growth will be further refined in the microchannels and it is now possible to make such wires with unprecedented length up to tens of microns by simply drying the precursor solution confined in the replicated microfluidic channels.

Moreover, the resulting wires have clean surfaces. TEM was used to further inspect the gold nanowires' crystallization and its surface. The surfactant free property making them ready to be used for surface sensitive studies and applications.

6.1.2 Experiment

Make micro-meter sized nanoarray

In order to make micro-meter sized PDMS mold, the imprinting technique would be used as below: We firstly used CD-R disk and peel it off to get the disk surface with micro channel structure on it. Then, put it into the petri dish and pour the PDMS into the petri dish. The whole petri dish was put into the pre-heated oven (at 60C) for 40min. This process will make PDMS cure into solid to further replicate the micro-structure. And after curing, the negatively replicate of CD-R disk' microstructure will transfer on to PDMS mold.

Preparation of gold nanoparticle precursor (NMP-based Au(1+) growth solution)

Typically, 39.4 mg HAuCl4·3H2O was dissolved in 10 ml NMP to prepare 0.01 M Au concentration in the 20 ml vial with a polypropylene cap. 2.3 ml H2O2 (30 wt. %) was added into the solution. The mixture solution was dipped in the preheated oil-bath of 110 °C with vigorous stirring. As the heating reaction proceeded, the initial yellow color of the mixture solution from Au(3+) was pale yellow. Finally, the solution color was clear and colorless after around 20 minutes of heating. The reaction was immediately terminated by taking out the

reactor from the oil bath. The clear and colorless solution was naturally cooled down to room temperature. The growth solution was stored at room temperature for further uses.

Preparation of clean wafers

The wafer was cut into the same size which will match the PDMS mold. And further use the piranha solution to clean the small wafer pieces. Piranha solution would be prepared by adding hydrogen peroxide to sulfuric acid slowly. Mixing the solution is extremely exothermic. It must be allowed to cool reasonably before it is used. The sudden increase in temperature can also lead to violent boiling of the extremely acidic solution. Once the mixture has stabilized, it can be further heated to sustain its reactivity. The hot (often bubbling) solution cleans organic compounds off substrates and oxidizes or hydroxylates most metal surfaces. Cleaning usually requires about 60 minutes, after which the substrates can be removed from the solution. And they will further be rinsed with the clean water for future usage.

Template-assisted gold nanowire growth

After the precursor and substrate with micro-channels are prepared, the template-assisted gold nanowire synthesis will further proceed by using the soft lithography experiment. The general experiment setup is shown in Figure 6.1.2. The PDMS mold with the replicated microchannels would cover a pre-cleaned silicon wafer. And the gold precursor solution will spread along the one side of channel entry. The capillary force will suck the solution into the microchannels. Then put the whole sample into the pre-heated oven and the reaction would start. After overnight, the sample will be taken out and the PDMS mold will be removed.

TEM sample preparation

In order to prepare the TEM sample, the gold nanowires on the substrate will be washed into the ethanol by sonication. And the nanowire sample will be further transferred onto TEM grid by drop casting the ethanol solution containing gold nanowires. HITACHI SEM 8300 and JOEL TEM 2100 were used for the characterization.

6.1.3 Results and discussion

The Principle of surfactant-free Au precursor (NMP-based Au (1+) solution)

In order to synthesize gold nanowire without any surfactant, our group developed a surfactant-free route for gold nanoparticle synthesis. We introduced H_2O_2 into NMP solvent, in which Au(3+) ions are dissolved. The H_2O_2 will further reduce the Au(3+) into Au(1+)[135]. As a reduction agent, H_2O_2's byproduct should be water or gaseous molecules. In addition, NMP could effectively stabilize H_2O_2 in liquid solution as forming NMP- H_2O_2 adduct[136-137]. This precursor solution could be reduced by thermal treatment. The H_2O_2 will be released and further reduce the ion into gold.

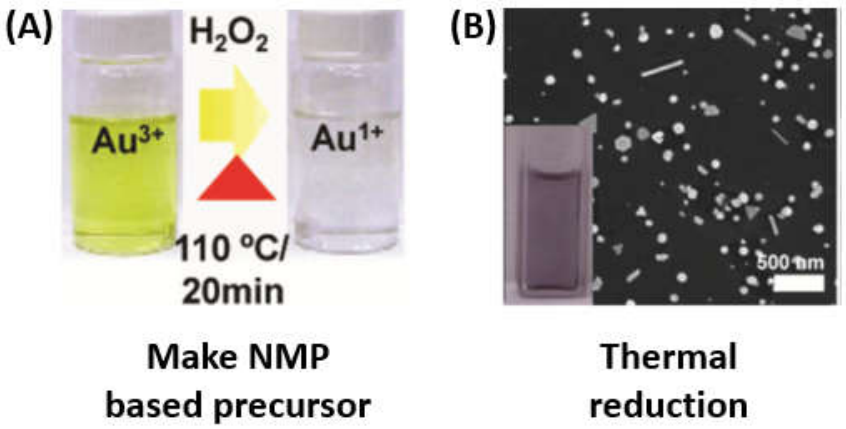

Figure 6.1.1 (A) The process of making surfactant-free NMP based precursor (B) Thermal reduction of precursor

Make micro-meter sized nanoarray

As mentioned in the experiment section, a soft lithography was used to get the microchannel space for the gold nanowire growth. Because PDMS was covered on the peeled CD-R disk, the structure on the PDMS replicated the negative structure on the CD-R disk. The hill on the CD-R would be the valley on the PDMS mold. For the CD-R bump, it has a width of 1um. And similarly, the PDMS mold will replicate this structure as trenches with the width of 1um for gold nanowire growth.

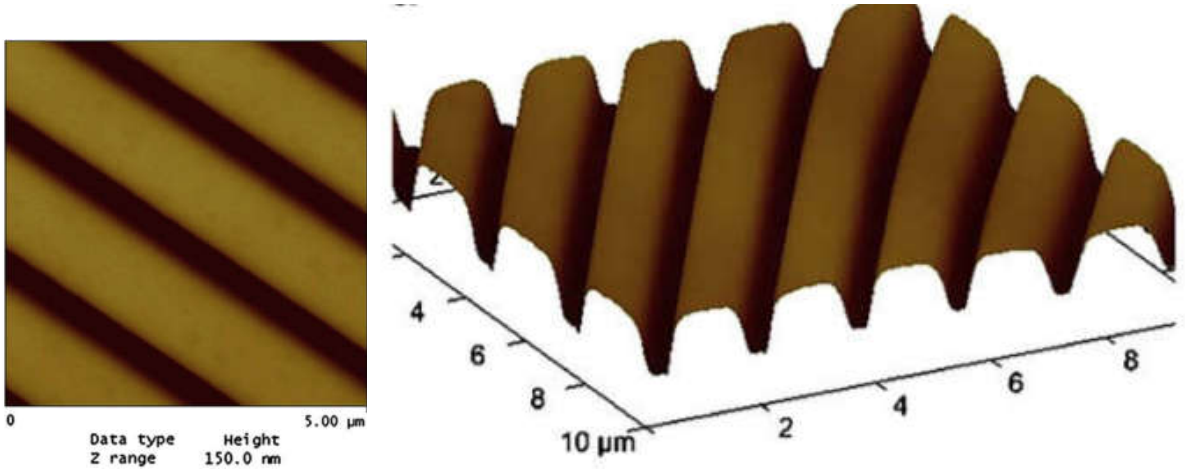

Figure 6.1.2 The top view and the AFM scan of CD-R disks. The Height is in the 100 nm scale and the width of the groove is 1um scale, which indicates that the width of trenches on the PDMS mold should be around 1um as well

Template-assisted gold nanowire synthesis

With the replicated PDMS mold, the one-dimensional confined channel will be formed by covering the silicon wafer with the PDMS mold as shown in Figure 6.1.3. The precursor solution will be absorbed into the channels with the capillary force.

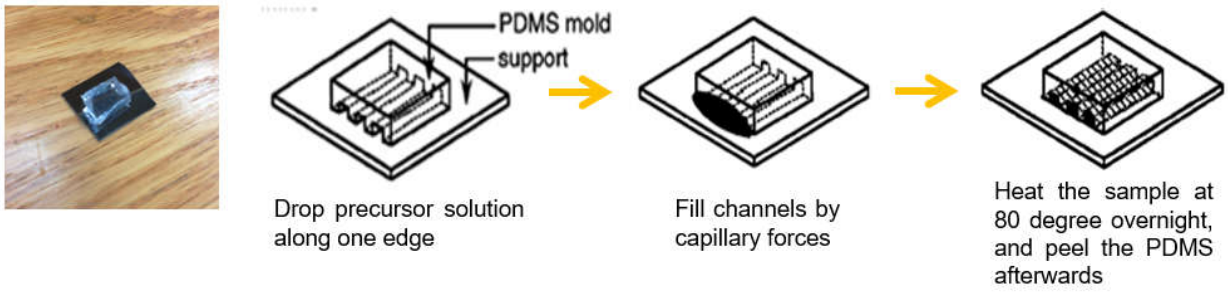

Figure 6.1.3 The template-assisted gold nanowire growth channel – the replicated PDMS mold will cover the silicon wafer to generate a more confined growth space. The micro-channel will further suck the precursor into the channel. And gold nanowire starts to grow under proper condition

Different as surfactant assisted gold nanowire synthesis, the template-assisted gold nanowire's growth was confined by the micro-channel geometry instead of the surfactant. Due to the capillary force of micro-channel, the gold precursor will be absorbed into the channel and further react inside of it. Their growth will not exceed the geometry confinement of the microchannels, especially the lateral direction, and the channel will further guide the growth along the channel longitude direction. After the reduction reaction overnight, the PDMS mode would be removed. The synthesized gold nanowires will align on the silicon wafer substrate as shown in the Figure 6.1.4. Gold nanowire and nanoparticles were scattered on the substrate, and they were all grown inside the micro-channels with a unidirectional distribution pattern. It is clear to observe that long gold nanowire could be made with this method: some wires even have a length of 80 um. It also generated some gold nanoparticles spreading inside the aligned grooves. Due to the non-continuous supply of precursor solution, some solution reacted and turned into gold nanowire and others only transformed into gold nanoparticles probably due to the lack of precursor's supply. That is why gold nanoparticles are all well spread on the silicon substrate. To further magnify the gold nanowire, it is clear to see that the gold nanowire was laid inside the channel as shown in Figure 6.1.5. From the mark of the channel, we could tell that the channel width is about

800nm. During the channel replication, there was some geometry lose to the original trench width of 1 um, which is reasonable. The width of the nanowire is 350nm, and we could tell that the channel could confine the growth of gold nanowire to further facilitate the wire growth instead of particle growth. If there is no channel under the similar condition, the precursor could only transform into gold nanoparticles without any nanowire with such length.

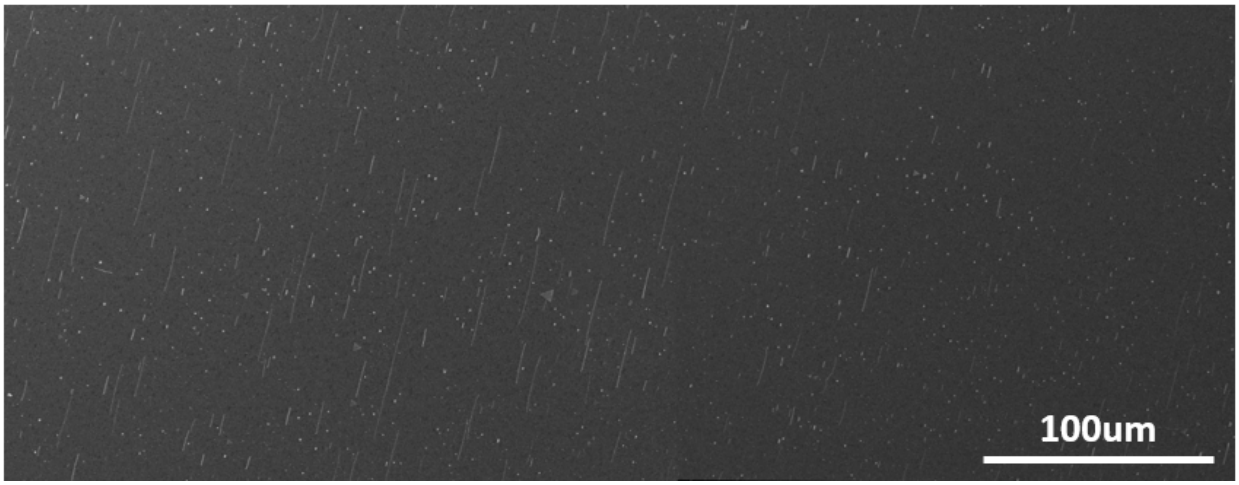

Figure 6.1.4 The SEM image of gold nanowire array made by the imprinted micro sized groove pattern. The gold nanowire has the uniform aligned direction due to the aligned grooves

Figure 6.1.5 The SEM image of a single gold nanowire array grown inside a channel. The width of nanowire is about 350nm, the channel width is about 800nm

Characterization of template-assisted grown gold nanowires

In order to further inspect the crystallization of template-assisted grown gold nanowire, TEM was used as shown in Figure 6.1.6. There were two wires corresponding to (A-B) and (C-D). Firstly, from the high-resolution TEM image of two wires (A and C), the images show a clear surface of gold nanowire without any surfactant. Secondly, the diffraction pattern of these two wires (B and D) indicated that gold nanowire made by this template-assisted method has Penta-twinned crystal structure. However, the width of this nanowire is way smaller than the one shown in the Figure 6.1.5. This further indicated that some of the gold nanowire didn't get enough precursor solution to support the continuous growth of longer and wider gold nanowire. And this would be worthy to be explored as the next step in the future.

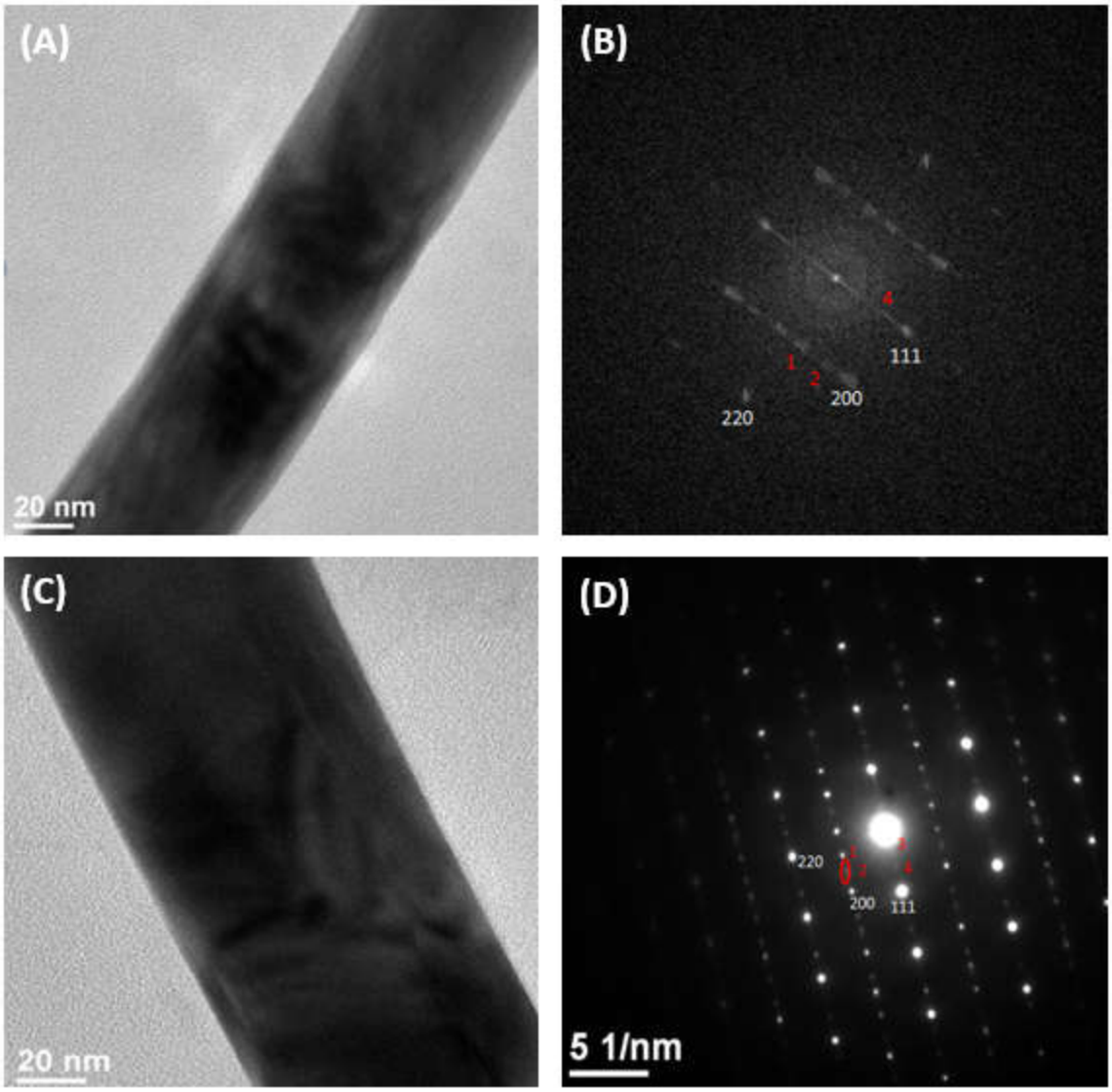

Figure 6.1.6 The TEM image of two gold nanowires (A and C) indicate a very clean surfaces without any surfactant. The diffraction pattern (B and D) of two wires further indicate that two wires have a Penta-twinned crystal structure

6.1.4 Conclusion and outlook

For the template-assisted grown gold nanowire, it could achieve high aspect ratio nanowires (length 40-80um, width 300-500nm) with the NMP-based surfactant free gold precursor solution. And this method provides another way to make surfactant free gold nanostructure. TEM image and diffraction pattern further identified that the pristine of the gold nanowire and its Penta-twined crystal structure. For the next step, it would be interesting to further explore that if it would be possible to further fulfill the continuous growth of gold nanowire by continuously suppling the precursor solution into the micro-channel. And also, the gold nanowire collection process would be a challenge, a washing process might be applied to remove the gold nanowires from those substrates.

Part II: Stretching induced formation of helical polymer ribbons

6.2.1 Introduction

For this helical polymer strip project, stretching the printed PVC polymer strip could automatically form into a helical curling structure after it was released from stretching. And stretching process is necessary to induct this deformation process. During the following elastic experiment, it is interesting that only the polymer strips which were dried 3-8 hours after printing could form into helical curling structure, and other samples within other time

ranges have different deformation behavior. Multiple repetitive tests were conducted, and the experiment results were consistent.

Why there is different elastic behavior within different time ranges? The reason for forming the helical structure was further explored by conducting experiments with different control factors. And different time length after the printing process turned out to be the determining factor. Similarly as other research works done by others[138-144], that was due to the asymmetric distribution of different strain properties during the evaporation of DMF solvent in the printed polymer strip, since dried PVC has different elastic property comparing to the wet PVC. Once the polymer strip was stretched, the inner layers at different levels relaxed at a different rate. The asymmetric elastic property further induces the formation of the helical structure during the relaxation stage.

6.2.2 Experiment

PVC solution

PVC powder (55,000 MW) was mixed with DMF solvent at 200mg per ml on the magnetic stirring stage. During the mixing, the water bath at 70C degree was used to further facilitate the dissolving and mixing process. The speed of the stirring bar was set at 500 rpm/min. About 45min later, the PVC powder could fully dissolve into the DMF solvent.

Glassware preparation

The microscopic glass slides were used as the substrate for the PVC strip printing process. In order to get the clean glasses, Piranha solution was used. The solution would be prepared by adding hydrogen peroxide to sulfuric acid slowly. Mixing the solution is extremely exothermic. It must be allowed to cool reasonably before it is used. The sudden increase in temperature can also lead to violent boiling of the extremely acidic solution. Once the mixture has stabilized, it can be further heated to sustain its reactivity. The hot (often bubbling) solution cleans organic compounds off substrates and oxidizes or hydroxylates most metal surfaces. Cleaning usually requires about 60 minutes, after which the glass slides can be removed from the solution. And they will further be rinsed with the clean water for future usage.

Printing process

In order to make the polymer strip, a syringe pump was used. Firstly, transfer the PVC in DMF solvent into the 5 or 10mL syringe. The PTFE tube connected the syringe on the one side with the flat top syringe needle on the other side. Set the pumping speed at the appropriate range and glass substrates were used to take the printed polymer strip. After printing, some DMF will be spread out on the substrate and let the printed PVC strip dry for a bit. After those DMF on the substrate dry out, the PVC strip could be easily removed from the substrate.

6.2.3 Results and Discussion

Strain-induced helical PVC strip

After the PVC strip was printed on the glass substrate, it could be easily removed from the substrate as shown in Figure 6.2.1 (a). Then, use the hands to stretch the polymer strip, it was elastic and could extend to 3-5 times of its original length as shown in Figure 6.2.1 (b). However, when the force is gradually released, the polymer strip would self-propagate into a helical curling structure. The whole relaxation process corresponds to Figure 6.2.1 (c-d).

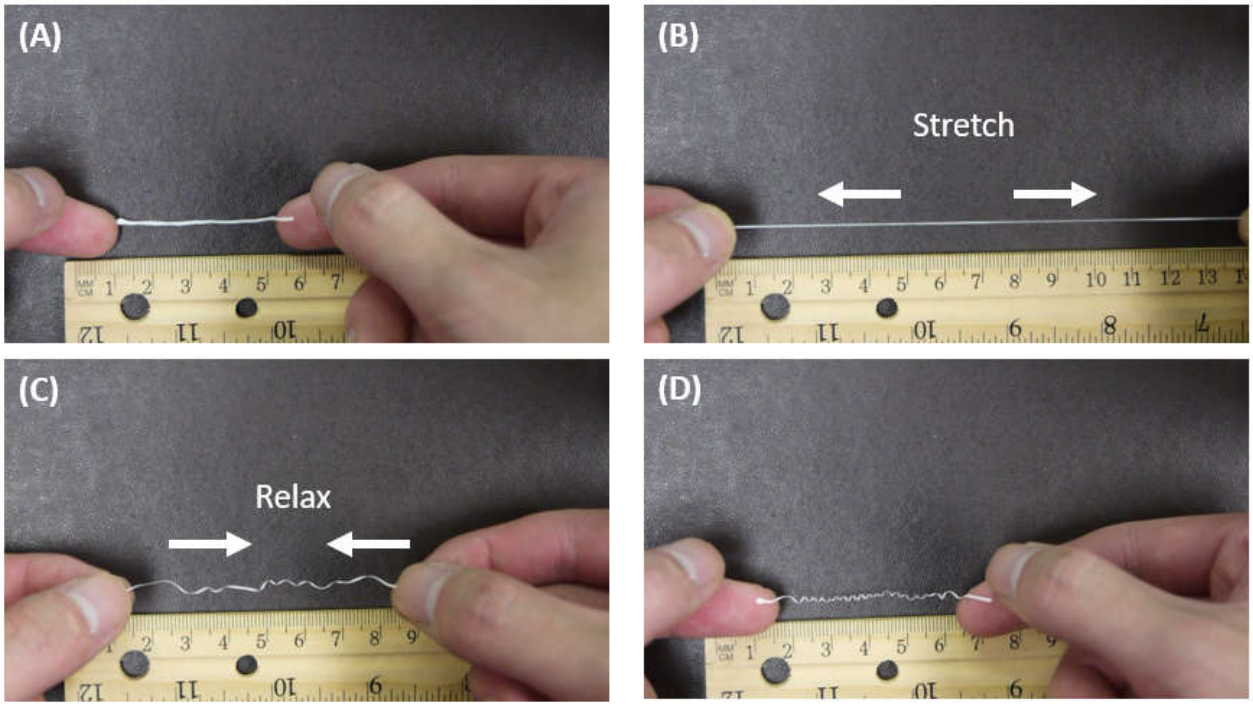

Figure 6.2.1 The whole stretching – relaxation process is recorded through those pictures. (a) Originally, the polymer strip was removed from the substrate; (b) the strip was stretched at relatively large extend to its original length; (c) after stretching, the polymer strip was released, and it started to relax into a helical curling shape (d) at full relaxation state

Self-propagated deformation varied by the time after printing

Once the PVC dispersed in DMF was printed on the substrate, the DMF will start to evaporate. During this process, the printed structure is transparent at the very beginning and DMF would start to evaporate, the color of printed structure turned to white and formed into PVC stripe. For the stretch tests, they were conducted at three different stages and different results were achieved. The three stages correspond to different time length – short term (10-30 min after printing), mid-term (3-8 hours after printing), long term (2-4 days after printing).

The printed polymer strip is stretchy but could not form into a helical structure upon releasing. Couple hours later, the polymer strip could form into the helical structure after stretching. And days later, the polymer strip would not be stretchy anymore and would break into half (as shown in Figure 6.2.3).

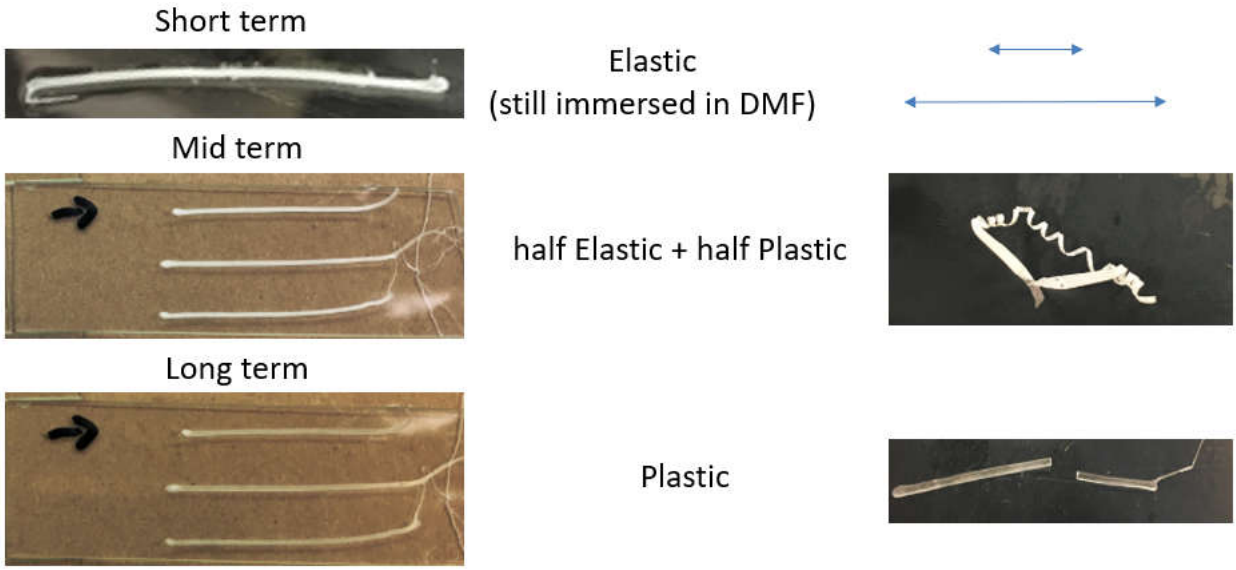

Figure 6.2.2 The different deformation behavior corresponding to the PVC polymer strips' different drying stages (from short term to long term). For the short term, the PVC polymer strip is pretty elastic and could maintain or recover to its original state. For the mid-term, the polymer strip will generate into helical curling structure

The reason why it has different deforming behavior is due to the evaporation of DMF. PVC itself was not elastic (as shown in Figure 6.2.3 below), however, DMF acted as a plasticizer to make it more elastic. For the original state, DMF didn't evaporate yet, the whole polymer strip was elastic. And days later, the DMF fully evaporated and only PVC left, which makes

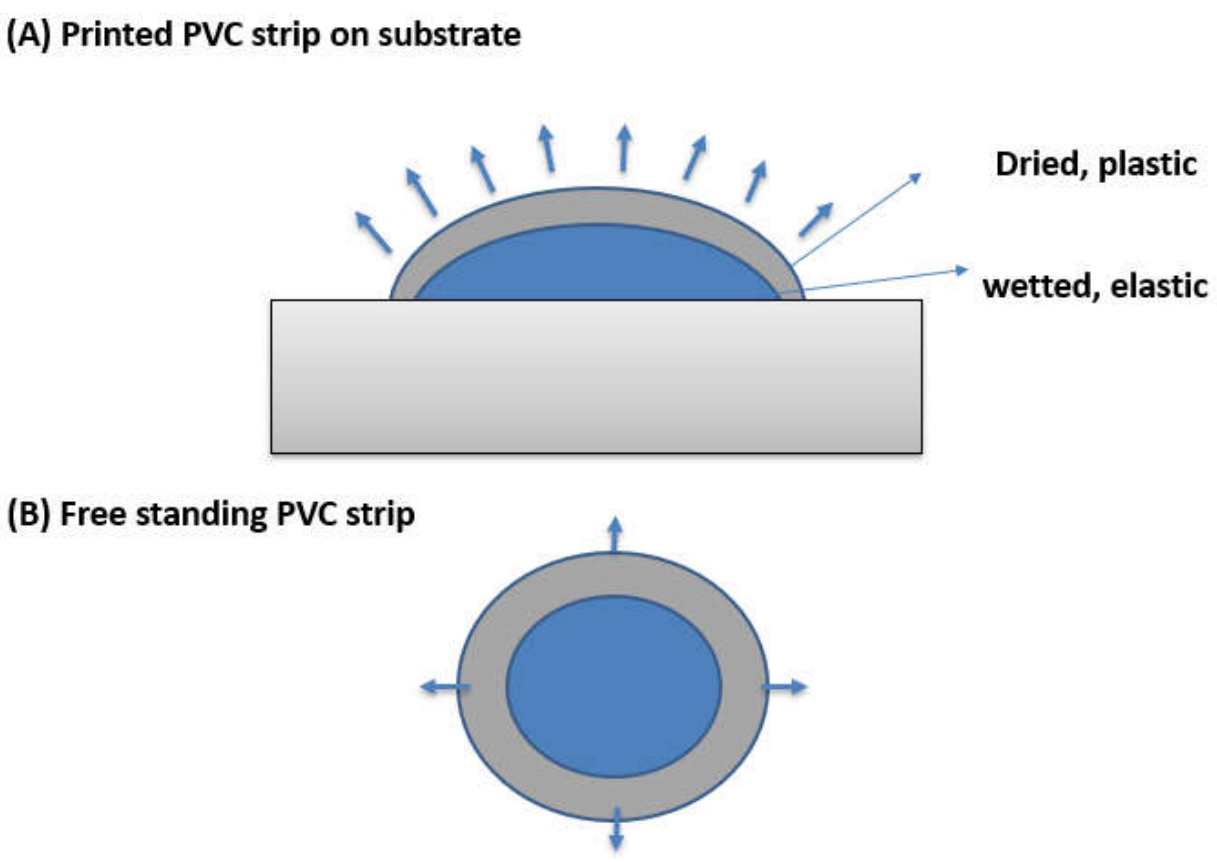

Figure 6.2.3 The cross-section of PVC strips showing in the evaporation process, which further explains the asymmetric elastic property distribution for the printed PVC strip (A) The PVC strip printed on the substrate - the outer shell tends to evaporate more than the inner shell which makes the PVC strip have the different mechanical property at different inner site. That is the reason why the PVC will self-propagate into a helical structure upon stretching. (b) the free-standing PVC strip without any substrate - it has a symmetric evaporation condition, which results into a symmetric elastic property distribution. No helical structure will be formed after the release of the stretching.

the polymer strip non-elastic. And fully dried PVC could be broken into parts easily upon the pull force. For the middle stage, the polymer strip could form into helical deformation upon force release because DMF was evaporating and therefore formed different concentration level inside the polymer strip. This concentration variation further caused a varied distribution of different elastic property. Because of the asymmetry of mechanical property inside the stripe at different spots of the cross-sections, it enables the polymer strip not only to bend but also to twist itself, which generated helical structure in general. To further prove that, a comparison test was made between the PVC strip printed on the substrate and the free-standing printed PVC strip (as shown in in Figure 6.2.3 B). And because of their different geometry and different evaporation process. They were used to further validate that the helical structure was caused by the asymmetry of the mechanical property. The PVC strip on the substrate will only evaporate the surface part first which exposed to the air (as shown in

Figure 6.2.3 A), and it created different elastic properties from outside to inside. And it is asymmetrically distributed compared to the free-standing PVC strip. Although it also had the same evaporation process, it has the symmetric elastic property distribution because the strip was all exposed to the air.

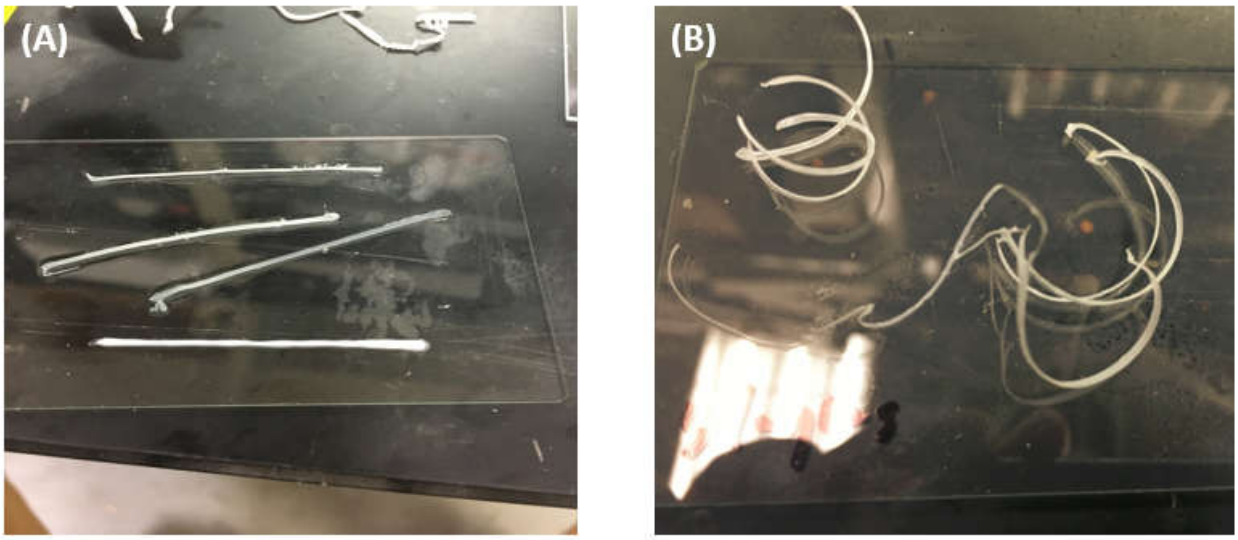

Figure 6.2.4 The PVC strip on the substrate (without stretching) (A) The PVC strips which was just printed on the substrate, and they were still immersed in the DMF solution. The width of the PVC strip is not uniformed either. (B) The PVC strips which was dried for 2 weeks. And they had already formed the buckled structure due to the asymmetric evaporation process

In the Figure 6.2.4, it further indicates the extreme condition for the asymmetric evaporation for the printed PVC strip. For the Figure 6.2.4 (A), the freshly printed PVC strip still have some DMF leaked out of the strip and make the whole PVC strip immersed into the DMF solution. The PVC strip under this state is completely elastic. Because the DMF was regarded as a plasticizer. However, after the PVC strip was completely dried out, it will further self-propagate into a big curve buckled structure.

The reason for the buckled structure is due to the asymmetric evaporation of the DMF solution. As mentions before in the Figure 6.2.3, the drying process start from the top surface of the printed PVC strip. It worked the same for the dried PVC strip in the Figure 6.2.4 (B), and in this process, the PVC will shrink when the DMF will further evaporate. It will also form into the different elastic property distribution inside the drying PVC strip. At a certain critical time or point, the upper part of the PVC stripe is more dried PVC and bottom or inside PVC strip is more elastic due to the remaining DMF. And at this point, the upper surface tends to shrink and at the same time, the bottom part does not tend to shrink, but it was more elastic. That is why the whole PVC tend to buckle and eventually, all the buckled strip dries out completely. This process further indicates the influence of the varied DMF concentration variation inside the PVC strip.

In addition, even for the helical deformed PVC strip itself, it will generate different helical micro-structure as well (as shown in the Figure 6.2.5 below).

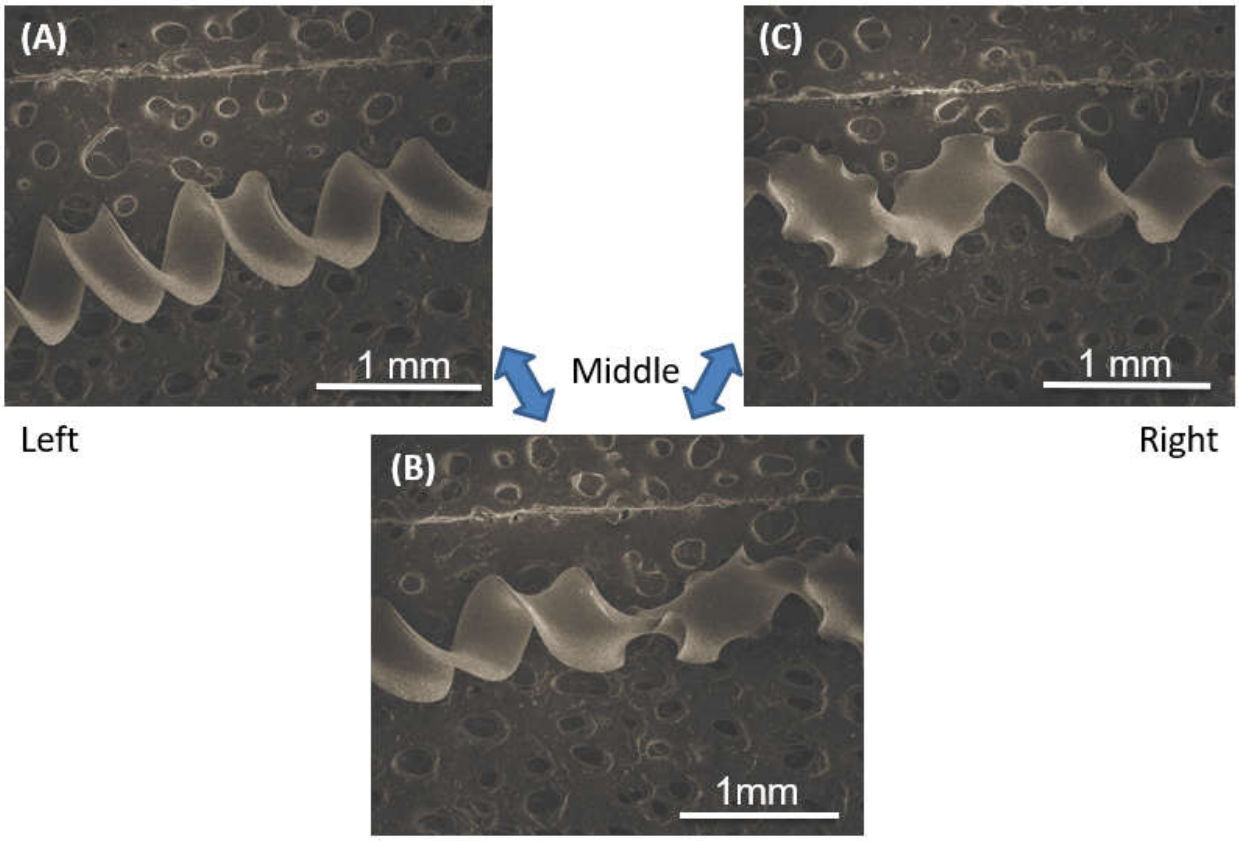

Figure 6.2.5 The different helical structure on the same stretched PVC strip. (A) and (B) show the different the helical structure from left to the right of the PVC strip. The left side has more smooth edges and right side also has wavy edges. (C) represents the transition from the smooth edge to the wavy edge (bi-fringes) in the middle which connected the left and right side of the PVC strip

The reason why there would be two different types of the helical structures on the same PVC strip is probably due to the non-uniformity of the printed PVC strips. From the previous Figure 6.2.2, those printed PVC strips were not uniform from left to right. Even being

stretched with the same load, the two different ends would have different height and width which might contribute to the different helical structures with different deformation pattern. And those structures with bi-fringes might be caused by the drying process of different edges caused by the non-uniformity of the printed PVC stripe as shown in the Figure 6.2.2. Because the different PVC strip edges will have the different geometry (cross-section shape and thickness), therefore the following drying process will result into the different mechanical properties comparing the two ends.

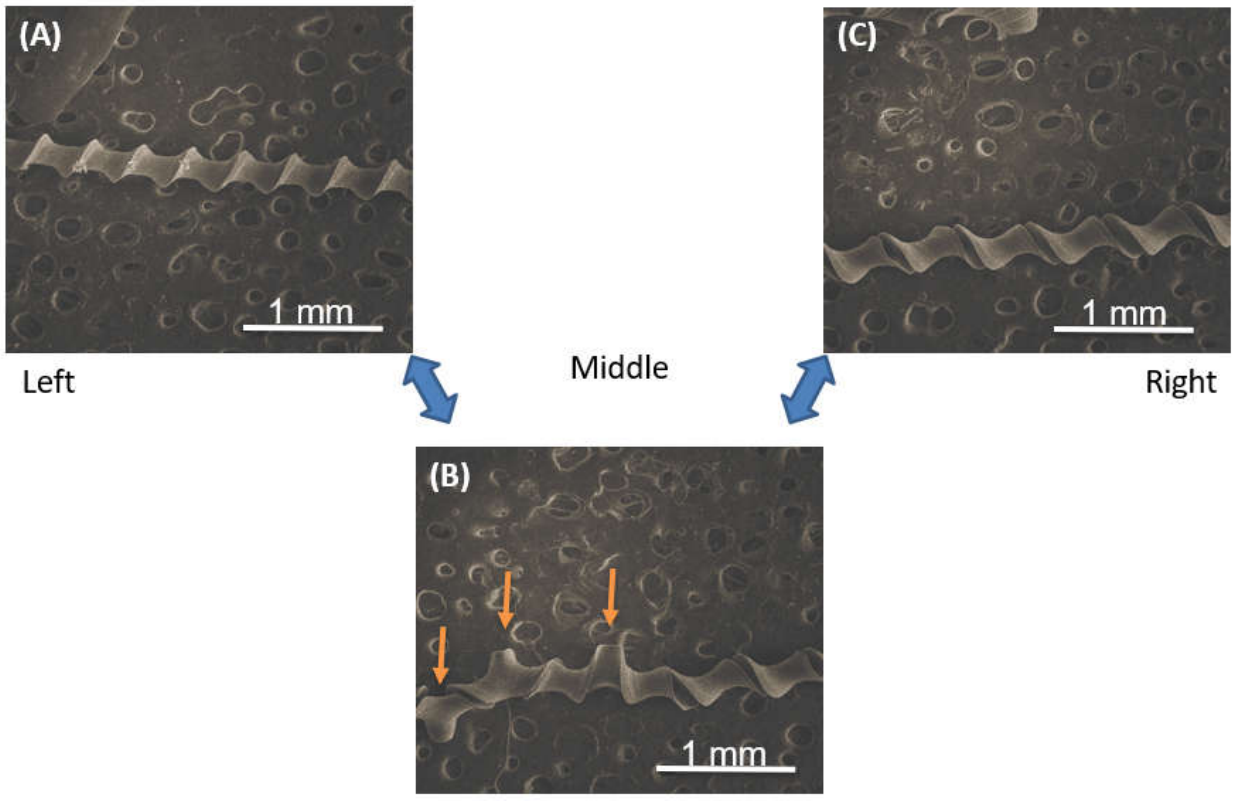

Figure 6.2.6 There are also perversions in the helical structure as shown in the (B), labeled with yellow arrows. The (A) and (B) are the left side and right side of the helical PVC strip.

The (C) is the middle part to connect (A) and (B) together. Because there are three perversions in this PVC strip, it changes the helical orientation and you could find the different orientation direction by comparing (A) and (B)

As the Figure 6.2.6 shown above, the perversion connected two oppositely handed helices. The reason why it generates the perversion after the stretching is because both ends of the PVC strip are fixed and cannot rotate during and after the stretching. This constrains the energy release at the end. If the box ends are fixed, the helical coiling will happen in the same direction which increases the writhe, which needs to be compensated by the twist. In order to minimize the twisting energy, the helical strip combines two helical coils into an opposite writhe and form the perversion.

6.2.4 Conclusion

The straight printed PVC strip could self-propagate into the helical structure after stretching. The reason why it has this different deformation behavior was due to the different evaporation condition of DMF. Because the PVC was dissolved into the DMF and the evaporation of DMF further created different concentration distribution of DMF content inside of polymer strip, which further results into different elastic properties at the different spots in the cross-section direction since DMF was regarded as a plasticizer. After the stretching, the asymmetric elastic property distribution in the cross section further resulted into the different elastic respond. This different elastic respond further results into the

helical structure. Because some of the parts could relax to the original state and some of the parts could not, however, they were bundled together and had to generate the twist and writhe to further release the energy stored in this asymmetric property distribution. However, once the DMF completely evaporate off, the PVC strip will be brittle. Therefore, it will be possible to mix PVC with other non-evaporative plasticizers with different concentration level to generate a stable strain induced PVC strip without the influence of the evaporating of DMF.

References

1. Holmberg, K.; Andersson, P.; Erdemir, A., Global energy consumption due to friction in passenger cars. *Tribology International* **2012,** *47*, 221-234.
2. Holmberg, K.; Erdemir, A., Influence of tribology on global energy consumption, costs and emissions. *Friction* **2017,** *5* (3), 263-284.
3. Geim, A. K.; Novoselov, K. S., The rise of graphene. *Nat Mater* **2007,** *6* (3), 183-191.
4. Lin, J.; Wang, L.; Chen, G., Modification of Graphene Platelets and their Tribological Properties as a Lubricant Additive. *Tribology Letters* **2010,** *41* (1), 209-215.
5. Berman, D.; Erdemir, A.; Sumant, A. V., Reduced wear and friction enabled by graphene layers on sliding steel surfaces in dry nitrogen. *Carbon* **2013,** *59*, 167-175.
6. Wang, S.; Zhang, Y.; Abidi, N.; Cabrales, L., Wettability and surface free energy of graphene films. *Langmuir* **2009,** *25* (18), 11078-11081.
7. Sun, C. Q.; Sun, Y.; Nie, Y. G.; Wang, Y.; Pan, J. S.; Ouyang, G.; Pan, L. K.; Sun, Z., Coordination-resolved C–C bond length and the C 1s binding energy of carbon allotropes and the effective atomic coordination of the few-layer graphene. *J Phys Chem C* **2009,** *113* (37), 16464-16467.
8. Lee, C.; Wei, X.; Kysar, J. W.; Hone, J., Measurement of the elastic properties and intrinsic strength of monolayer graphene. *Science* **2008,** *321* (5887), 385-8.
9. Novoselov, K. S.; Geim, A. K.; Morozov, S. V.; Jiang, D.; Zhang, Y.; Dubonos, S. V.; Grigorieva, I. V.; Firsov, A. A., Electric field effect in atomically thin carbon films. *Science* **2004,** *306* (5696), 666-669.
10. Kim, K. S.; Lee, H. J.; Lee, C.; Lee, S. K.; Jang, H.; Ahn, J. H.; Kim, J. H.; Lee, H. J., Chemical vapor deposition-grown graphene: the thinnest solid lubricant. *ACS Nano* **2011,** *5* (6), 5107-5114.
11. Lee, H.; Lee, N.; Seo, Y.; Eom, J.; Lee, S., Comparison of frictional forces on graphene and graphite. *Nanotechnology* **2009,** *20* (32).
12. Filleter, T.; McChesney, J. L.; Bostwick, A.; Rotenberg, E.; Emtsev, K. V.; Seyller, T.; Horn, K.; Bennewitz, R., Friction and dissipation in epitaxial graphene films. *Phys Rev Lett* **2009,** *102* (8), 086102.
13. Kou, R.; Shao, Y.; Mei, D.; Nie, Z.; Wang, D.; Wang, C.; Viswanathan, V. V.; Park, S.; Aksay, I. A.; Lin, Y.; Wang, Y.; Liu, J., Stabilization of Electrocatalytic Metal Nanoparticles at Metal-Metal Oxide-Graphene Triple Junction Points. *Journal of the American Chemical Society* **2011,** *133* (8), 2541-2547.
14. Lee, C.; Li, Q.; Kalb, W.; Liu, X. Z.; Berger, H.; Carpick, R. W.; Hone, J., Frictional characteristics of atomically thin sheets. *Science* **2010,** *328* (5974), 76-80.
15. Xu, L.; Ma, T.-b.; Hu, Y.-z.; Wang, H., Molecular dynamics simulation of the interlayer sliding behavior in few-layer graphene. *Carbon* **2012,** *50* (3), 1025-1032.
16. Ye, Z. J.; Tang, C.; Dong, Y. L.; Martini, A., Role of wrinkle height in friction variation with number of graphene layers. *J Appl Phys* **2012,** *112* (11), 116102.

17. Xu, L.; Ma, T. B.; Hu, Y. Z.; Wang, H., Vanishing stick-slip friction in few-layer graphenes: the thickness effect. *Nanotechnology* **2011,** *22* (28), 285708.
18. Egberts, P.; Han, G. H.; liu, X. Z.; Johnson, A. T. C.; Carpick, R. W., Frictional behavior of atomically thin sheets Hexagonal shaped graphene islands grown on copper by chemical vapor deposition. *ACS Nano* **2014,** *8* (5), 5010-5021.
19. Li, Q.; Lee, C.; Carpick, R. W.; Hone, J., Substrate effect on thickness-dependent friction on graphene. *physica status solidi (b)* **2010,** *247* (11-12), 2909-2914.
20. Smolyanitsky, A.; Killgore, J. P.; Tewary, V. K., Effect of elastic deformation on frictional properties of few-layer graphene. *Phys Rev B* **2012,** *85*, 035412.
21. Yang, L.; Zhang, Q.; Diao, D., Cross linking induced frictional behavior of multilayer graphene: Origin of friction. *Tribol Lett* **2016,** *62* (2), 33-40.
22. Buzio, R.; Gerbi, A.; Uttiya, S.; Bernini, C.; Castillo, A. E. D.; Palazon, F.; Siri, A. S.; Pellegrini, V.; Pellegrino, L.; Bonaccorso, F., Ultralow friction of ink-jet printed graphene flakes. *Nanoscale* **2017,** *9* (22), 7612-7624.
23. Reguzzoni, M.; Fasolino, A.; Molinari, E.; Righi, M. C., Friction by shear deformations in multilayer graphene. *J Phys Chem C* **2012,** *116* (39), 21104-21108.
24. Zeng, X. Z.; Peng, Y. T.; Lang, H. J., A novel approach to decrease friction of graphene. *Carbon* **2017,** *118*, 233-240.
25. Gong, P.; Li, Q. Y.; Liu, X. Z.; Carpick, R. W.; Egberts, P., Adhesion Mechanics between Nanoscale Silicon Oxide Tips and Few-Layer Graphene. *Tribology Letters* **2017,** *65* (2).
26. Deng, Z.; Smolyanitsky, A.; Li, Q.; Feng, X. Q.; Cannara, R. J., Adhesion-dependent negative friction coefficient on chemically modified graphite at the nanoscale. *Nat Mater* **2012,** *11* (12), 1032-7.
27. Ye, Z.; Egberts, P.; Han, G. H.; Johnson, A. T.; Carpick, R. W.; Martini, A., Load dependent friction hysteresis on graphene. *ACS Nano* **2016,** *10* (5), 5161-5168.
28. Almeida, C. M.; Prioli, R.; Fragneaud, B.; Cancado, L. G.; Paupitz, R.; Galvao, D. S.; De Cicco, M.; Menezes, M. G.; Achete, C. A.; Capaz, R. B., Giant and Tunable Anisotropy of Nanoscale Friction in Graphene. *Scientific Reports* **2016,** *6*.
29. Liu, Z. H.; Ma, T.; Liu, L. Q., Optical-assistant characterization of friction anisotropy properties of single-crystal graphene domains. *Tribology International* **2017,** *110*, 131-139.
30. Zhang, Y.; Liu, L.; Xi, N.; Wang, Y.; Dong, Z.; Wejinya, U. C., Friction anisotropy dependence on lattice orientation of graphene. *Science China Physics, Mechanics and Astronomy* **2014,** *57* (4), 663-667.
31. Kim, D.-I.; Park, S.-M.; Hong, S. W.; Jeong, M. Y.; Kim, K. H., The periodicity in interfacial friction of graphene. *Carbon* **2015,** *85* (0), 328-334.
32. Zhang, Y.; Dong, M.; Gueye, B.; Ni, Z.; Wang, Y.; Chen, Y., Temperature effects on the friction characteristics of graphene. *Appl Phys Lett* **2015,** *107* (1), 011601.
33. Peng, Y.; Wang, Z.; Zou, K., Friction and Wear Properties of Different Types of Graphene Nanosheets as Effective Solid Lubricants. *Langmuir* **2015,** *31* (28), 7782-91.
34. Ko, J.-H.; Kwon, S.; Byun, I.-S.; Choi, J. S.; Park, B. H.; Kim, Y.-H.; Park, J. Y., Nanotribological Properties of Fluorinated, Hydrogenated, and Oxidized Graphenes. *Tribology Letters* **2013,** *50* (2), 137-144.

35. Dong, Y.; Wu, X.; Martini, A., Atomic roughness enhanced friction on hydrogenated graphene. *Nanotechnology* **2013,** *24* (37), 375701.
36. Bonelli, F.; Manini, N.; Cadelano, E.; Colombo, L., Atomistic simulations of the sliding friction of graphene flakes. *J Phys Condens Mat* **2009,** *70* (4), 449-459.
37. Zhang, L.; Pu, J.; Wang, L.; Xue, Q., Frictional dependence of graphene and carbon nanotube in diamond-like carbon/ionic liquids hybrid films in vacuum. *Carbon* **2014,** *80,* 734-745.
38. Kwon, S.; Ko, J. H.; Jeon, K. J.; Kim, Y. H.; Park, J. Y., Enhanced nanoscale friction on fluorinated graphene. *Nano Lett* **2012,** *12* (12), 6043-8.
39. Elinski, M. B.; Menard, B. D.; Liu, Z. T.; Batteas, J. D., Adhesion and Friction at Graphene/Self-Assembled Monolayer Interfaces Investigated by Atomic Force Microscopy. *Journal of Physical Chemistry C* **2017,** *121* (10), 5635-5641.
40. Vilhena, J. G.; Pimentel, C.; Pedraz, P.; Luo, F.; Serena, P. A.; Pina, C. M.; Gnecco, E.; Perez, R., Atomic-Scale Sliding Friction on Graphene in Water. *Acs Nano* **2016,** *10* (4), 4288-4293.
41. Guo, Y. F.; Guo, W.; Chen, C. F., Modifying atomic-scale friction between two graphene sheets: A molecular-force-field study. *Phys Rev B* **2007,** *76*, 155429-155434.
42. Zhang, H.; Guo, Z.; Gao, H.; Chang, T., Stiffness-dependent interlayer friction of graphene. *Carbon* **2015,** *94*, 60-66.
43. Feng, X. F.; Kwon, S.; Park, J. Y.; Salmeron, M., Superlubric sliding of graphene nanoflakes on graphene. *ACS Nano* **2013,** *7* (2), 1718-1724.
44. van Wijk, M. M.; Dienwiebel, M.; Frenken, J. W. M.; Fasolino, A., Superlubric to stick-slip sliding of incommensurate graphene flakes on graphite. *Physical Review B* **2013,** *88* (23).
45. Wang, J. J.; Wang, F.; Li, J. M.; Wang, S. J.; Song, Y. L.; Sun, Q.; Jia, Y., Theoretical study of superlow friction between two single-side hydrogenated graphene sheets. *Tribol Lett* **2012,** *48* (2), 255-261.
46. Wang, L. F.; Ma, T. B.; Hu, Y. Z.; Wang, H., Atomic-scale friction in graphene oxide: An interfacial interaction perspective from first- principles calculations. *Phys Rev B* **2012,** *86* (12), 125436.
47. Wijk, M. M.; Wijn, A. S.; Fasolino, A., Collective superlubricity of graphene flakes. *J Phys Condens Matter* **2016,** *28* (13), 134007.
48. Bhushan, B., *Introduction to tribology*. John Wiley & Sons: 2013.
49. Rudnick, L. R., *Lubricant additives: chemistry and applications*. CRC press: 2009.
50. Mungse, H. P.; Khatri, O. P., Chemically Functionalized Reduced Graphene Oxide as a Novel Material for Reduction of Friction and Wear. *Journal of Physical Chemistry C* **2014,** *118* (26), 14394-14402.
51. Ota, J.; Hait, S. K.; Sastry, M. I. S.; Ramakumar, S. S. V., Graphene dispersion in hydrocarbon medium and its application in lubricant technology. *Rsc Advances* **2015,** *5* (66), 53326-53332.
52. Eswaraiah, V.; Sankaranarayanan, V.; Ramaprabhu, S., Graphene-Based Engine Oil Nanofluids for Tribological Applications. *Acs Applied Materials & Interfaces* **2011,** *3* (11), 4221-4227.
53. Shao, J. J.; Wu, S. D.; Zhang, S. B.; Lv, W.; Su, F. Y.; Yang, Q. H., Graphene oxide hydrogel at solid/liquid interface. *Chem Commun (Camb)* **2011,** *47* (20), 5771-3.

54. Zin, V.; Barison, S.; Agresti, F.; Colla, L.; Pagura, C.; Fabrizio, M., Improved tribological and thermal properties of lubricants by graphene based nano-additive. *RSC Adv* **2016,** *00* (1-3).
55. Zhang, W.; Zhou, M.; Zhu, H. W.; Tian, Y.; Wang, K. L.; Wei, J. Q.; Ji, F.; Li, X.; Li, Z.; Zhang, P.; Wu, D. H., Tribological properties of oleic acid-modified graphene as lubricant oil additives. *J Phys D Appl Phys* **2011,** *44*, 205303-305307.
56. Choudhary, S.; Mungse, H. P.; Khatri, O. P., Dispersion of alkylated graphene in organic solvents and its potential for lubrication applications. *Journal of Materials Chemistry* **2012,** *22* (39), 21032.
57. Ismail, N. A.; Bagheri, S., Highly oil-dispersed functionalized reduced graphene oxide nanosheets as lube oil friction modifier. *Materials Science and Engineering: B* **2017,** *222*, 34-42.
58. Fan, X.; Wang, L.; Li, W., In Situ Fabrication of Low-Friction Sandwich Sheets Through Functionalized Graphene Crosslinked by Ionic Liquids. *Tribology Letters* **2015,** *58* (1).
59. Fu, H.; Fan, X.; Li, W.; Zhu, M.; Peng, J.; Li, H., In situ modified multilayer graphene toward high-performance lubricating additive. *RSC Adv.* **2017,** *7* (39), 24399-24409.
60. Li, Y.; Zhao, J.; Tang, C.; He, Y.; Wang, Y.; Chen, J.; Mao, J.; Zhou, Q.; Wang, B.; Wei, F.; Luo, J.; Shi, G., Highly Exfoliated Reduced Graphite Oxide Powders as Efficient Lubricant Oil Additives. *Advanced Materials Interfaces* **2016,** *3* (22), 1600700.
61. Yang, J.; Xia, Y.; Song, H.; Chen, B.; Zhang, Z., Synthesis of the liquid-like graphene with excellent tribological properties. *Tribology International* **2017,** *105*, 118-124.
62. Zheng, D.; Cai, Z.-b.; Shen, M.-x.; Li, Z.-y.; Zhu, M.-h., Investigation of the tribology behaviour of the graphene nanosheets as oil additives on textured alloy cast iron surface. *Applied Surface Science* **2016,** *387*, 66-75.
63. Li, H.; Chen, L.; Zhang, Y.; Ji, X.; Chen, S.; Song, H.; Li, C.; Tang, H., Synthesis of $MoSe_2$/Reduced graphene oxide composites with improved tribological properties for oil-based additives. *Crystal Research and Technology* **2014,** *49* (4), 204-211.
64. Liang, S.; Shen, Z.; Yi, M.; Liu, L.; Zhang, X.; Ma, S., In-situ exfoliated graphene for high-performance water-based lubricants. *Carbon* **2016,** *96*, 1181-1190.
65. Peng, Y.; Wang, Z., Tribological properties of sodium dodecyl sulfate aqueous dispersion of graphite-derived carbon materials. *RSC Advances* **2014,** *4* (20), 9980.
66. Dou, X.; Koltonow, A. R.; He, X. L.; Jang, H. D.; Wang, Q.; Chung, Y. W.; Huang, J. X., Self-dispersed crumpled graphene balls in oil for friction and wear reduction. *Proceedings of the National Academy of Sciences of the United States of America* **2016,** *113* (6), 1528-1533.
67. Zin, V.; Agresti, F.; Barison, S.; Colla, L.; Mercadelli, E.; Fabrizio, M.; Pagura, C., Tribological Properties of Engine Oil with Carbon Nano-horns as Nano-additives. *Tribology Letters* **2014,** *55* (1), 45-53.
68. Wu, X.; Zhao, G.; Zhao, Q.; Gong, K.; Wang, X.; Liu, W.; Liu, W., Investigating the tribological performance of nanosized MoS2on graphene dispersion in perfluoropolyether under high vacuum. *RSC Adv.* **2016,** *6* (101), 98606-98610.
69. Xu, Y.; Peng, Y.; Dearn, K. D.; Zheng, X.; Yao, L.; Hu, X., Synergistic lubricating behaviors of graphene and MoS2 dispersed in esterified bio-oil for steel/steel contact. *Wear* **2015,** *342-343*, 297-309.

70. Gong, K.; Wu, X.; Zhao, G.; Wang, X., Nanosized MoS 2 deposited on graphene as lubricant additive in polyalkylene glycol for steel/steel contact at elevated temperature. *Tribology International* **2017,** *110*, 1-7.
71. Pu, J.; Mo, Y.; Wan, S.; Wang, L., Fabrication of novel graphene-fullerene hybrid lubricating films based on self-assembly for MEMS applications. *Chem Commun (Camb)* **2014,** *50* (4), 469-71.
72. Liu, X.; Pu, J.; Wang, L.; Xue, Q., Novel DLC/ionic liquid/graphene nanocomposite coatings towards high-vacuum related space applications. *Journal of Materials Chemistry A* **2013,** *1* (11), 3797.
73. Yan, Z.; Shi, X.; Huang, Y.; Deng, X.; Yang, K.; Liu, X., Tribological Performance of Ni3Al Matrix Self-Lubricating Composites Containing Multilayer Graphene and Ti3SiC2 at Elevated Temperatures. *Journal of Materials Engineering and Performance* **2017,** *26* (9), 4605-4614.
74. Bai, G.; Wang, J.; Yang, Z.; Wang, H.; Wang, Z.; Yang, S., Preparation of a highly effective lubricating oil additive – ceria/graphene composite. *RSC Adv.* **2014,** *4* (87), 47096-47105.
75. Zhou, Q.; Huang, J.; Wang, J.; Yang, Z.; Liu, S.; Wang, Z.; Yang, S., Preparation of a reduced graphene oxide/zirconia nanocomposite and its application as a novel lubricant oil additive. *RSC Adv.* **2015,** *5* (111), 91802-91812.
76. Berman, D.; Deshmukh, S. A.; Sankaranarayanan, S. K. R. S.; Erdemir, A.; Sumant, A. V., Macroscale superlubricity enabled by graphene nanoscroll formation. *Science* **2015,** *348* (6239), 1118-1122.
77. Pu, J.; Wan, S.; Zhao, W.; Mo, Y.; Zhang, X.; Wang, L.; Xue, Q., Preparation and Tribological Study of Functionalized Graphene–IL Nanocomposite Ultrathin Lubrication Films on Si Substrates. *The Journal of Physical Chemistry C* **2011,** *115* (27), 13275-13284.
78. Akbulut, H.; Hatipoglu, G.; Algul, H.; Tokur, M.; Kartal, M.; Uysal, M.; Cetinkaya, T., Co-deposition of Cu/WC/graphene hybrid nanocomposites produced by electrophoretic deposition. *Surface & Coatings Technology* **2015,** *284*, 344-352.
79. Zhang, X.; Dong, P.; Chen, Y.; Yang, W.; Zhan, Y.; Wu, K.; Chao, Y., Fabrication and tribological properties of copper matrix composite with short carbon fiber/reduced graphene oxide filler. *Tribology International* **2016,** *103*, 406-411.
80. Uysal, M.; Akbulut, H.; Tokur, M.; Algül, H.; Çetinkaya, T., Structural and sliding wear properties of Ag/Graphene/WC hybrid nanocomposites produced by electroless co-deposition. *Journal of Alloys and Compounds* **2016,** *654*, 185-195.
81. Zou, J.; Shi, X.; Shen, Q.; Yang, K.; Zhai, W.; Huang, Y., Dry Sliding Wear of TiAl-Graphene-Silver Composite at Elevated Temperatures. *Journal of Materials Engineering and Performance* **2017,** *26* (9), 4615-4625.
82. Xu, Z. S.; Zhang, Q. X.; Shi, X. L.; Zhai, W. Z.; Yang, K., Tribological Properties of TiAl Matrix Self-Lubricating Composites Containing Multilayer Graphene and Ti3SiC2 at High Temperatures. *Tribology Transactions* **2015,** *58* (6), 1131-1141.
83. Shen, Q.; Shi, X. L.; Zou, J. L.; Yang, K.; Huang, Y. C.; Zhang, A.; Ibrahim, A. M. M.; Wang, Y. F., Tribological Performance and Self-Lubricating Film Formation Mechanism of TiAl-Based Composites at Elevated Temperatures. *Journal of Materials Engineering and Performance* **2017,** *26* (1), 268-276.

84. Zou, J.-L.; Shi, X.-L.; Shen, Q.; Yang, K.; Huang, Y.-C.; Zhang, A.; Wang, Y.-F.; Zhang, Q.-X., Tribological Behavior of TiAl–Multilayer Graphene–Ag Composites at Different Temperatures and Sliding Speeds. *Acta Metallurgica Sinica (English Letters)* **2017,** *30* (3), 193-200.
85. Yazdani, B.; Xu, F.; Ahmad, I.; Hou, X.; Xia, Y.; Zhu, Y., Tribological performance of Graphene/Carbon nanotube hybrid reinforced Al_2O_3 composites. *Sci. Rep.* **2015,** *5*, 11579.
86. Yang, M.; Zhang, Z.; Yuan, J.; Guo, F.; Men, X.; Liu, W., Growth of Mo2C nanoparticles on graphene as lubricant filler for high tribological performances of fabric self-lubricating liner composites. *RSC Adv.* **2016,** *6* (111), 110070-110076.
87. Chen, Z.; Yan, H.; Liu, T.; Niu, S., Nanosheets of MoS2 and reduced graphene oxide as hybrid fillers improved the mechanical and tribological properties of bismaleimide composites. *Composites Science and Technology* **2016,** *125*, 47-54.
88. Liu, C.; Yan, H.; Chen, Z.; Yuan, L.; Liu, T., Enhanced tribological properties of bismaleimides filled with aligned graphene nanosheets coated with Fe3O4nanorods. *J. Mater. Chem. A* **2015,** *3* (19), 10559-10565.
89. Li, H. L.; Jin, L.; Dong, J. L.; Liu, L.; Li, M.; Liu, Y.; Xiao, L. H.; Ao, Y. H., Tribological performance and thermal conductivity of graphene-Fe3O4/poly(phenol-formaldehyde resin) hybrid reinforced carbon fiber composites. *Rsc Advances* **2016,** *6* (65), 60200-60205.
90. Masood, M. T.; Papadopoulou, E. L.; Heredia-Guerrero, J. A.; Bayer, I. S.; Athanassiou, A.; Ceseracciu, L., Graphene and polytetrafluoroethylene synergistically improve the tribological properties and adhesion of nylon 66 coatings. *Carbon* **2017,** *123*, 26-33.
91. Pan, B. L.; Peng, S. G.; Song, S. Y.; Chen, J.; Liu, J. C.; Liu, H. Y.; Zhang, Y. Z.; Niu, Q. S., The Adaptive Tribological Investigation of Polycaprolactam/Graphene Nanocomposites. *Tribology Letters* **2017,** *65* (1).
92. Xin, Y. S.; Li, T. S.; Xu, F. L.; Wang, M. M., Multidimensional structure and enhancement performance of modified graphene/carbon nanotube assemblies in tribological properties of polyimide nanocomposites. *Rsc Advances* **2017,** *7* (34), 20742-20753.
93. Zhang, S.; Yang, J.; Chen, B.; Guo, S.; Li, J.; Li, C., One-step hydrothermal synthesis of reduced graphene oxide/zinc sulfide hybrids for enhanced tribological properties of epoxy coatings. *Surface and Coatings Technology* **2017,** *326*, 87-95.
94. Meng, Y.; Su, F.; Chen, Y., Supercritical Fluid Synthesis and Tribological Applications of Silver Nanoparticle-decorated Graphene in Engine Oil Nanofluid. *Sci Rep* **2016,** *6*, 31246.
95. Ramón-Raygoza, E. D.; Rivera-Solorio, C. I.; Giménez-Torres, E.; Maldonado-Cortés, D.; Cardenas-Alemán, E.; Cué-Sampedro, R., Development of nanolubricant based on impregnated multilayer graphene for automotive applications: Analysis of tribological properties. *Powder Technology* **2016,** *302*, 363-371.
96. Berman, D.; Deshmukh, S. A.; Sankaranarayanan, S. K. R. S.; Erdemir, A.; Sumant, A. V., Extraordinary Macroscale Wear Resistance of One Atom Thick Graphene Layer. *Advanced Functional Materials* **2014,** *24* (42), 6640-6646.
97. Zheng, D.; Wu, Y.-p.; Li, Z.-y.; Cai, Z.-b., Tribological properties of WS2/graphene nanocomposites as lubricating oil additives. *RSC Adv.* **2017,** *7* (23), 14060-14068.
98. Hummers, W. S.; Offeman, R. E., PREPARATION OF GRAPHITIC OXIDE. *Journal of the American Chemical Society* **1958,** *80* (6), 1339-1339.

99. Kim, F.; Luo, J.; Cruz-Silva, R.; Cote, L. J.; Sohn, K.; Huang, J., Self-Propagating Domino-like Reactions in Oxidized Graphite. *Advanced Functional Materials* **2010,** *20* (17), 2867-2873.
100. Jang, H. D.; Chang, H.; Cho, K.; Kim, F.; Sohn, K.; Huang, J., Co-Assembly of Nanoparticles in Evaporating Aerosol Droplets: Preparation of Nanoporous Pt/TiO2 Composite Particles. *Aerosol Science and Technology* **2010,** *44* (12), 1140-1145.
101. Schniepp, H. C.; Li, J. L.; McAllister, M. J.; Sai, H.; Herrera-Alonso, M.; Adamson, D. H.; Prud'homme, R. K.; Car, R.; Saville, D. A.; Aksay, I. A., Functionalized single graphene sheets derived from splitting graphite oxide. *Journal of Physical Chemistry B* **2006,** *110* (17), 8535-8539.
102. Zhu, Y.; Murali, S.; Stoller, M. D.; Velamakanni, A.; Piner, R. D.; Ruoff, R. S., Microwave assisted exfoliation and reduction of graphite oxide for ultracapacitors. *Carbon* **2010,** *48* (7), 2118-2122.
103. Coleman, J. N., Liquid Exfoliation of Defect-Free Graphene. *Accounts Chem Res* **2013,** *46* (1), 14-22.
104. Hanlon, D.; Backes, C.; Doherty, E.; Cucinotta, C. S.; Berner, N. C.; Boland, C.; Lee, K.; Harvey, A.; Lynch, P.; Gholamvand, Z.; Zhang, S. F.; Wang, K. P.; Moynihan, G.; Pokle, A.; Ramasse, Q. M.; McEvoy, N.; Blau, W. J.; Wang, J.; Abellan, G.; Hauke, F.; Hirsch, A.; Sanvito, S.; O'Regan, D. D.; Duesberg, G. S.; Nicolosi, V.; Coleman, J. N., Liquid exfoliation of solvent-stabilized few-layer black phosphorus for applications beyond electronics. *Nat Commun* **2015,** *6*.
105. Nicolosi, V.; Chhowalla, M.; Kanatzidis, M. G.; Strano, M. S.; Coleman, J. N., Liquid Exfoliation of Layered Materials. *Science* **2013,** *340* (6139), 1420-+.
106. O'Neill, A.; Khan, U.; Coleman, J. N., Preparation of High Concentration Dispersions of Exfoliated MoS2 with Increased Flake Size. *Chem Mater* **2012,** *24* (12), 2414-2421.
107. Bakunin, V. N.; Suslov, A. Y.; Kuzmina, G. N.; Parenago, O. P., Synthesis and application of inorganic nanoparticles as lubricant components - a review. *J Nanopart Res* **2004,** *6* (2-3), 273-284.
108. Hsu, S. M., Nano-lubrication: concept and design. *Tribol Int* **2004,** *37* (7), 537-545.
109. Luo, J. Y.; Kim, J.; Huang, J. X., Material Processing of Chemically Modified Graphene: Some Challenges and Solutions. *Accounts Chem Res* **2013,** *46* (10), 2225-2234.
110. Luo, J. Y.; Jang, H. D.; Sun, T.; Xiao, L.; He, Z.; Katsoulidis, A. P.; Kanatzidis, M. G.; Gibson, J. M.; Huang, J. X., Compression and Aggregation-Resistant Particles of Crumpled Soft Sheets. *Acs Nano* **2011,** *5* (11), 8943-8949.
111. Luo, J. Y.; Jang, H. D.; Huang, J. X., Effect of Sheet Morphology on the Scalability of Graphene-Based Ultracapacitors. *Acs Nano* **2013,** *7* (2), 1464-1471.
112. Berman, D.; Erdemir, A.; Sumant, A. V., Graphene: a new emerging lubricant. *Mater Today* **2014,** *17* (1), 31-42.
113. Bollmann, W.; Spreadborough, J., Action of Graphite as a Lubricant. *Nature* **1960,** *186* (4718), 29-30.
114. Dwyerjoyce, R. S.; Sayles, R. S.; Ioannides, E., An Investigation into the Mechanisms of Closed 3-Body Abrasive Wear. *Wear* **1994,** *175* (1-2), 133-142.
115. Lee, C. G.; Hwang, Y. J.; Choi, Y. M.; Lee, J. K.; Choi, C.; Oh, J. M., A Study on The Tribological Characteristics of Graphite Nano Lubricants. *Int J Precis Eng Man* **2009,** *10* (1), 85-90.

116. Lin, J. S.; Wang, L. W.; Chen, G. H., Modification of Graphene Platelets and their Tribological Properties as a Lubricant Additive. *Tribol Lett* **2011,** *41* (1), 209-215.
117. Zhang, W.; Zhou, M.; Zhu, H. W.; Tian, Y.; Wang, K. L.; Wei, J. Q.; Ji, F.; Li, X.; Li, Z.; Zhang, P.; Wu, D. H., Tribological properties of oleic acid-modified graphene as lubricant oil additives. *J Phys D Appl Phys* **2011,** *44* (20).
118. Baik, S.; Yoon, D.; Lee, H. I.; Kim, J. M.; Lee, G. S.; Lee, Y. Z., Frictional Performances of Activated Carbon and Carbon Blacks as Lubricant Additives. *Tribol T* **2009,** *52* (1), 133-137.
119. Kim, F.; Luo, J. Y.; Cruz-Silva, R.; Cote, L. J.; Sohn, K.; Huang, J. X., Self-Propagating Domino-like Reactions in Oxidized Graphite. *Adv Funct Mater* **2010,** *20* (17), 2867-2873.
120. Grzelczak, M.; Perez-Juste, J.; Mulvaney, P.; Liz-Marzan, L. M., Shape control in gold nanoparticle synthesis. *Chemical Society Reviews* **2008,** *37* (9), 1783-1791.
121. Hardy, W. B., Boundary lubrication - The paraffin series. *P R Soc Lond a-Conta* **1922,** *100* (707), 550-574.
122. Udofia, I. J.; Jin, Z. M., Elastohydrodynamic lubrication analysis of metal-on-metal hip-resurfacing prostheses. *J Biomech* **2003,** *36* (4), 537-544.
123. Hess, D. P.; Soom, A., Normal Vibrations and Friction under Harmonic Loads .1. Hertzian Contacts. *J Tribol-T Asme* **1991,** *113* (1), 80-86.
124. Willis, J. R., Hertzian Contact of Anisotropic Bodies. *J Mech Phys Solids* **1966,** *14* (3), 163-&.
125. Silbert, L. E., Jamming of frictional spheres and random loose packing. *Soft Matter* **2010,** *6* (13), 2918-2924.
126. Ronen, A.; Malkin, S., Wear Mechanisms of Statically Loaded Hydrodynamic Bearings by Contaminant Abrasive Particles. *Wear* **1981,** *68* (3), 371-389.
127. Guo, Q.; Mehta, A. K.; Grover, M. A.; Chen, W.; Lynn, D. G.; Chen, Z., Shape selection and multi-stability in helical ribbons. *Applied Physics Letters* **2014,** *104* (21).
128. Huang, X. H.; Neretina, S.; El-Sayed, M. A., Gold Nanorods: From Synthesis and Properties to Biological and Biomedical Applications. *Advanced Materials* **2009,** *21* (48), 4880-4910.
129. Jones, M. R.; Osberg, K. D.; Macfarlane, R. J.; Langille, M. R.; Mirkin, C. A., Templated Techniques for the Synthesis and Assembly of Plasmonic Nanostructures. *Chemical Reviews* **2011,** *111* (6), 3736-3827.
130. Rycenga, M.; Cobley, C. M.; Zeng, J.; Li, W. Y.; Moran, C. H.; Zhang, Q.; Qin, D.; Xia, Y. N., Controlling the Synthesis and Assembly of Silver Nanostructures for Plasmonic Applications. *Chemical Reviews* **2011,** *111* (6), 3669-3712.
131. Tao, A. R.; Habas, S.; Yang, P. D., Shape control of colloidal metal nanocrystals. *Small* **2008,** *4* (3), 310-325.
132. Xia, Y. N.; Xiong, Y. J.; Lim, B.; Skrabalak, S. E., Shape-Controlled Synthesis of Metal Nanocrystals: Simple Chemistry Meets Complex Physics? *Angewandte Chemie-International Edition* **2009,** *48* (1), 60-103.
133. Guo, S.; Wang, L.; Wang, E., Templateless, surfactantless, simple electrochemical route to rapid synthesis of diameter-controlled 3D flowerlike gold microstructure with "clean" surface. *Chem Commun* **2007,** (30), 3163-3165.

134. Lopez-Sanchez, J. A.; Dimitratos, N.; Hammond, C.; Brett, G. L.; Kesavan, L.; White, S.; Miedziak, P.; Tiruvalam, R.; Jenkins, R. L.; Carley, A. F.; Knight, D.; Kiely, C. J.; Hutchings, G. J., Facile removal of stabilizer-ligands from supported gold nanoparticles. *Nat Chem* **2011,** *3* (7), 551-556.
135. Panda, B. R.; Chattopadhyay, A., Synthesis of Au nanoparticles at "all" pH by H2O2 reduction of HAuCl4. *Journal of Nanoscience and Nanotechnology* **2007,** *7* (6), 1911-1915.
136. Fan, C. L.; Lee, W. D.; Teng, N. W.; Sun, Y. C.; Chen, K. M., Epoxidation of chiral camphor N-enoylpyrazolidinones with methyl(trifluoromethyl)dioxirane and urea hydrogen peroxide/acid anhydride: Reversal of stereoselectivity. *Journal of Organic Chemistry* **2003,** *68* (25), 9816-9818.
137. Marigo, M.; Franzen, J.; Poulsen, T. B.; Zhuang, W.; Jorgensen, K. A., Asymmetric organocatalytic epoxidation of alpha,beta-unsaturated aldehydes with hydrogen peroxide. *Journal of the American Chemical Society* **2005,** *127* (19), 6964-6965.
138. Gerbode, S. J.; Puzey, J. R.; McCormick, A. G.; Mahadevan, L., How the Cucumber Tendril Coils and Overwinds. *Science* **2012,** *337* (6098), 1087-1091.
139. Liu, J.; Huang, J. S.; Su, T. X.; Bertoldi, K.; Clarke, D. R., Structural Transition from Helices to Hemihelices (vol 9, e93183, 2014). *Plos One* **2015,** *10* (9).
140. Robertson, J. M.; Torbati, A. H.; Rodriguez, E. D.; Mao, Y. Q.; Baker, R. M.; Qi, H. J.; Mather, P. T., Mechanically programmed shape change in laminated elastomeric composites. *Soft Matter* **2015,** *11* (28), 5754-5764.
141. Huang, J. S.; Liu, J.; Kroll, B.; Bertoldi, K.; Clarke, D. R., Spontaneous and deterministic three-dimensional curling of pre-strained elastomeric bi-strips. *Soft Matter* **2012,** *8* (23), 6291-6300.
142. Studart, A. R.; Erb, R. M., Bioinspired materials that self-shape through programmed microstructures. *Soft Matter* **2014,** *10* (9), 1284-1294.
143. Forterre, Y.; Dumais, J., Generating Helices in Nature. *Science* **2011,** *333* (6050), 1715-1716.
144. Liu, S. P.; Yao, Z. W.; Chiou, K.; Stupp, S. I.; de la Cruz, M. O., Emergent perversions in the buckling of heterogeneous elastic strips. *Proceedings of the National Academy of Sciences of the United States of America* **2016,** *113* (26), 7100-7105.